

Aim and Scope

The objective of the *Journal of Residuals Science & Technology* (JRS&T) is to provide a forum for technical research on the management and disposal of residuals from pollution control activities. The Journal publishes papers that examine the characteristics, effects, and management principles of various residuals from such sources as wastewater treatment, water treatment, air pollution control, hazardous waste treatment, solid waste, industrial waste treatment, and other pollution control activities. Papers on health and the environmental effects of residuals production, management, and disposal are also welcome.

Editor-in-Chief

P. Brent Duncan
Department of Biology
University of North Texas
Denton, TX, USA
pduncan@unt.edu

Assistant Editor

James Lee
james.lee3918@gmail.com

Editorial Advisory Board

Muhammad Abu-Orf
AECOM, USA
mohammad.abu-orf@aecom.com

Nafissa M. Bizo
City of Philadelphia Water Department
nafissa.bizo@phila.gov

Richard Dick
Cornell University, USA
rid1@cornell.edu

Eliot Epstein
Epstein Environmental Consultants
epsteinee@comcast.net

Guor-Cheng Fang, Ph.D.
Hungkuang University, Taiwan
gcfang@sunrise.hk.edu.tw

Robert Hale
Virginia Institute of Marine Science, USA
hale@vims.edu

Paul F. Hudak
University of North Texas, USA
hudak@unt.edu

Blanca Jimenez Cisneros
Inst. de Ingenieria, UNAM, Mexico
bjc@mumas.iingen.unam.mx

Julia Kopp
Technische Universitat Braunschweig,
Germany
j.kopp@tu-bs.de

Uta Krogmann
RutgersUniversity, USA
krogmann@aesop.rutgers.edu

D. J. Lee
National Taiwan University, Taiwan
djlee@ntu.edu.tw

Giuseppe Mininni
Via Reno 1, Italy
mininni@irsa.rm.cnr.it

Lynne H. Moss
CDM Smith
mosslh@cdmsmith.com

John Novak
Virginia Tech, USA
jtnov@vt.edu

Nagaharu Okuno
The University of Shiga Prefecture,
Japan
okuno@ses.usp.ac.jp

Jan Oleszkiewicz
University of Manitoba, Canada
oleszkie@ms.umanitoba.ca

Banu Örmeci
Carleton University, Canada
banu_ormeci@carleton.ca

Ian L. Pepper
University of Arizona, USA
ipepper@ag.arizona.edu

Ioana G. Petrisor
Co-Editor-in-Chief
Environmental Forensics Journal, USA
Environmental.Forensics@gmail.com

Bob Reimers
Tulane University, USA
rreimers@tulane.edu

Dilek Sanin
Middle East Technical University,
Turkey
dsanin@metu.edu.tr

Heidi Snyman
Golder Associates Africa (Pty) Ltd.,
South Africa
hsnyman@golder.co.za

Ludovico Spinosa
Consultant at Commissariat
for Env. Energ. in Region,
Puglia, Italy
ludovico.spinosa@fastwebnet.it

P. Aarne Vesilind
Bucknell University, USA
aarne.vesilind@gmail.com

Doug Williams
California Polytechnic State
University, USA
wmsengr@thegrid.net

JOURNAL OF RESIDUALS SCIENCE & TECHNOLOGY—Published quarterly—January, April, July and October by DEStech Publications, Inc., 439 North Duke Street, Lancaster, PA 17602.

Indexed by Chemical Abstracts Service. Indexed/abstracted in Science Citation Index Expanded. Abstracted in Current Contents/Engineering, Computing & Technology. Listed in ISI Master Journal.

Subscriptions: Annual \$219 per year. Single copy price \$60. Foreign subscriptions add \$45 per year for postage.

(ISSN 1544-8053)

 DEStech Publications, Inc.

439 North Duke Street, Lancaster, PA 17602-4967, U.S.A.

©Copyright by DEStech Publications, Inc. 2016—All Rights Reserved

C O N T E N T S

Research

- Comparison on Copper (II) Desorption from Loess Soil with and without Biochars Derived from Flax and Rape Straws** 81
BAOWEI ZHAO, TINGTING SHANG, FENGFENG MA, LIJUAN YAN and LIPING HUANG
- Physiological-Biochemical Effects of Inoculation with a Resistant Strain on *L.perenne*, *Farundinace* and Cadmium Enrichment** 89
CHEN MING, XU HUI, YANG TAO, NIE JIN-XIA and YANG QUAN
- Adsorbent Preparation from Oily Scum for Oily Wastewater Treatment** 97
TANG CHAO, ZHAO LIN, GUAN JIAO-JIAO and XIE SHUI-XIANG
- Changes in Nitrogen Form in Paper Mill Wastewater Treated by Ozone Oxidation** 105
KE ZENG, TIANLI HAO, YIRAN LI, HONGCHAO ZHANG and HONGYOU WAN
- Pyrolysis and Carbocoal Characteristics for Biophysical Drying Sewage Sludge** 111
TAO ZHU, XIAOYANG LI, WENJING ZHANG, WENJUAN ZHAO, NI XIA and XIAOJIA WANG
- A Three-Dimensional Model Coupled Mechanical Consolidation and Contaminant Transport** 121
ZHIHONG ZHANG and YUANFANG FANG
- Synthesis and Mechanism of Flocculating-Decolorizing Agent PAD used for Polymer-Sulphonated Drilling Wastewater** 135
QINGYANG LI, YAN LUO, BING HOU and ZIXUAN HAN
- A Positional Method for Accidental Chemical Oxygen Demand to Determine a River's Pollution Source** 145
LIU YING, LI YONG, OUYANG FENG and CHEN YU
- Biosolids Application for Barley Production** 153
AKRUM H. TAMIMI, B. ATHAMNEH, C. P. GERBA and W. SULEIMAN
- Corrosion Behaviors of Carbon Steel in the Presence of Iron Oxidizing Bacteria Cultured in Reclaimed Water** 165
LI PENG, YAJUN ZHANG, PING XU and LIPING LU

Comparison on Copper (II) Desorption from Loess Soil with and without Biochars Derived from Flax and Rape Straws

BAOWEI ZHAO*, TINGTING SHANG, FENGFENG MA, LIJUAN YAN and LIPING HUANG
School of Environmental and Municipal Engineering, Lanzhou Jiaotong University, Lanzhou 730070, P. R. China

ABSTRACT: It has been reported that biochar is capable of adsorbing and immobilizing heavy metals in soils due to its prominent properties, such as the porous structure, large and charged surface, and functional groups on surface. The desorption of Cu (II) (Cu) from loess soil was studied and compared using batch washing method, with and without biochars derived from flax and rape straws. The effects of contact time, initial pH value of solution, temperature, initial concentration of Cu in soil, and co-existing Ca^{2+} on desorptions were investigated. The pseudo-second-order kinetic model could be used to describe the desorbing process well. The leaching ability (η) of Cu from solid phase increased in overly acidic solutions. Increasing temperature improved desorption of Cu from loess soil. When the initial concentration of Cu in soil increased, the η values of Cu decreased. Slight effect of Ca^{2+} on the η value of Cu was found. No significant immobilization of Cu by biochars was found because loess soil is much capable of holding Cu, possibly due to high content of carbonates. The results could provide references for immobilization remediation of loess soils contaminated with heavy metals using biochars as amendment.

INTRODUCTION

IN recent years, increasingly more soils are found to be contaminated with heavy metals due to waste emissions from industrial production, mining activities, waste application and wastewater irrigation, which has brought serious environmental problems [1–3]. For example, the arable land area subjected to heavy metal contamination is about 20 million ha, accounting for 20% of the total agricultural land area in China [4]. Heavy metals in soils are not only harmful to ecosystem and agricultural production but also serious threat to human being [5,6]. Loess, a special soil spreading over the large area of northwestern China and central Asia, being different from the acidic soils due to its high pH value, high calcareous content, loose structure, large porosity and water permeability, and low agglomerating force and organic carbon content, is also found to have suffered much heavy metal contamination due to the mining activity and sewage irrigation [7–9]. Therefore, it was quite necessary for the research on heavy metal pollution in loess, and on how to effectively control and manage pollution, which has

gained the attention of the government and scholars. At the present time, biochar is a promising amendment into soils, improving soil properties and remediating the contaminated soils [10,11].

Biochar is produced by so-called thermal decomposition of organic materials (wood, straw, leaves, manure and sludge etc.) under limited supply of oxygen (O_2) and at relatively low temperatures ($< 700^\circ\text{C}$). Biochar is carbonaceous with microporous structure, active surface charge and functional groups [12–14]. These properties have sparked strong interesting in mitigating climate change, improving soils, enhancing crop production and controlling contamination in soils [15]. Although the effect of biochar on heavy metal mobility and bioavailability in soils has been investigated, the results may be quite different when the biochars derived from various biomasses are used. Biochar addition led to immobilization of both Cd and Zn in soil in a column leaching experiment [16]. Consequently, Cd and Zn concentrations in pore water were reduced 300 and 45-fold, respectively [16]. Namgay *et al.* reported that the concentrations of extractable As and Zn in soil increased with biochar addition, whereas the concentration of extractable Pb decreased, that of Cu did not change, and that of Cd showed an inconsistent trend [17]. Heavy metal ions (Cu) were tested for their mobility in San Joaquin soil

*Author to whom correspondence should be addressed.
No. 88, West Anning Road, School of Environmental and Municipal Engineering,
Lanzhou Jiaotong University, Lanzhou 730070, P. R. China;
E-mail: zhbw2001@sina.com; Tel: +86-931-4938017; Fax: +86-931-4956017

amended with 5–20% (w/w) biochars, which resulted in negligible remediation in soluble Cu concentrations [18]. Cu contamination in soils is very common in the research area. Baiyin for example being 80 km from the research site is an important industrial base of copper metal. Because of the history of metal smelting and sewage irrigation, the average concentration of heavy metals in farmland is high, and the average concentration of Cu (II) is $90.12 \text{ mg} \cdot \text{kg}^{-1}$, which is much higher than that of background in soil [19]. In the previous studies, researchers have mainly focused on the acidic type of soils amended with biochar derived from the local biomasses. However, there are few studies on the effect of biochars on heavy metal (e. g. Cu) migration and conversion in loess soils, to our knowledge.

In this study, the flax (*Linum usitatissimum L.*) straw and rape (*Brassica campestris L.*) straw, which are widely planted and abandoned in loess areas, were pyrolyzed into biochars at 600°C . A comparison was conducted on the effects of biochars on copper (II) (Cu) desorption from loess soil using batch washing method. The factors influencing the leaching ability (η) of Cu such as contact time, initial pH value of solution, initial Cu concentration in soil, temperature, and co-existing cation (Ca^{2+}) were tested. The objective is to investigate preliminarily whether the immobilization of heavy metals occurs and the pattern of heavy metal desorption changes in loess soil-water system in the presence of biochar.

EXPERIMENTAL SECTION

Chemicals

Copper nitrate ($\text{Cu}(\text{NO}_3)_2 \cdot 3\text{H}_2\text{O}$), sodium nitrate ($\text{Na}(\text{NO}_3)$), calcium nitrate ($\text{Ca}(\text{NO}_3)_2$), sodium hydroxide (NaOH), and nitric acid (HNO_3) were purchased from Guangfu Chemical Research Institution, China. All reagents used were of analytical grade. The deionized water was used for all procedures.

Materials

The loess soil (light sierozem) sample (0–20 cm) was collected at a hill in Lanzhou Jiaotong University, China, where few low artemisia plants grew. The soil was air dried, removed weeds and gravels, and passed through a 40 mesh sieve. The pH value of the soil was determined as 8.11 [1:2.5 of soil mass (g) to volume of water (mL)] on a pH meter (PHS-3C, Electronics and Scientific Instrument Corporation, Shanghai, China).

The background content of Cu is $22.5 \text{ mg} \cdot \text{kg}^{-1}$ [20]. Its value of the point of zero charge (pH_{PZC}) is 2.82 [21] and the carbonate content is 3.9% [22]. The loess organic matter was determined as 0.53% using digestion method by potassium dichromate. The soil contains 18.65% grave, 28.50% silt and 52.85% clay. The loess was artificially prepared as Cu-contaminated soil with $\text{Cu}(\text{NO}_3)_2 \cdot 3\text{H}_2\text{O}$ solution. Desired amounts of $\text{Cu}(\text{NO}_3)_2$ was dissolved in deionized water and added to the contaminant-free soils. The slurry mixtures were evaporated under a hood, and the soils spiked with Cu were mixed, homogenized, passed through a 40 mesh sieve and aged for 20 days in order to achieve a relative stable distribution of species fraction of Cu. The final Cu concentrations in the loess soils were 400, 600, 700, 1000 and $1500 \text{ mg} \cdot \text{kg}^{-1}$, respectively.

The used biochars derived from flax and rape straw were prepared and characterized through the same processes as reported in our previous study [23]. In brief, the cleaned flax straw and rape straw chips were pyrolyzed in muffle oven at temperature 600°C for 4 h. The results from pre-experiment showed that the biochars obtained from 600°C and 4 h pyrolysis exhibited much adsorption capacities for Cu [23]. After cooling to room temperature, the resulting biochars were washed with $0.1 \text{ mol} \cdot \text{L}^{-1}$ HCl to remove excess ash [8], rinsed with deionized water, oven-dried for 12h at 80°C , and then sieved to 100 mesh. The biochars were termed as LS600 and BS600, respectively. The physical and chemical parameters of two biochars are listed in Table 1 [23], where the pH values and ash contents of the biochars were determined according to the national standards of China [24]. The point of zero charge (pH_{PZC}) was determined by potentiometric titration. Elemental analysis was completed on an elemental analyzer (Vario EL, Germany). The biochar contents of C, N, H and S were determined directly, while the O content was calculated by subtracting the contents of C, N, H, S and the ash contents from the total mass of the sample. The specific surface areas of the biochars were determined on a surface and porosimetry analyzer (Micromeritics ASAP 2020, USA). The surface areas were measured with N_2 adsorption at 77 K using BET adsorption isotherms.

Batch Washing Procedure

A series of 0.2 g of the contaminated soil, 0.2 g of the contaminated soil with 0.05 g of LS600, or 0.2 g of the contaminated soil with 0.05 g of BS600 were added to 20 mL of $0.01 \text{ mol} \cdot \text{L}^{-1}$ NaNO_3 solutions in 50-mL

Table 1. Physical and Chemical Parameters of Biochars.

Biochar	pH	pH _{pzc}	Ash, %	BET Surface Area, m ² g ⁻¹	Element Content, wt%				
					C	H	N	S	O
BS600	9.98	5.08	29.2	158	53.6	1.56	0.86	0.76	14.0
LS600	10.7	4.73	19.1	109	60.1	1.80	14.83	0.61	16.5

flasks with taps. 0.1 mL of 1 g L⁻¹ NaN₃ was added to inhibit microbial growth [25]. Duplicate samples were prepared. Then the samples were placed on a reciprocating shaker (THZ-82A, Jiangsu Quartz Glass Factory, China) at 150 rpm and 25°C. After shaking, each suspension was centrifuged at 3500 rpm for 30 min, and the supernatant was carefully decanted into a clear glass vial and filtered through a 0.45 μm membrane. The concentration of Cu in the filtrate was measured by atomic absorption spectrophotometry (AAS). The pH values of the solutions were adjusted to the target ones by 1 mol L⁻¹ HNO₃ and 1 mol L⁻¹ NaOH solutions [8]. The contact time, initial pH value of solution, dosage of contaminated soil, temperature, initial Cu concentration in soil and electrolyte concentration were kept as 24 h, 7.0, 0.2 g, 25°C, 600 mg Cu kg⁻¹ soil, and 0.01 mol L⁻¹ NaNO₃ respectively except that one of the factors was tested and changed.

Analytical Method

The concentration of Cu in aqueous phase was determined on an atomic absorbance spectrophotometer (Varian, Spectrum AA110/220, USA) at 324.8 nm. The flame type was air-acetylene one. Standard solutions were prepared and used to automatically draw the standard calibration. The leaching ability (η , %) of Cu can be calculated as follows in Equation (1) [26]:

$$\eta = \frac{C_e V_e}{Cm} \times 100\% \quad (1)$$

where C_e is the Cu concentration in elution (mg L⁻¹), V_e is the volume of elution (mL), C is the initial Cu concentration in soil (mg kg⁻¹), and m is the weight of soil (g). All of the values of η were the means of parallel determination.

RESULTS AND DISCUSSION

Effect of Contact Time

Figure 1 presents the plots of η values versus the

contact time varying from 0 to 24 h. It is indicated that the removal of Cu from solid phase increased as time increasing but the removal amount was not large and less than 3%. Within 1 h, sharp enhancements of η were observed in the three cases. The rates increased slow with time ranging from 1 to 6 h and then leveled off after 6 h [27]. For the single loess system, it was found that a strong immobilizing ability of loess for Cu occurred because only up to 2.8% of the total amount of Cu was desorbed into aqueous phase. In our previous study, it was found that the adsorptive capacity of loess soil for Cu could reach 16.13 g kg⁻¹ [28]. This is attributed to the high content of carbonates in loess soil [29,30]. It was demonstrated that binding of Cu(II) bonded to carbonates is dominant in the copper sorption by loess soils [29]. Zhao *et al.* pointed out that the direct precipitation and co-precipitation of Cu (II) with carbonates in loess soils were the main mechanisms on Cu (II) sorption onto loess soils, which resulted in a large fraction of carbonate-bound copper and a large holding capacity of loess for copper [22]. For example, the capacity of 5.5 g of Malan loess for copper (II) was still unsaturated even while the initial concentration of copper in aqueous solution was up to 957.0 mg L⁻¹. The sorption of copper decreased significantly after extrac-

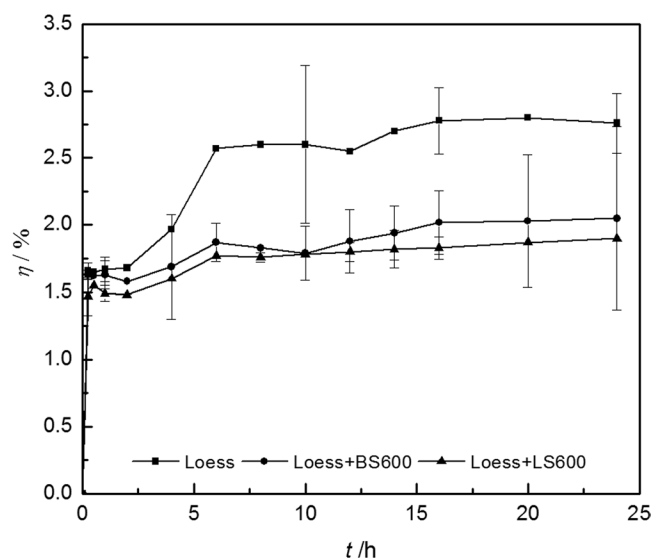


Figure 1. Effect of contact time on leaching ability of Cu.

tion of carbonates [22]. The possible precipitates of Cu on loess soils, e.g. $\text{Cu}_3(\text{OH})_2(\text{CO}_3)_2$ and $\text{Cu}_2(\text{OH})_2\text{CO}_3$, are extremely undissolved, e.g. $\text{Cu}_3(\text{OH})_2(\text{CO}_3)_2$ $pK_{sp} = 21.53$ and $\text{Cu}_2(\text{OH})_2\text{CO}_3$ $pK_{sp} = 21.55$ [22]. Thus, ultralow concentrations of Cu in aqueous phase would be found.

As for the systems of loess with BS600 and LS600, the whole patterns of desorption processes were similar to that of the single loess system. However, the Cu leaching abilities decreased by 1.9% and 1.8% at large. This indicated that the immobilization of Cu was somewhat enhanced in the presence of used biochars. No doubt, the additional immobilized amount of Cu was due to the adsorptive capacity of BS600 and LS600 [23] and the negligible difference of the Cu leaching abilities between in the presence of BS600 and LS600 might be due to their similar adsorptive capabilities for Cu [23], because their structure and surface properties are not significantly different (See Table 1) [23]. Frišták *et al.* reported Cu^{2+} ions adsorption onto the biochars derived from two woody biomasses at the same pyrolysis conditions [31]. It was found that the adsorption of Cu^{2+} onto the biochars followed pseudo-second-order kinetic model, Langmuir and Freundlich isotherm model and it was confirmed that the crucial roles in adsorption processes were mainly hydroxyl and carboxyl functional groups on the biochars' surface by chemical modification (esterification of carboxyl, and methylation of hydroxyl and phenolic functional groups of biochar) and FTIR analyses [31]. In our previous study [28], no significant difference occurred between the results of surface functional group determination for BS600 and LS600 using Boehm titration and the adsorption of Cu onto BS600 and LS600 followed pseudo-second-order kinetic model and Langmuir isotherm model. Therefore, although there was a large difference between the BET surface area of BS600 and LS600 (See Table 1), very similar values of the maximum adsorptive capacities of Cu (30.8 mg g^{-1} for BS600 and 26.7 mg g^{-1} for LS600) were found [28]. The values of standard Gibbs energy (ΔG°) for the adsorption of Cu onto loess, BS600 and LS600 were determined as

$-13.87 \text{ kJ mol}^{-1}$, $-8.78 \text{ kJ mol}^{-1}$ and $-9.16 \text{ kJ mol}^{-1}$ at 25°C [28], which indicate Cu ions are much easier to be adsorbed onto loess, rather than the used biochars. It can be deduced that it was impossible that most of Cu adsorbed on loess phase was transferred into biochar phase at the tested experimental conditions. Thus, BS600 and LS600 did not exhibit much immobilization results compared with the results mentioned above [16] although their adsorptive capacities for Cu (30.8 mg g^{-1} and 26.7 mg g^{-1}) were large [23] and the used amount of biochars was up to 25% of the total solid weight. The main reason might be the prominent holding ability of loess soils to Cu, which led to ultralow concentrations of Cu in aqueous phase and thus the immobilization by BS600 and LS600 was not significant.

The desorption mechanism for Cu could be explained using pseudo-first-order kinetic and pseudo-second-order kinetic [26]. The model's linear forms may be expressed as seen in Equations (2) and (3):

$$\log(q_e - q_t) = \log q_e - \frac{k_1}{2.303} t \quad (2)$$

$$\frac{t}{q_t} = \frac{1}{k_2 q_e^2} + \frac{1}{q_e} t \quad (3)$$

where q_e (mg g^{-1}) denotes the desorbed amount of metal per unit mass of solid at equilibrium; q_t (mg g^{-1}) is the desorbed amount of metal per unit mass of solid at time t (h); k_1 (h^{-1}) is the constant of pseudo-first-order kinetic model; k_2 ($\text{g mg}^{-1} \text{ h}^{-1}$) is the constant of pseudo-second-order kinetic one. According to data seen in Figure 1 and Equations (2) and (3), regression results were obtained and listed in Table 2. It is apparent the pseudo-second-order kinetic model was better used to describe the desorption processes than the pseudo-first-order kinetic one due to high values of correlation coefficients (R^2), 0.9960, 0.9960 and 0.9980 for single loess, loess with BS600 and loess with LS600 systems, together with the slight difference between the desorbed amount of Cu tested at equilibrium ($q_{e,ex}$, mg g^{-1}) and calculated from regression ($q_{e,cal}$, mg g^{-1}). The

Table 2. Regression Results for Kinetic Models.

System	$q_{e,ex}$, mg g^{-1}	Pseudo-First-Order			Pseudo-Second-Order		
		$q_{e,cal}$, mg g^{-1}	k_1 , h^{-1}	R^2	$q_{e,cal}$, mg g^{-1}	k_1 , h^{-1}	R^2
Loess	0.0168	0.0069	0.168	0.857	0.0170	66.35	0.996
Loess + BS600	0.0123	0.0035	0.147	0.860	0.0124	137.0	0.996
Loess + LS600	0.0114	0.0025	0.122	0.952	0.0114	198.5	0.998

values of $q_{e,ex}$ in the three cases were 0.017, 0.0124 and 0.0114 mg g⁻¹, which were very close to those values of $q_{e,cal}$ from the regression results for pseudo-second-order kinetic model.

Effect of pH Value

Figure 2 shows the relationship between the leaching ability (η) of Cu and the initial pH value of solution, with pH values ranging from 2 to 6. As pH values located from 6 to 4, no obvious change in the leaching ability occurred in each system. The variation trends of η in three cases were somewhat different when the pH values decreased, especially in overly acidic solutions. For the single loess system, when the pH values were less than 3.5, obvious increment in the values of η was observed. Firstly, the reason might be the dissolution of carbonate precipitates of Cu on loess soil and more Cu ions were released into aqueous phase [32]. Secondly, when the pH values were less than pH_{ZPC} 2.82, the dominant charge on loess soil was positive and the sorption of Cu ions was inhibited. Thirdly, more hydrogen ions in acidic solution would compete the adsorption of Cu ions onto soils. The Cu desorptive efficiencies from loess increased up to 4.95%, 4.24%, and 3.83% while the initial pH values of solutions were 2.0, 2.5 and 3.0, respectively.

As for the loess with biochar systems, when the pH values decreased from 4.0 to 2.5, slight increments in the leaching ability (η) of Cu were obtained. It is no doubt that dissolution of copper carbonates began in this pH value range. On paper, the Cu concentrations in aqueous phase would increase at a rate as that in the

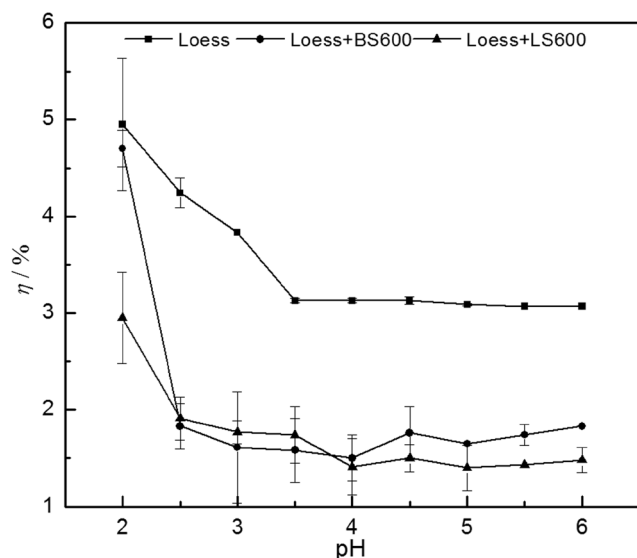


Figure 2. Effect of initial solution pH values on leaching ability of Cu.

single loess system. However, it was the adsorption of Cu onto biochars that slowed down the rate. It is indicated that the predominance of Cu²⁺ ions in solution is shown for the pH range less than 7.0 in water-biochar system [31]. Our previous study indicated that the mechanisms on adsorption of Cu on BS600 and LS600 were ion exchange and coordination of Cu with biochar surface [23]. The results reported by Uchimiya *et al.* suggested that higher pyrolysis temperature lead to the disappearance (e.g., aliphatic -CH₂ and -CH₃) and the formation (e.g., C=O) of certain surface functional groups of biochars [33]. Moreover, with higher carbonized fractions and loading of chars, Cu immobilization by cation exchange becomes increasingly outweighed by other controlling factors such as the coordination by n electrons (C=C) of carbon and precipitation [33]. On the one hand, as shown in Table 1, the values of pH_{ZPC} for BS600 and LS600 are 5.08 and 4.73, which demonstrates that positive charge occurred on the biochar surface and the adsorptive capacity of biochars for Cu decreased when the pH values were located in this range. On the other hand, the dissociation degree of oxygen-containing functional groups binding Cu such as -COOH and -OH [23] would decrease, which also led to reduction in adsorption ability of biochars [15,34]. The leaching ability (η) of Cu increased at a slow rate. After all, the positive charge and the acidic functional groups would be dominant when the solutions were much too acidic (pH < 2.5). Meanwhile, the competition of free protons and metal ions for unoccupied binding sites with lowered solution pH increased, which also caused the reduction of adsorption effectiveness for bivalent metal ions [31]. Then the leaching ability of Cu increased sharply, with 4.70% and 2.95% values in the presence of BS600 and LS600, respectively.

Effect of Temperature

Figure 3 illustrates the variation of η values with temperature in three systems. It is showed that the desorptive rate of Cu increased continuously in the single loess system when the tested temperature increased from 25–40°C. Although the adsorption of Cu onto loess soil is endothermic [28], increasing of temperature will result in the water solubilities of carbonates on loess soil [35]. It is possible the latter action was dominant in the desorption process in the single loess system. As the systems with biochars were concerned, the desorptive rates of Cu did not obviously change when temperatures were set up as 25°C, 30°C, 35°C and 40°C. These results indicated that parts of

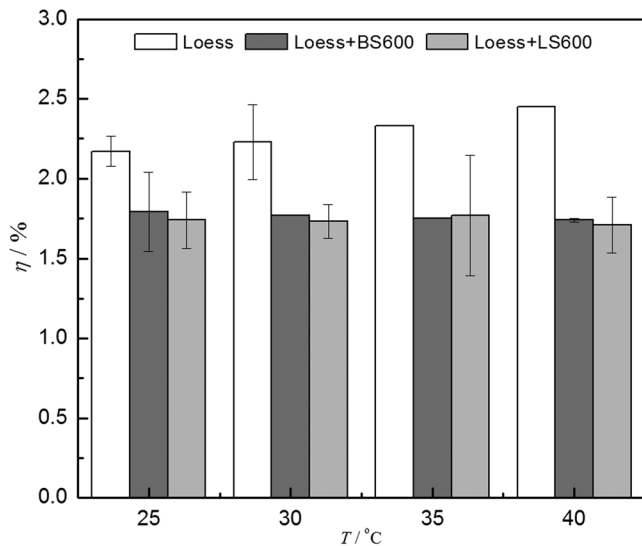


Figure 3. Effect of temperature on leaching ability of Cu.

dissolved Cu were transferred and immobilized by the biochars through adsorption. Because the adsorption of Cu onto BS600 and LS600 was endothermic, the adsorptive capacity of the two biochars would increase with temperature increasing [28] which inhibited the Cu concentrations in aqueous phase.

Effect of Initial Cu Concentration

The effect of initial Cu concentration in loess soil on the leaching ability of Cu is seen in Figure 4. For all cases, the leaching ability of Cu decreased with the initial Cu concentrations increasing in loess soil. As 400 mg kg⁻¹ of the contaminated soil was used, the leaching ability of Cu was 3.55%, 3.00% and 2.80% in the single loess, loess with BS600 and loess with LS600 systems, respectively. While the initial Cu concentration in loess increased up to 1500 mg kg⁻¹, those values reduced to 0.78%, 0.61% and 0.6%, being low as about 5 times as those with 400 mg kg⁻¹ of the contaminated soil. As mentioned above, the concentration of Cu in aqueous phase depended mainly upon the weak dissolution of carbonates on loess soil and loess had a high adsorptive capacity for Cu [36]. The concentrations of Cu in aqueous phase changed slightly in all the cases. Therefore, the leaching ability of Cu decreased much because the denominator in Equation (1) increased rapidly when the initial Cu in soil was added too much.

Effect of Co-existing Cation (Ca²⁺)

The effect of co-existing Ca²⁺ on the leaching ability of Cu is illustrated in Table 3. It is observed that the

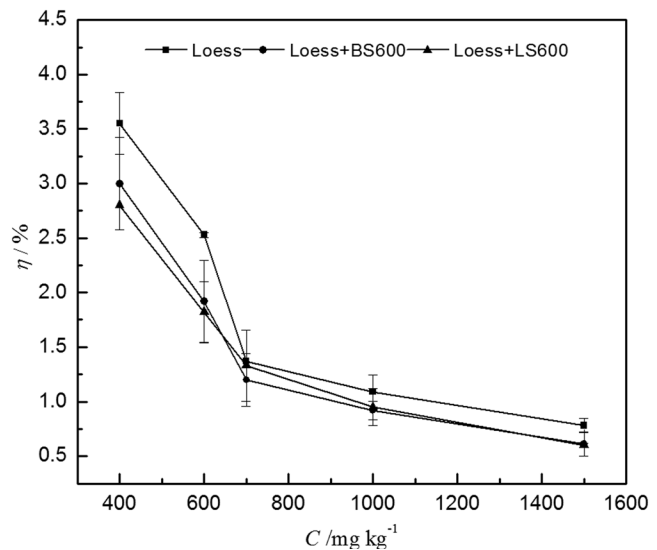


Figure 4. Effect of initial Cu concentration on leaching ability of Cu.

desorption of Cu was not significantly changed when the concentration of Ca²⁺ increased from 0–0.5 mmol L⁻¹ (0–20 mg L⁻¹). For the single loess system, slight decrease in the leaching ability of Cu was found. This could be attributed to the weak alkalinity of Ca(NO₃)₂ further reduced the solubility of carbonates. For the loess with biochar systems, a U shape of variation of the η values was observed. On the one hand, the alkaline Ca(NO₃)₂ could reduce the solubility of carbonates, which led to the reduction in Cu concentrations in aqueous phase, as shown when Ca²⁺ concentrations ranged from 0–0.03 mol L⁻¹. On the other hand, it was possible that much Ca²⁺ would result in the desorption of Cu having been adsorbed on biochar due to the competitive adsorption, conversely, which resulted in increase of Cu in aqueous phase [37]. When the heavy metal ions enter the soil environment, the sorption mechanisms may include four types, i.e. (1) electrostatic action adsorption; (2) ion exchange; (3) complexing with organic and inorganic ligands; (4) chemical precipitation. If the sorption of a metal onto soil is based on one of the two formers, the adsorbed metal ions can usually be replaced in the neutral salt or buffer solution [38]. As discussed above, the main sorption

Table 2. Effect of Ca²⁺ on leaching ability of Cu.

System	η, %						
	Ca ²⁺ , mmol L ⁻¹	0	0.1	0.2	0.3	0.4	0.5
Loess		2.62	2.74	2.45	2.13	2.04	2.02
Loess + BS600		1.77	1.64	1.40	1.28	1.41	1.57
Loess + LS600		1.50	1.19	1.07	1.04	1.50	1.44

mechanism of Cu onto loess is chemical precipitation. The cations of electrolytes are difficult in replacement of Cu in carbonates.

CONCLUSIONS

The desorptions of Cu in the loess and loess with biochars BS600 and LS600 could reach equilibrium at 24 h. The data of desorptions were well fitted by pseudo-second-order kinetic model. The leaching ability (η) of Cu from solid phase improved when the initial pH values of solution were less than 3.5 in loess system and 4.0 in loess with biochar systems. The values of η in the single loess system increased and those in the loess with biochar systems did not change with temperature increasing. When the initial concentration of Cu in soil increased, the η values of Cu decreased. No obvious effect of Ca^{2+} on the η value was found. The desorption patterns seemed similar among three cases but the η values of Cu in the presence of biochars were less than those in the absence of biochars. The used biochars, BS600 and LS600, did not exhibit much immobilization of Cu, possibly due to the strong holding capability of loess soil to Cu.

ACKNOWLEDGEMENTS

This work was financially supported by the National Natural Science Foundation of China (No. 21167007, 21467013), the Specialized Research Fund for the Doctoral Program of Higher Education of China (No.20136204110003), and the Youth Science Foundation of Lanzhou Jiaotong University (No.2013015).

REFERENCES

- Sfakianakis, D. G., Renieri, E., Kentouri, M., and Tsatsakis, A. M., "Effect of heavy metals on fish larvae deformities: A review", *Environ. Res.* Vol. 137, 2015, pp. 246–255. <http://dx.doi.org/10.1016/j.envres.2014.12.014>
- Song, Q., and Li, J., "A review on human health consequences of metals exposure to e-waste in China", *Environ. Pollut.* Vol. 196, 2015, pp. 450–461. <http://dx.doi.org/10.1016/j.envpol.2014.11.004>
- Peng, C., Zhao, X., Han, Y., Shi, W., Liu, S., and Liu, G., "Toxic effects of chronic sub-lethal Cu^{2+} , Pb^{2+} and Cd^{2+} on antioxidant enzyme activities in various tissues of the Blood Cockle, *Anadara granosa*", *J. Residuals Sci. Technol.* Vol. 12, No. 3, 2015, pp. 125–131. <http://dx.doi.org/10.12783/issn.1544-8053/12/3/2>
- Xi, J. F., Yu, X. Z., Zhou, L. X., Li, D. C., and Zhang, G. L., "Comparison of soil heavy metal pollution in suburb fields of different regions", *Soils*, Vol. 43, No. 5, 2011, pp. 769–775.
- Zhang, X., Wang, H., He, L., Lu, K., Sarmah, A., Li, J., Bolan, N. S., Pei, J., and Huang, H., "Using biochar for remediation of soils contaminated with heavy metals and organic pollutants", *Environ. Sci. Pollut. Res.* Vol. 20, No. 12, 2013, pp. 8472–8483. <http://dx.doi.org/10.1007/s11356-013-1659-0>
- Yu, C., Zhang, J., Wu, L., Liu, Y., and Ge, G., "Effects of heavy metal and nutrients on benthic microbial communities in freshwater sediment of Poyang Lake (China)", *J. Residuals Sci. Technol.* Vol. 12, No. 2, 2015, pp. 105–111. <http://dx.doi.org/10.12783/issn.1544-8053/12/2/11>
- Wang, Y., Tang, X., Chen, Y., Zhan, L., Li, Z., and Tang, Q., "Adsorption behavior and mechanism of Cd(II) on loess soil from China", *J. Hazard. Mater.* Vol. 172, No. 1, 2009, pp. 30–37. <http://dx.doi.org/10.1016/j.jhazmat.2009.06.121>
- Pellera, F. M., Giannis, A., Kalderis, D., Anastasiadou, K., Stagmann, R., Wang, J. Y., and Gidararakos, E., "Adsorption of Cu(II) ions from aqueous solutions on biochars prepared from agricultural by-products", *J. Environ. Manage.* Vol. 96, No. 1, 2012, pp. 35–42. <http://dx.doi.org/10.1016/j.jenvman.2011.10.010>
- Hu, Y., Wang, D., Wei, L., Zhang, X., and Song, B., "Bioaccumulation of heavy metals in plant leaves from Ya'an city of the Loess Plateau, China", *Ecotoxic. Environ. Safety*, Vol. 110, 2014, pp. 82–88. <http://dx.doi.org/10.1016/j.ecoenv.2014.08.021>
- Lehmann, J., "A handful of carbon", *Nature*, Vol. 447, No. 7141, 2007, pp. 143–144. <http://dx.doi.org/10.1038/447143a>
- Janus, A., Pelfrène, A., Heymans, S., Deboffe, C., Douay, F., and Waterlot, C., "Elaboration, characteristics and advantages of biochars for the management of contaminated soils with a specific overview on Miscanthus biochars", *J. Environ. Manage.* Vol. 162, 2015, pp. 275–289. <http://dx.doi.org/10.1016/j.jenvman.2015.07.056>
- Lehmann, J. and Joseph, S. 2009. *Biochar for environmental management: science and technology*. London, Earthscan.
- Fraser, B., "High-tech charcoal fights climate change", *Environ. Sci. Technol.* Vol. 44, No. 2, 2010, pp. 548–549. <http://dx.doi.org/10.1021/es903696x>
- Ladygina, N. and Rinceau, F. 2013. *Biochar and soil biota*. New York, CRC Press. <http://dx.doi.org/10.1201/b14585>
- Jiang, J., Xu, R. K., Jiang, T. Y., and Li, Z., "Immobilization of Cu(II), Pb(II) and Cd(II) by the addition of rice straw derived biochar to a simulated polluted Ultisol", *J. Hazard. Mater.* Vol. 229–230, 2012, pp. 145–150. <http://dx.doi.org/10.1016/j.jhazmat.2012.05.086>
- Beesley, L. and Marmiroli, M., "The immobilization and retention of soluble arsenic, cadmium and zinc by biochar", *Environ. Pollut.* Vol. 159, No. 2, 2011, pp. 474–480. <http://dx.doi.org/10.1016/j.envpol.2010.10.016>
- Namgay, T., Singh, B., and Singh, B. P., "Influence of biochar application to soil on the availability of As, Cd, Cu, Pb, and Zn to maize (*Zea mays L.*)", *Aust. J. Soil Res.* Vol. 48, No. 7, 2010, pp. 638–647. <http://dx.doi.org/10.1071/SR10049>
- Uchimiya, M., Klasson, K. T., Wartelle, L. H., and Lima, I. M., "Influence of soil properties on heavy metal sequestration by biochar amendment: 1. Copper sorption isotherms and the release of cations", *Chemosphere*, Vol. 82, No. 10, 2011, pp. 1431–1437. <http://dx.doi.org/10.1016/j.chemosphere.2010.11.050>
- Zhao, B., and Wang, G., 2010, "Preliminary investigation and assessment of farmland soils contaminated by heavy metal around Baiyin City", *Environ. Sci. Technol.* 2010, Vol. 33, No. 11, pp. 79–81, 105.
- Tian, J., Li, Y., and Chen, D., "Study on Rules of differentiation of background elements in loess in China", *Acta Scientiae Circumstantiae*, Vol. 11, No. 3, 1991, pp. 253–262.
- Liu, J. 2014. *Competitive adsorption and desorption of Pb(II), Cu(II), and Cd(II) onto loess soils*. Ph.D. thesis, Hangzhou, Zhejiang University.
- Zhao, R., Ni, J., Zhang, L., Deng, B., and Sun, W., "Effects of carbonates in loess on copper sorption and speciation", *Environ. Chem.* Vol. 21, No. 4, 2002, 349–355.
- Shi, X. 2014. *Preparation and characterization of biochars derived from oil crops and its adsorptive properties for Cr(VI) and Cu(II)*. Ms. D. thesis, Lanzhou, Lanzhou Jiaotong University.
- Liu, F. and Liu, X. 2007. *Monitoring and analysis technology for soils and waste solids*. Beijing, Chemical Industry Press.
- Tang, J., Lv, H., Gong, Y., and Huang, Y., "Preparation and characterization of a novel graphene/biochar composite for aqueous phenanthrene and mercury removal", *Bioresour. Technol.* Vol. 196, 2015, pp. 355–363. <http://dx.doi.org/10.1016/j.biortech.2015.07.047>

26. Liang, Y., Cao X. D., and Zhao, L., "Biochar- and phosphate-induced immobilization of heavy metals in contaminated soil and water: implication on simultaneous remediation of contaminated soil and groundwater", *Environ. Sci. Pollut. Res.* Vol. 21, No. 6, 2014, pp. 4665–4674. <http://dx.doi.org/10.1007/s11356-013-2423-1>
27. Hossain, M. A., Ngo, H. H., Guo, W. S., and Setiadi, T., "Adsorption and desorption of copper (II) ions onto garden grass", *Bioresource Technol.* Vol. 121, 2012, pp. 386–395. <http://dx.doi.org/10.1016/j.biortech.2012.06.119>
28. Shang, T., Zhao, B., Ma, F., Yan, Li., and Huang, L., "Adsorption of Cu(II) by biochar derived from *Linum usitatissimum* L. straw with loess", *J. Lanzhou Jiaotong Univ.* Vol. 34, No. 3, 2015, pp. 145–152.
29. Zhang, L., Sun, W., Zhao, R., Deng, B., and Ni, J., "Effects of adding copper of different chemical forms on its sorption and speciation by loess", *Environ. Chem.* Vol. 21, No. 3, 2002, pp. 225–229.
30. Wang, M., Wu, H., Liao, Y., Fang, F., Gao, Y., and Xu, Y., "Pilot study of partial extraction geochemistry for base metal exploration in a thick loess-covered region", *J. Geochem. Explorat.* Vol. 148, 2015, pp. 231–240. <http://dx.doi.org/10.1016/j.gexplo.2014.10.003>
31. Frišták, V., Pipiška, M., Lesný J., Soja, G., Friesl-Hanl, W., and Packová A., "Utilization of biochar sorbents for Cd²⁺, Zn²⁺ and Cu²⁺ ions separation from aqueous solutions: Comparative study", *Environ. Monit. Assess.* Vol. 187, 2015, pp. 4093–4108. <http://dx.doi.org/10.1007/s10661-014-4093-y>
32. Martinez, C. E., and Motto, H. L., "Solubility of lead, zinc and copper added to mineral soils", *Environ. Pollut.* Vol. 107, No. 1, 2000, pp. 153–158. [http://dx.doi.org/10.1016/S0269-7491\(99\)00111-6](http://dx.doi.org/10.1016/S0269-7491(99)00111-6)
33. Uchimiya, M., Lima, I M., and Klasson, K. T., 2010, "Immobilization of heavy metal ions (Cu(II), Cd(II), Ni(II), and Pb(II)) by broiler litter-derived biochars in water and soil", *J. Agri. Food Chem.* 2010, Vol. 58, No. 9, pp. 5538–5544. <http://dx.doi.org/10.1021/jf9044217>
34. Jiang, T. Y., Jiang, J., and Xu, R. K., "Effect of biochar from rice straw on adsorption of Cd(II) by variable charge soils", *J. Agro-Environ. Sci.* Vol. 31, No. 6, 2012, pp. 1111–1117.
35. Xu, R. K., "Effect of pH, temperature and ratios of water to soil on distribution of Al³⁺ species in acid soil solution", *Tropical Subtropical Soil Sci.* Vol. 7, No. 1, 1998, pp. 26–30.
36. Li, Z. Z. 2009. *Mechanism of sorption, desorption, diffusion and remediation of heavy metal in soils.* Ph.D. thesis, Hangzhou, Zhejiang University.
37. Chen, T., Zhou, Z., Han, R., Meng, R., Wang, H., and Lu, W., "Adsorption of cadmium by biochar derived from municipal sewage sludge: Impact factors and adsorption mechanism", *Chemosphere*, Vol. 134, No. 9, 2015, pp. 286–293. <http://dx.doi.org/10.1016/j.chemosphere.2015.04.052>
38. Zhang, F. 2011. *Experimental study on Tl⁺ adsorption and desorption in red soil and loess.* Ph. D. thesis, Guangzhou, Guangzhou University.

Physiological-Biochemical Effects of Inoculation with a Resistant Strain on *L.perenne*, *F.arundinace* and Cadmium Enrichment

CHEN MING*, XU HUI, YANG TAO, NIE JIN-XIA and YANG QUAN

Jiangxi Key Laboratory of Mining and Metallurgy Environmental Pollution Control, Jiangxi University of Science and Technology, Ganzhou, 341000, China

ABSTRACT: Pot experiments were conducted to investigate the effects of incubation of a resistant microbe on Cd phytoremediation by *L.perenne* and *F.arundinace*. Results show that after inoculation of the resistant microbe, the plant heights of *L.perenne* and *F.arundinace* are extended significantly with the addition of 20 and 50 mg/kg Cd, respectively. The inoculation of resistant strain into *L.perenne* and *F.arundinace* enhances total biomass of 1.3–4.5% and 4.2–6.3%, respectively, and also promotes the Cd enrichment. The inoculation also strengthens the photosynthesis, and first increases, and then decreases, the chlorophyll contents. Inoculation of the resistant microbe into *L.perenne* and *F.arundinace* enhances the activities of SOD, POD and CAT under Cd stress, and reduces the MDA contents in leaves.

INTRODUCTION

HEAVY metal pollution has gradually attracted wide attention since the outbreak of Cd-caused Itaiitai disease in 1950s in Japan. Pb and Cd with high mobility and toxicity are the main heavy metals causing severe concern. According to statistics, the annual global discharge of Cd is about 1.0×10^6 t, which is still rising with industrial development [1–2].

The 1972 report on food contamination and toxicity by the Joint FAO/WHO Expert Committee lists Cd as the third food contaminant only after aflatoxins and arsenic. Moreover, Cd is ranked first among the 12 harmful substances with global significance by United Nations Environment Program (UNEP) in 1984. Cd is listed sixth among all health-threatening toxic substances by U.S. Agency for Toxic Substances and Disease Registry (ATSDR).

With modernization, however, the industry, agriculture and other activities have destroyed the natural environment and caused large-area Cd pollution to groundwater, farming land, and rivers/lakes. Through circulation on food chains, Cd will finally endanger the ecoenvironment and human health. Thus, how to remediate heavy-metal-polluted soils has become a hot topic in recent years. The common methods for processing of heavy metal pollution include physical and chemical

methods, such as soil replacement and electrochemical method [3]. Because of high costs, these methods are unpractical and may potentially cause secondary pollution. The recently-developed phytoremediation has gained much attention owing to low investment and no secondary pollution. However, the heavy metal adsorption efficiency by phytoremediation is very low, because of short growth cycle, small plant height, and low adsorption capacity. Thus, how to improve the Cd absorption by plants and to increase the phytoremediation rate become two hotspots. In recent years, microbial combined remediation that promotes plant growth is used to improve the efficiency of phytoremediation. Microbes are good for plants as they can enhance the ability of nutrient absorption by plants and alter the rhizosphere morphology [4–5]. As reported, when microbes were inoculated into ryegrass and bahia grass for absorption of ^{98}Sr , the inoculation modestly enhanced the ^{98}Sr absorption [6]. When ryegrass was planted on a regular bioreactor, modest efficiency of toluene purification was achieved by using rhizospheric enhanced microorganism [7]. Microbes modestly enhanced the ability of tall fescue in remediation of oil-contaminated soils [8]. A plant-microbe joint remediation system has two functions: bio-fixation and bio-removal of heavy metals from soils. Through mycorrhiza and endophytic fungi, the microbes can form clusters with the rhizosphere, and by improving plant resistance and optimizing rhizosphere environment, they accelerate rhizosphere development and enhance the absorption and

*Author to whom correspondence should be addressed. Email: 261984014@qq.com

upward transport of heavy metals [9]. When Guizhou Rapeseed was used into remediation of Cd-polluted soils, after addition of different Cd concentrations, the effects of cadmium-resistant fungi on the growth and Cd remediation ability of Guizhou Rapeseed were studied. Results show that the inoculation significantly promoted the biomass, Cd enrichment *in vivo*, and migration of Cd from roots to aground [10].

In the present study, a Cd-resistant bacterium was inoculated into *L.perenne* and *F.arundinace* for remediation of Cd pollution. We studied the effects of such inoculation on the plant growth and Cd absorption, and the effects of inoculation on the physiological- biochemical properties of plants.

MATERIALS AND METHODS

Test Plants

L.perenne and *F.arundinace* are vital and strong perennial terrestrial herbs which are subjected to few diseases and insect pests [11]. The seeds of these two herbs were provided by Hebei binary seed industry co., LTD.

Test Microbe

The Cd-resistant test strain was isolated from the polluted soils near a tungsten ore in south Jiangxi Province. The culture medium—potato dextrose agar—was prepared as follows: potato (200 g), dextrose (20 g), agarose (15–20 g), distilled water (1000 ml), and natural pH. The resistance of the strain was tested: different concentrations of Cd were added into the culture medium, and whether the strain could propagate and grow under the maximum 300 mg/L Cd was tested. This strain was proved very Cd-resistant and after inoculation into Cd-containing soils, it could normally propagate in rhizospheric soils.

Test Soil

The test soil was typical red earth in south Jiangxi. Its physiochemical properties are listed in Table 1.

Preparation of Cd-Polluted Soil

The test soil was clean and un-polluted. Four concentrations were set: 0, 20, 50, and 100 mg/kg Cd. Water solutions of $\text{Cd}(\text{NO}_3)_2 \cdot 4\text{H}_2\text{O}$ were spilled by a watering, and add the same amount of water dilution into pots, to the different concentrations of Cd. Plastic pots were used. To each pot, 7 kg of soil (soil: sand ratio = 3:1) was added. The soil passed through a 5-mm screen. Each treatment (inoculation or no inoculation) was conducted in triplicate. The soils added with Cd were placed in dark for ageing for 30 d, while 60% field moisture capacity was maintained.

Methods

Seeds of *L.perenne* and *F.arundinace* were soaked in rooting water for 2 h and then washed with clean water. To each pot, 50 seeds were uniformly scattered for germination. After 2 weeks, 20 plants of both herbs with uniform and similar growing condition were selected for planting. Pot experiments were conducted in a greenhouse. After that, the Cd-resistant strain was inoculated into the liquid medium for reactivation, and oscillated at constant temperature for 24 h, which was marked as the first generation. 5% was taken from the first-generation strain solution and inoculated into the liquid culture medium which was oscillated at constant temperature for 24 h and marked as the second generation. The second-generation solution was used in the pot experiments. During the experiments, normal watering and daily maintenance management were performed.

The plants were all harvested at day 45. The plant height, fresh weight, and dry weight (aboveground part and underground part) were measured, and according to the previous data get the tolerance index. Ti is an index explains plant tolerance.

The plants were washed with deionized water, dried naturally, crushed, and gradually decomposed before measurement of Cd *in vivo*. Physiological-biochemical indicators including chlorophyll, catalase (CAT), superoxide dismutase (SOD), peroxidase (POD), and malonyldialdehyde (MDA) were also detected. The

Table 1. Basic Physical and Chemical Properties of Test Soil.

PH	Organic Matter (g/kg)	Total N (g/kg)	Total P (g/kg)	Total K (g/kg)	Cation Exchange Capacity (mol/kg)	Cd Content (mg/kg)
5.5	8.57	0.86	0.56	10.21	15	0.03

methods are as follows: chlorophyll content, spectrophotometry; POD, guaiacol method; SOD, nitroblu-tetrazolium (NBT) reductive method; CAT, ultraviolet absorption method; MDA, thiobarbituric acid (TBA) method [12–15].

RESULTS AND ANALYSIS

Effects of Inoculation with Resistant Strain on Plant Heights for *L.perenne* and *F.arundinace*

CK is not inoculated microorganisms, inoculation is inoculated microorganism. Seen in Figure 1, this resistant strain has unique effect under a specific Cd concentration. Whether inoculation with the strain or not, the plant heights first increase and then decrease with the rise of Cd concentration. These results indicate that low Cd concentrations can promote the plant growth, but too high concentrations will inhibit plant growth, showing the stress effect. After the incubation, the microbe effect in the blanks is not significant and the plant height does not increase largely. After addition of 20 and 50 mg/kg Cd, the plant heights of both herbs increase significantly; but the plants are stressed severely at too high concentration (100 mg/kg), and the increase of plant height is not significant.

Effects of Inoculation of a Resistant Strain on Biomass, Tolerance Index (TI), and Root Length for *L.perenne* and *F.arundinace*

CK is not inoculated microorganisms, inoculation is inoculated microorganism. the previous sentence has odd punctuation and does not make sense The results of biomass and TI are listed in Table 2. Without inoculation of the tolerant strain, the growth of both *L.perenne* and *F.arundinace* first increases and then de-

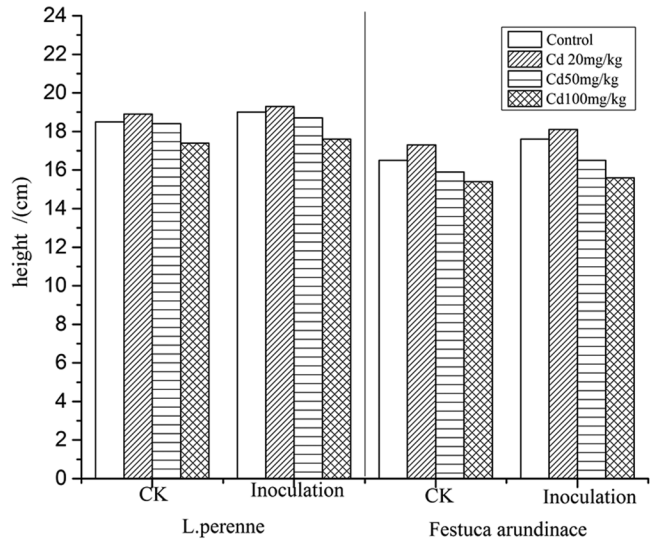


Figure 1. Effects of inoculation of a resistant strain on plant heights of *L.perenne* and *F.arundinace*.

creases, and the biomass and root height are optimized at concentration of 20 mg/kg Cd. With the increase of soil Cd level, both biomass and root length are reduced significantly.

After inoculation of the tolerant strain, the above-ground biomasses of *L.perenne* and *F.arundinace* are increased by 1.3–4.5% and 4.2–6.3%, respectively. The root lengths at the blank part are increased significantly, but not at other parts. After the inoculation, the TI of *L.perenne* is basically increasing all the time, while that of *F.arundinace* decreases.

Effects of Inoculation of a Resistant Strain on Chlorophyll Contents for *L.perenne* and *F.arundinace*

Plant growth is closely related with photosynthe-

Table 2. Effects of Inoculation of a Resistant Strain on Biomass, Ti, and Root Length for *L.perenne* and *F.arundinace*.

Plant	Cd (mg/kg)	Biomass/g		Ti		Root Length/cm	
		CK	Inoculation	CK	Inoculation	CK	Inoculation
<i>L.perenne</i>	0	7.68	8.03	1.00	1.00	3.59	3.93
	20	7.82	8.07	1.01	1.04	3.96	4.17
	50	7.58	7.68	0.98	0.96	3.57	3.70
	100	7.07	7.24	0.90	0.90	3.29	3.30
<i>F.arundinace</i>	0	5.68	6.26	1.00	1.00	3.30	3.90
	20	5.90	6.39	1.03	0.97	4.16	4.50
	50	5.58	5.98	0.98	0.95	3.19	3.53
	100	5.07	5.39	0.89	0.86	2.98	3.11

sis, or the synthesis of photoassimilates, and thus, the chlorophyll content reflects the growing status. The reduction of chlorophyll content will interfere with light absorption by plants. Under Cd stress, the chlorophyll contents in *L.perenne* and *F.arundinace* both first increase and then decrease, and are maximized after addition of 20 mg/kg Cd, and the increasing amplitudes are optimized at 20 and 50 mg/kg, respectively. The growth is insignificant at the level of 100 mg/kg Cd.

Effects of Inoculation of a Resistant Strain on CAT, POD, SOD Activities, and MDA Contents in *L.perenne* and *F.arundinace*

Under environmental stress such as high temperature, high salinity or heavy metal contamination, plants will produce abundant O-containing free radicals, and rapidly induce the generation of enzymes (CAT,SOD,POD) against these O-containing radicals. Thus, plant enzymes reflect the contaminated state to some extent [16–17]. The enzyme activities and MDA contents for both herbs are listed in Figure 4. Clearly, with the increase of soil Cd concentrations, the SOD, POD and CAT activities in *L.perenne* and *F.arundinace* are all increased significantly. Without addition of Cd, the inoculation of the tolerant strain does not significantly affect the enzyme activities of either herb. With addition of 20, 50 and 100 mg/kg Cd, the SOD, POD and CAT activities in *L.perenne* after inoculation are enhanced by 0.6–14%, 6.1–20.0%, and 0.9–10.1%, respectively; while those of *F.arundinace* are improved by 2–7.4%, 1.9–19.1%, 2.1–11.83%, respectively. These improvements in the two herbs are especially

evident after the addition of 20 and 50 mg/kg Cd, respectively.

MDA is a main product from membrane lipid peroxidation which is induced by the accumulation of reactive oxygen species (ROS) and closely related with the damages to plants under environmental stress [18–19]. The generation of MDA is a major index reflecting the damages of environmental stress to biomembranes, and indicates the stress undertaken by plants. The MDA content in leaf significantly increases with the gradual rise of Cd concentration in soils, indicating that the stress is gradually enhanced with the rise of heavy metal concentration. With the absence of Cd in soils, the MDA content after inoculation of the tolerant strain does not change significantly. With the presence of 20, 50 and 100 mg/kg Cd in soils, the inoculation of the tolerant strain significantly reduces the MDA contents in leaves of *F.arundinace*, while MDA contents in *L.perenne* decline by 2.95–43.3%. The decreasing amplitude is most significant with addition of 50 mg/kg Cd, as the MDA contents in *F.arundinace* drop by 6.7–13.0%, but without obvious regularity.

Effects of Inoculation with Resistant Strain on Cd Enrichment in Plants

Enrichment of heavy metals by plants is the most direct and effective index reflecting the heavy metal repair in soils. Generally, the absorption of heavy metals is promoted by the increase of heavy metal concentration [20]. As shown in Figure 5 and Figure 6, (a), (b) are the aboveground and underground parts after inoculation of the tolerant strain; (c), (d) are the

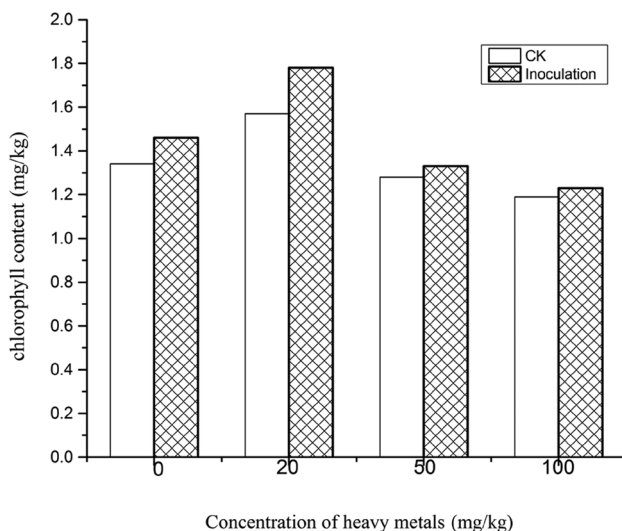


Figure 2. Chlorophyll contents in *L.perenne*.

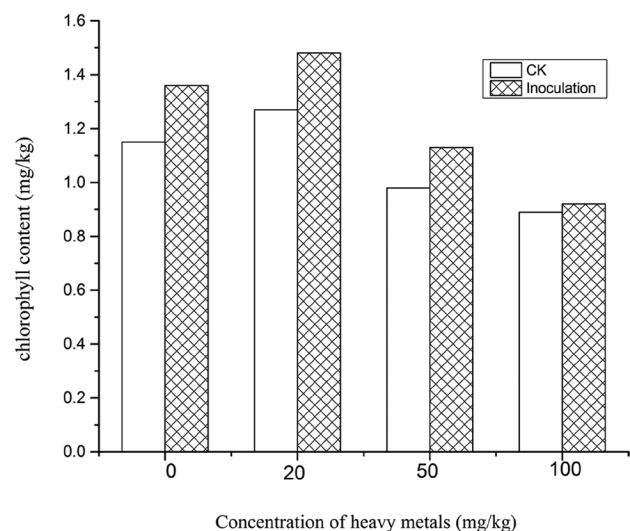


Figure 3. Chlorophyll contents in *F.arundinace*.

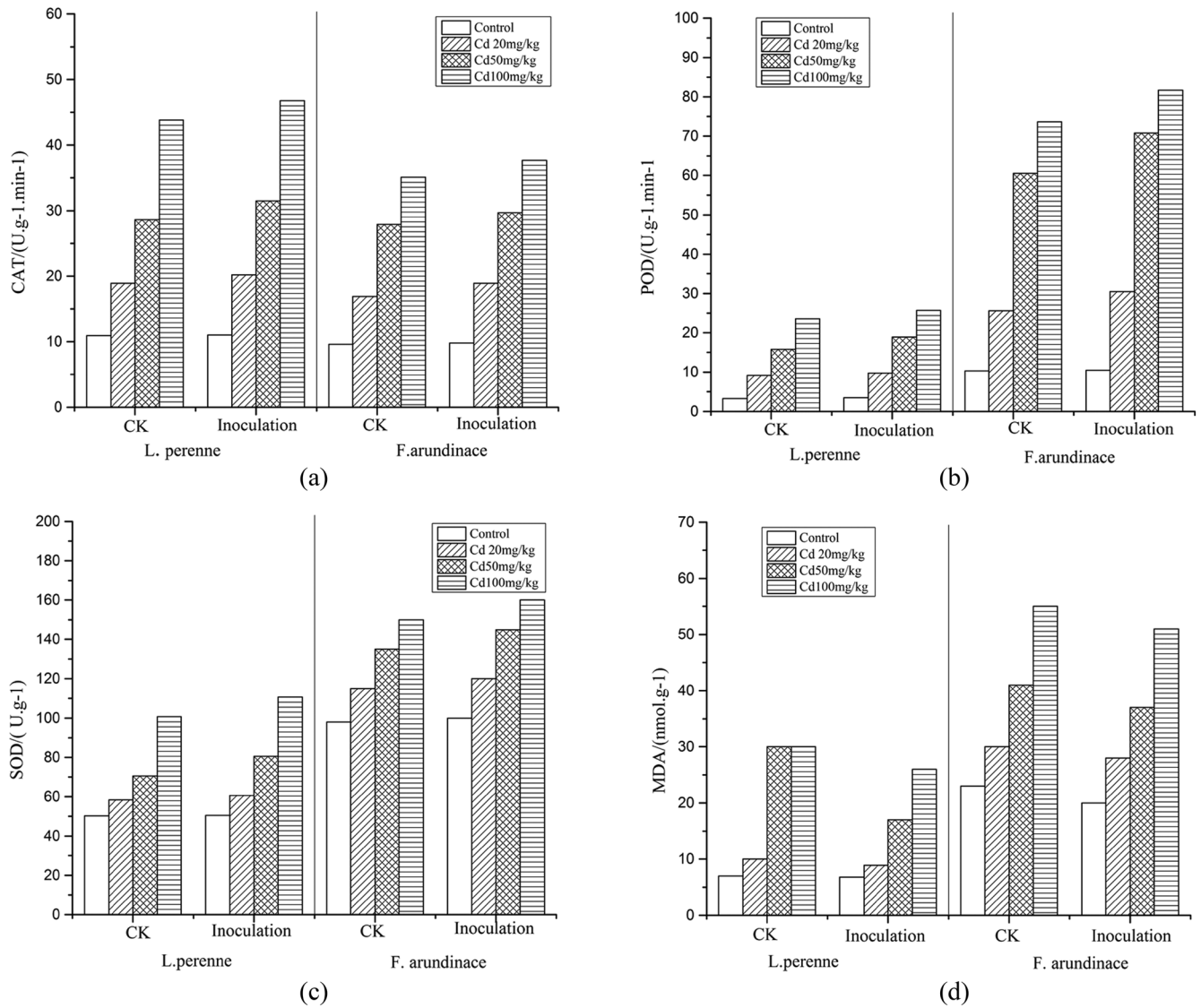


Figure 4. Effects of inoculation with resistant strain on (a) CAT, (b) POD, (c) SOD activities, and (d) MDA content in leaves of *L.perenne* and *F.arundinace*.

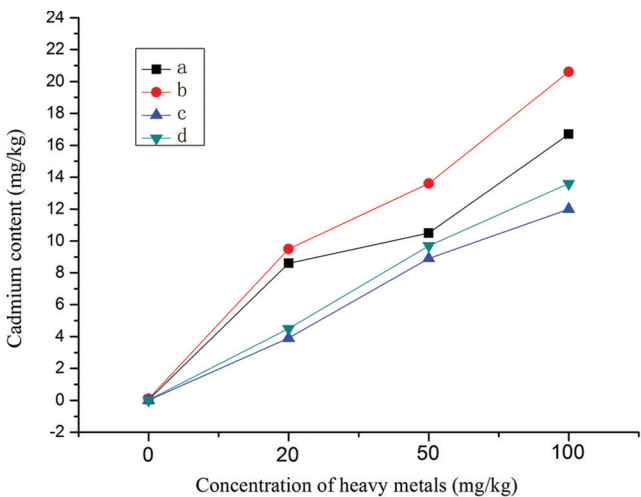


Figure 5. Characteristics of inoculation with resistant strain on Cd adsorption in the ground portion of *L.perenne*.

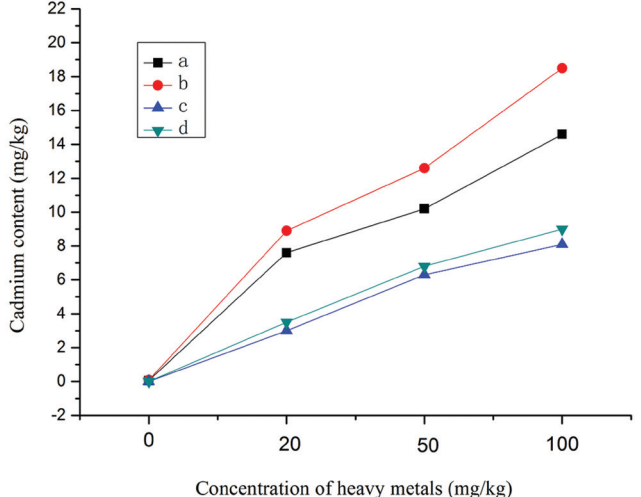


Figure 6. Characteristics of inoculation with resistant strain on absorption of Cd in the ground portion of *F.arundinace*.

Table 3. TF and BF of Cd Absorption for *L.perenne* and *F.arundinace*.

Plant	Cd (mg/kg)	TF		BF	
		CK	Inoculation	CK	Inoculation
<i>L.perenne</i>	0	5	5	0.16	0.33
	20	2.2	2.1	0.43	0.48
	50	1.17	1.4	0.21	0.27
	100	1.39	1.5	0.17	0.21
<i>F.arundinace</i>	0	6	9	0.20	0.30
	20	2.53	2.54	0.38	0.45
	50	1.62	1.85	0.20	0.25
	100	1.8	2	0.15	0.19

aboveground and underground parts without such inoculation), the addition of the resistant strain positively promotes the Cd enrichment in plants. With the addition of 0 and 20 mg/kg Cd, the adsorption quantities by the aboveground and underground parts of *L.perenne* do not increase significantly. With increase of Cd concentration, the enrichment by the aboveground part is very obvious, but not significantly different versus the underground part, after incubation of the strain. Without incubation of the strain, the adsorption quantities by *F.arundinace* are lower versus *L.perenne*. At the addition of 100 mg/kg Cd, the adsorption quantity by the aboveground part in *F.arundinace* is most significantly higher with incubation versus without incubation of the strain, while underground parts do not perform very differently.

Translocation factor (TF) and bioconcentration factor (BF) are major indicators reflecting the enrichment of heavy metals by plants. TF is the stems-to-roots ratio of heavy metal contents in a plant, while BF is the aboveground-to-medium ratio of heavy metal contents. BF modestly indicates the difficulty of element migration in the medium-plant system. It is generally believed that TF and BF should both be > 1 in plants [21].

The TFs and BFs of both herbs under different Cd concentrations are listed in Table 3. The TFs of both herbs are > 1 , whether incubation or not, but the TFs are all larger after the inoculation. The BFs after inoculation are larger. Thus, the addition of the strain promotes the migration and enrichment of Cd, and improves the efficiency of Cd phytoremediation.

CONCLUSIONS

Three major conclusions were reached. First, under different Cd concentrations the inoculation of the resistant microbe enhances biomass, plant height, root

length, and tolerance index for both *L.perenne* and *F.arundinace*. This indicates a growth-promoting effect.

Second, under Cd stress inoculation improves chlorophyll contents, photosynthetic rate, water use efficiency, and basic metabolism in plants. The inoculation also enhances activities of SOD, POD, and CAT *in vivo* and reduces MDA contents. A possible physiological mechanism is the Cd-tolerant microbe promotes Cd absorption by *L.perenne* and *F.arundinace*.

Lastly, under different Cd concentrations inoculation enhances enrichment of Cd by the two herbs of interest. Also, it increases TF and phytoremediation efficiency.

ACKNOWLEDGEMENTS

The authors would like to thank the financial support for this work by the National Science & Technology Pillar Program during the twelfth “Five-year Plan” Period (2012BAC11B07) and Jiangxi International Science & Technology Cooperation Plan (20133BDH80027).

REFERENCES

1. Wu, Q. L., Yang, Y. and Xie, Z. M. 2000. *Trace elements and biological health*. Guiyang, Guizhou Science and Technology Press.
2. Wang, S. C., Wei, Z. C. and Zhou, Y., *et al.*, A Research on the Leaching Toxicity of the Solid Waste of a Pb-Zn Mine, *Journal of Residuals Science & Technology*, Vol. 12, No. 1, 2015, pp. 25–30. <http://dx.doi.org/10.12783/issn.2376-578X/12/1/4>
3. Slolzhenko, E. G., Soboleva, N. M. and Goncharuk, V. V., Decolorization of azodye solutions by fenton's oxidation. *Water Research*, Vol. 29, No. 9, 1995, pp. 2006.
4. Jiang, C. Y., Sheng, X. F. and He, L. Y., *et al.*, Isolation and characteristics of heavy metal-resistant strain WS34 and its effects on the phytoremediation of soils contaminated with lead and cadmium, *Journal of Agro-Environment Science*, Vol. 28, No. 10, 2008, pp. 1961–1968.
5. Luo, Q. Y., Wang, X. J. and Lin, S. S. *et al.*, Mechanism and application of bioremediation to heavy metal polluted soil using arbuscular-mycorrhizal fungi, *Acta Ecologica Sinica*, Vol. 33, No. 13, 2013, pp. 3898–3906. <http://dx.doi.org/10.5846/stxb201206260900>
6. Zhong, W. L. and Liu, K. X., Effects of soil microorganisms on uptake of 89 Sr by ryegrass and bahia grass, *Journal of Nuclear Agricultural Sciences*, Vol. 20, No. 4, 2006, pp. 341–344.
7. Wu, M. and Xu, Z. J., Purification of toluene by enhanced microorganisms in ryegrass rhizo sphere, *Chinese Journal of Environmental Engineering*, Vol. 8, No. 9, 2014, pp. 3871–3874.
8. Ouyang, W., Liu, H. and Yu, Y. Y., *et al.*, The combined effects of tall fescue (*Festucaarundinace*) phyto-remediation and bio-augmentation on treatment of oil-contaminated soil, *Techniques and Equipment for Environmental Pollution Control*, Vol. 7, No. 1, 2006, pp. 94–97.
9. Li, Y. S., Feng, C. L. and Wu, X. F. *et al.*, A review on functions of microorganisms in phytoremediation of heavy metal contaminated soils, *Acta Ecologica Sinica*, Vol. 35, No. 20, 2015, pp. 1–13.
10. Zhu, S. C., Zeng, X. X. and Tang, J. X. *et al.*, Augmentation Effects of Mucor QS1 on Phytoremediation of Cadmium Contaminated Soils with Guizhou Rapeseed, *Hubei Agricultural Sciences*, Vol. 58, No. 18, 2014, pp. 4283–4285.
11. Yang, B., T. J. and Li, H. Y., Effect of Several Herbaceous Plants on

- Purification of Sewage, *Guizhou Agricultural Sciences*, Vol. 42, No. 12, 2014, pp. 217–220.
12. Li, H. S. 2002. *Modern plant physiology*, Beijing, Higher Education Press.
 13. Zhang, Z. L., Qu, W. Q. and Li, X. F. 2009. *Experiment guidance on plant physiology 4th ed.* Beijing, Higher Education Press.
 14. Stobart, A. K., Griffiths, W. T. and Ameen, B. I., The effect of Cd²⁺ on the biosynthesis of chlorophyll in leaves of barley, *Physiology of Plant*, Vol. 63, 1985, pp. 293–298. <http://dx.doi.org/10.1111/j.1399-3054.1985.tb04268.x>
 15. Gonzalez, C. M., Casanovas, S. S. and Pignata, M. L., Biomonitoring of air pollutants from traffic and industries employing *Ramalinaecklonii* (Spreng). *Mey and Flot in Cordoba Argentina Environmental Pollution*, Vol. 91, No. 3, 1996, pp. 269–277.
 16. Fatima, R. A. and Ahmad, M. C., Certain antioxidant enzymes of *Alliumcepa* as biomarkers for the detection of toxic heavy metals in wastewater, *Science of The Total Environment*, Vol. 346, No. 3, 2005, pp. 256–273. <http://dx.doi.org/10.1016/j.scitotenv.2004.12.004>
 17. Peng, C., Zhao, X. G., and Han, Y., *et al.*, Toxic Effects of Chronic Sub-Lethal Cu²⁺, Pb²⁺ and Cd²⁺ on Antioxidant Enzyme Activities in Various Tissues of the Blood Cockle, *Anadaragranosa*. *Journal of Residuals Science & Technology*, Vol. 12, No. 3, 2015, pp. 125–131. <http://dx.doi.org/10.12783/issn.1544-8053/12/3/2>
 18. Zhang, L. H., Li, P. and Li, X. M., *et al.*, Effects of cadmium stress on the growth and physiological characteristics of wheat seedlings, *Chinese Journal of Ecology*, Vol. 24, No. 4, 2005, pp. 458–460.
 19. Yang, Z., Chen, J. and Li, B., Effects of Cd Contamination on Number of Microbes, Physiological and Biochemical Characteristics of *Brassica juncea*. *Journal of Agro-Environment Science*, Vol. 30, No. 12, 2011, pp. 2428–2433.
 20. Liu, Z. Q. and Zhang, S. C. 1993. *Plant resistance physiology*. Beijing, China Agriculture Press.
 21. Zhang, X. F., Cadmium tolerance and accumulation characteristics of *Commelina communis* Linn, *Guangdong Agricultural Sciences*, Vol. 1, 2013, pp. 167–169.

Adsorbent Preparation from Oily Scum for Oily Wastewater Treatment

TANG CHAO^{1,2,*}, ZHAO LIN², GUAN JIAO-JIAO¹ and XIE SHUI-XIANG³

¹Key Laboratory of Oil and Gas Drilling and Production Engineering, Yangtze University, Wuhan, China

²Engineering and Technology College, Yangtze University, JingZhou, China

³CNPC Research Institute of Safety & Environment Technology, Beijing, China

ABSTRACT: A large amount of pollutants mainly of oil, COD and suspended solids in produced water are generated during the oilfield development. The existing domestic sewage treatment technique is focused on the separation of oil slick and mechanical impurities which cannot meet the emission standard after treating. In this paper, a kind of carbon-based adsorbent was prepared by oily scum from sewage treatment plant in the oilfield united station on the basis of research and indoor experiments. The analysis of elements and microstructure indicated that high carbon content, pore-evolution properties were included in the preparation of adsorbent with pore size distribution mainly composed of mesoporous and the specific surface area was 477.49 m²/g, iodine value was 376.48 mg/g. Meanwhile, using the produced water from Liao He oilfield as a research object indoors, the adsorption capacity of carbon-based adsorbent and activated carbon on COD and oil in the wastewater was evaluated. The results showed that the adsorption capacity of carbon-based adsorbent on COD and oil in wastewater was superior to activated carbon. The concentration of COD and oil in wastewater decreased from 502.12 mg/L and 45.31 mg/L to 42.64 mg/L and 5.826 mg/L. The removal rate was 91.5% and 87.1% respectively after handling, which can meet the requirements of grade two of "The National Integrated Wastewater Discharge Standard" (GB8978) and provide a way for oily scum utilization as a resource.

INTRODUCTION

DURING the oilfield development, the most common wastewater is the oilfield produced water. In most cases, the produced water return to the reservoir by the means of injecting water or steam to maintain the formation energy. Along with the oilfield development in China coming into the middle-late period, water content of produced fluids is increasing accompanied by higher investment on treatment facilities and operating cost, which means it is becoming more difficult for the treatment and disposal of wastewater. At present, there are a great many methods for wastewater treatment including electrochemical treatment, membrane filtration, biological treatment, etc. Because of the difficulty of efficient treatment to remove the fluctuating compositions of different components in wastewater under real operating conditions, there is no one-size-fits-all approach for the removal technology [1]. While in China, the use of "old three sets" process

(oil removal, coagulation and filtration or oil removal, air flotation and filtration) on the treatment of oilfield wastewater, only focusing on the separation of oil slick and mechanical impurities [2]. Wasterwater treated by this process cannot meet the national discharged standard.

According to the current statistics, the first category of hazardous waste pollutants in oilfield wastewater does not exceed the national discharge standard in terms of environmental impact. Therefore, the treatment of oilfield wastewater aiming at discharge, its content of COD and oil pollutants should be controlled [2,3].

Oily scum, as a kind of oily sludge, is hazardous waste generated during the process of oilfield sewage treatment, which is an urgent and difficult problem for handling and disposal in environmental protection of oil production [4,5]. Due to large amount of hydrocarbons in the oily sludge there is a good value for oil and gas recovery. Components particularity determines that the resource utilization is bound to become the mainstream of oily sludge treatment technology [6,7].

There has been a large amount research on oily sludge utilization technology at home and abroad. In-

*Author to whom correspondence should be addressed.
E-mail: 395450161@qq.com; Tel: +86 0716 8067503; fax: +86 0716 8067507

cineration for example is using organic composition with a certain calorific value to deal with oily sludge [8]. Solvent extraction is using organic solvent as extractant to recycle oil in the oily sludge [9]. A hot washing process uses a chemical agent to wash the oily sludge making it a three-phase separation and recycling the oil components [10]. Pyrolysis of oily sludge using isolated air pyrolysis leads to three fractions: gas is mainly comprised of methane and carbon dioxide, liquid is mainly comprised of fuel oil and water, and the solid form is mainly comprised of inorganic minerals and carbon residue. It is possible to recycle both the gas and liquid. The solid fraction could be incinerated, disposed in the landfill, or used as a cheap adsorbent [11].

Based on the observation the solid fraction obtained after pyrolysis could be used as adsorbent the objective of this study was to prepare a kind of carbon-based adsorbent with oily scum used as a raw material for pyrolysis technology. The prepared adsorbent is applied to COD and the oil adsorption process in produced water. Results suggest that COD and oil after handling could meet requirements of grade two of "The National Integrated Wastewater Discharge Standard" (GB8978). This process has achieved reasonable treatment of oily scum as well as afforded an effective adsorption material for disposal of oilfield wastewater. This makes the recycling target of "waste-resource-product" in the oilfield sewage treatment plant come to fruition.

EXPERIMENTAL

Source of Materials

Two kinds of materials were derived from LiaoHe Oilfield. Oily scum was provided from the HuanSanlian sewage treatment plant and oily wastewater was provided from the ShuGuang oil recovery factory.

Analytical Method

Composition of Oily Scum Analysis

Oil and water content of the oily scum were measured separately according to standards GB/T8929-2006 and SY/T5118-2005. Residual content was calculated using a dispersion method.

Heavy Metals in Lixivium of Oily Scum Combustion Ash Measurement

Content of heavy metal in lixivium was in accor-

dance with GB/T17141-1997 Standards. This provided an oily scum combustion ash measurement.

Characterization Methods for Carbon-based Adsorbent and Activated Carbon

Iodine number was measured according to GB/T7702.7-2008. Elements analysis was measured using GENES IS Apex X-ray Fluorescence (EDAX corp. USA).

Analysis of surface properties and SEM were determined by N₂ adsorption ASAP (JinAipu Science and Technology Ltd. corp. Beijing) and a Quanta 200 tungsten filament scanning electron microscope (FEI H.K. Ltd. corp.).

Testing Contents of COD and Oil in Oilfield Wastewater

The oilfield produced water was first filtrated using filter paper for removal of oil slick and suspended solids. Contents of COD in wastewater after pretreatment were measured by a spectrophotometer according to HJ/T339-2007. Determination of oil content was performed using an infrared spectrophotometer based on HJ637-2012.

RESULTS AND DISCUSSION

Analysis of Oily Scum Composition and Heavy Metal Pollutants

Tables 1 and 2 summarized the composition of oily scum and heavy metal pollutants. Table 1 displays that moisture content is high but oil and solid content are relatively low. Table 2 displays that extraction toxicity of the heavy metals in oily scum combustion ash was less than regulation values for an identification standard for hazardous wastes and for the second-order of "National Overall Discharge Standard for Sewage."

Preparation and Characterization of Carbon-based Adsorbent

Adsorbent Preparation

Methods involved heating 500 g of oily scum in an electric heating pyrolysis furnace using a heating rate of 10°C/min. Pyrolysis temperature was 650°C maintained for 2 h and the whole process occurred under an N₂ atmosphere. The non-condensable gas, oil, and

Table 1. Contents of Oily Scum Components.

Sample	Water Content, W, %	Oil Content, W, %	Residue Content, W, %
Oily scum	85.4	8.1	6.5

water separated through condensation during pyrolysis may be recycled. After the reaction the solid product obtained was washed with a specific concentration mixture of HCl, HF, and NaOH solution, respectively, until ash and oxides were dissolved thoroughly. Then, the product was washed to neutral and dried and ground through a 200 mesh sieve. 27.64 g of black powder of solid material obtained was carbon-based adsorbent.

Analysis of Elements in carbon-based Adsorbent

Elements in carbon-based adsorbent and activated carbon (KangHong activated carbon factory, LiYang City) were analyzed respectively. Results are seen in Table 3 indicating total carbon content in carbon-based adsorbent is as high as 90% and almost similar to that of activated carbon.

Surface Properties and Iodine Number in Carbon-based Adsorbent and Activated Carbon

Surface properties and the iodine number of adsorbent and activated carbon were analyzed. Results are seen in Table 4 indicating the specific surface area of carbon-based adsorbent was relatively small but pore volume and mean pore size was big. Due to the different pore size of molecular adsorption the pores can be divided into the following three categories according to the IUPAC: pore width greater than 50 nm called macroporous, pore width between 2–5 nm called mesoporous, and pore width less than 2 nm called microporous [12]. Thus, carbon-based adsorbent was mainly composed of mesoporous structure. Activated carbon with small pore diameter is mainly made up of microporous with a large specific surface area. Size of the io-

Table 3. Elemental Analysis of Adsorbent and Activated Carbon.

Sample	C, Wt, %	O, Wt, %	Na, Wt, %	Al, Wt, %	S, Wt, %	Si, Wt, %
Adsorbent	90.72	6.57	0.89	0.29	1.05	0.41
Activated Carbon	92.49	7.51	—	—	—	—

dine number is associated with degree of development of the microporous [13] which reflects development of microporous in adsorbent is worse than activated carbon.

SEM Analysis

Surface appearance for the oily scum, carbon-based adsorbent, and activated carbon were analyzed respectively under the scanning electron microscope (SEM). Results are seen in Figure 1 indicating the surface of oily scum was relatively flat and smooth with a noticeable oil phase. Carbon-based adsorbent had a rough surface with an irregular porous structure, large aperture, and wide pore size distribution. The texture of activated carbon was tight with smaller aperture and equal distribution.

Oily Wastewater Treatment with Carbon-Based Adsorbent

Experimental Method

A certain amount of carbon-based adsorbent was placed into a conical flask filled with 100 mL of oily wastewater after pretreatment. It was then vibrated for a period of time in a water-bathing constant temperature vibrator. Adsorption temperature could be adjusted. COD and oil concentration in wastewater were measured before and after adsorption respectively. The removal rate of COD and oil was calculated. COD content in the oily wastewater was 502.12 mg/L and oil content was 45.31 mg/L. The oil in the

Table 2. Extraction Toxicity of Heavy Metals in Oily Combustion Ash.

Test Items	Pollutants Content, mg/L							
	Cu	Pb	Zn	Cd	Ni	As	Cr ⁶⁺	Hg
Combustion Ash	0.072	0.099	0.058	0.007	0.006	0.022	0.092	—
1	50	3	50	0.3	10	1.5	1.5	0.05
2	2.0	1.0	5.0	0.1	1.0	0.5	0.5	0.05

1: GB5085.3-1996 standard

2: Second-order of GB8978-1996 standard

Table 4. Surface Physical Characteristics and Iodine Value of Adsorbent and Activated Carbon.

Sample	BET Specific Surface Area, m ² /g	Pore Volume, cm ³ /g	Average Pore Size, nm	Iodine Number, mg/g
Adsorbent	477.49	0.6308	6.753	376.48
Activated Carbon	941.2	0.501	2.129	724.06

wastewater existed in the form of emulsified oil and pH was 7.

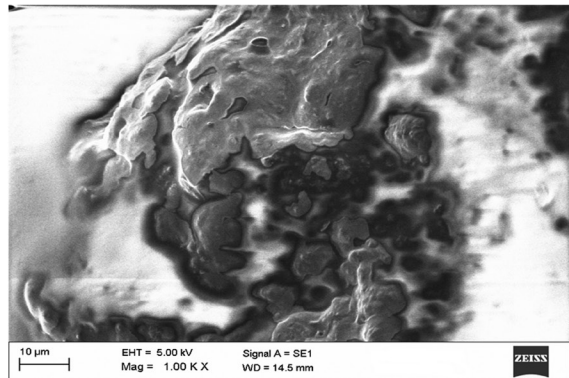
Influence Factors Analysis for the Treatment of Oily Wastewater

A solid-liquid adsorption system's main influence factors are concluded as dosage, adsorption time, and temperature [14–16]. A response surface method was performed as follows according to three main factors. Three levels were chosen from each factor to do a central composite design (CCD) [17–18]. The results of factors coding are seen in Table 5. Experiments were carried out according to a combination designed by a CCD-designing plan and experimental results are seen

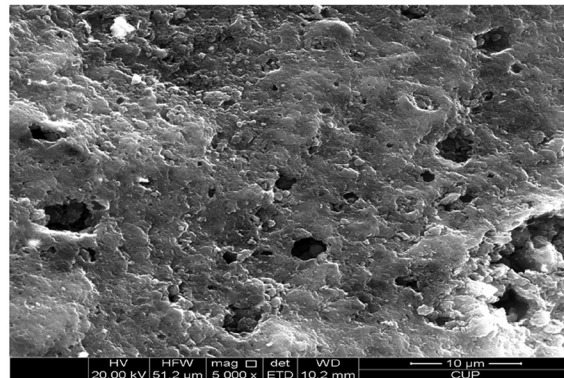
Table 5. CCD Design Factors and Level Coding Table.

Factors	Level		
	-1	0	1
A (dosage/g)	1	2.5	4
B (adsorption time/min)	30	75	120
C (temperature/°C)	10	30	50

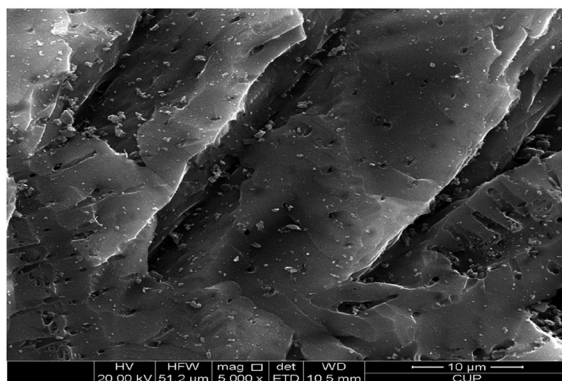
in Table 6. Variance and significant analysis of COD removal rate and oil removal rate are seen in Table 7 and Table 8 indicating that for COD removal rate the Model F-value of 26.41 implies the model is significant. Values of “Prob>F” less than 0.05 indicate model terms are significant, in this case A, B, A², B² are significant model terms. Values greater than 0.10 indicate the model terms are not significant. For oil removal rate, the Model F-value of 27.42 implies the model is significant. Values of “Prob>F” less than 0.05 indicate model terms are significant and in this case A, A², B² are significant model terms. For COD and oil removal rate, A was the smallest, B took second place, and C was the biggest. Influence relations were as follows: adsorbent dosage > adsorption time > temperature.



(a)



(b)



(c)

Figure 1. SEM images of (a) oily scum, (b) carbon-based adsorbent, and (c) activated carbon.

Table 6. Experiments and Design Results.

Number	Factors Coding			Results	
	A (dosage/g)	B (adsorption time/min)	C (temperature/°C)	COD Removal Rate, %	Oil Removal Rate, %
1	1	1	0	89.34	86.82
2	-1	0	1	88.92	70.03
3	0	1	1	89.07	81.87
4	-1	-1	0	85.48	67.18
5	0	0	0	91.07	86.53
6	1	-1	0	91.76	89.13
7	0	0	0	91.07	86.53
8	0	0	0	91.07	86.53
9	0	0	0	91.07	86.53
10	0	1	-1	89.24	82.96
11	-1	0	-1	87.64	74.31
12	0	-1	1	90.13	82.76
13	1	0	-1	92.08	88.81
14	-1	1	0	84.62	61.93
15	0	0	0	91.07	86.53
16	0	-1	-1	90.62	84.24
17	1	0	1	91.82	88.04

Results using optimum factors suggested that when dosage was 3.94 g the adsorption temperature was 10°C and lasted for 60.5 min. COD removal rate could reach the maximum at 92.94%. When dosage was 3.54 g the adsorption temperature was 10°C and lasted for 70.22 min. Oil removal rate can reach a maximum at 90.92%.

According to these results, COD and oil removal rate could reach the maximum when the adsorbent dosage was close to 4 g. Considering the adsorbent dosage influence on treatment cost and the rational wastewater discharge standard rules, adsorbent dosage was studied by means of single factor analysis in order to find out the best sewage treatment conditions.

Influence of Adsorbent Dosage on Wastewater Treatment

During practical wastewater treatment the adsorption temperature is usually hard to change. Therefore, the experiment was conducted at room temperature in the single factor experiment. The aforementioned analysis results indicate COD removal rate could reach a maximum when adsorption time lasted 60.5 min. Oil removal rate could reach a maximum when it lasted 70.22 min. This time the purpose of single factor experiment was to study dosage influence on COD and oil removal rate on the following conditions. A median adsorption time of 65 min was chosen at a room tem-

Table 7. COD Removal Rate Variance and Significance Analysis.

Source	df	Mean Square	F Value	p-value
Model	9	7.98	26.41	0.0001(significant)
A-dosage	1	42.04	139.12	< 0.0001
B-adsorption time	1	4.09	13.53	0.0079
C-temperature	1	0.016	0.054	0.8235
AB	1	0.61	2.01	0.1989
AC	1	0.59	1.96	0.02040
BC	1	0.026	0.085	0.7794
A ²	1	8.98	29.70	0.0010
B ²	1	13.79	45.64	0.0003
C ²	1	1.07	3.55	0.1014

Table 8. Oil Removal Rate Variance and Significance Analysis.

Source	df	Mean Square	F Value	p-value
Model	9	117.80	27.42	0.0001(significant)
A-dosage	1	787.05	183.22	< 0.0001
B-adsorption time	1	11.83	2.75	0.1409
C-temperature	1	7.26	1.69	0.2348
AB	1	2.16	0.50	0.5011
AC	1	3.08	0.72	0.4251
BC	1	0.038	0.009	0.9277
A ²	1	175.85	40.94	0.0004
B ²	1	60.88	14.17	0.0070
C ²	1	0.22	0.052	0.8264

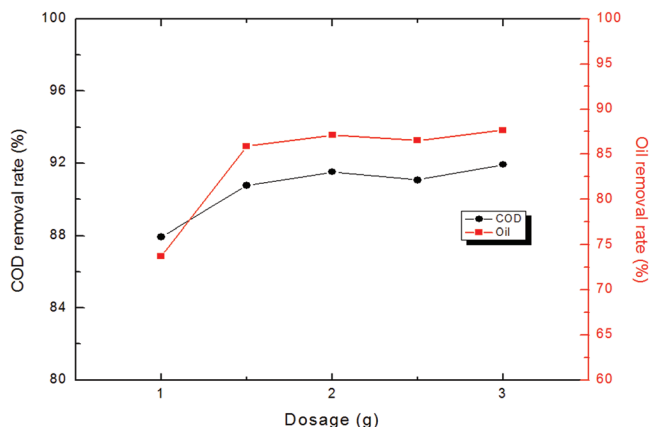


Figure 2. Dosage influence on COD and oil removal rate.

perature of 28°C. Results seen in Figure 2 indicate that COD and oil removal rate increased with an increase of dosage. When the quantity was 2 g COD and oil concentration in wastewater decreased to 42.62 mg/L and 5.83 mg/L respectively meeting requirements of grade two of the national highest emission concentration standard (GB8978). Therefore, a 2 g adsorbent dosage was appropriate in view of its direct impact on the cost of wastewater treatment.

A 2 g adsorption dosage was vibrated and adsorbed for 65 min at a room temperature of 28°C. COD and oil concentration in 100 mL wastewater decreased to 42.62 mg/L and 5.83 mg/L. Removal rate was 91.51% and 87.14%, respectively, and can meet requirements for grade two of “The National Integrated Wastewater Discharge Standard” (GB8978).

Comparative Evaluation between Carbon-based Adsorbent and Activated Carbon

Adsorption capacity of COD and oil in 100 mL oily wastewater was performed using a 2 g adsorbent dosage at a room temperature of 28°C for 65 min for comparison of carbon-based adsorbent and activated carbon. Results are seen in Table 9 indicating the adsorption capacity of carbon-based adsorbent was superior to activated carbon for treatment of COD and oil in

oilfield wastewater. Because carbon-based adsorbent is mainly mesoporous and within a shorter diffusion time when it comes to liquid phase adsorption this is conducive to adsorption of COD, emulsified oil, and other macromolecular organic matter in the wastewater. However, activated carbon pore size is small. Its microporous structure is not conducive to liquid phase diffusion. Specific surface area is bigger but mainly composed of microporous which has little contribution to macromolecular material adsorption. Therefore, the treatment is not as effective as carbon-based adsorbent [19].

CONCLUSION

Carbon-based adsorbent prepared from oily scum contained high carbon content with a rough surface, irregular porous structure, and was mainly composed of mesoporous determined by SEM and ASAP. Its specific surface area was 477.49 m²/g and iodine value was 376.48 mg/g. 100 mL oilfield wastewater absorbed by 2 g carbon-based adsorbent at a room temperature of 28°C for 65 min. COD and oil removal rate was 91.51% and 87.14%, respectively, after adsorption. COD and oil concentration decreased to 42.62 mg/L and 5.83 mg/L. Adsorption efficiency was superior to activated carbon which can meet requirements for grade two of “The National Integrated Wastewater Discharge Standard” (GB8978). Carbon-based adsorbent can be viewed as a new type of adsorbing material. Further study is necessary for mass production and application purposes.

ACKNOWLEDGEMENTS

The authors greatly appreciate financial support from Scientific Research Development Foundation of Engineering and Technology College (14j0102, 14j0101).

REFERENCES

1. Sanaa J., Adewale G., Shadi W. H., Recent improvements in oily

Table 9. Adsorption Properties Comparison between Carbo-based Adsorbent and Activated Carbon.

Sample	COD Concentration before Adsorption, mg/L	Oil Concentration before Adsorption, mg/L	COD Concentration after Adsorption, mg/L	Oil Concentration after Adsorption, mg/L	COD Removal Rate, %	Oil Removal Rate, %
Carbon-based Adsorbent	502.12	45.310	42.62	5.826	91.51	87.14
Activated Carbon	502.12	45.310	90.42	9.672	81.99	78.65

- wastewater treatment: Progress, challenges, and future opportunities, *Journal of Environmental Sciences*, Vol. 37, 2015, pp. 15–30. <http://dx.doi.org/10.1016/j.jes.2015.04.011>
2. Dong G. Y., Zhou A. G., Deng H., 2006, *Developments in Petroleum Environment Protection Technology*, Petroleum Industry Press, pp. 21–25 (in Chinese).
 3. Yang C. Z., 1998, *Environmental Engineering Science*, Beijing: Metallurgy Industry Press, pp. 65–81 (in Chinese).
 4. Yang F., Kang L. W., Liu F., Oily Sludge Treatment Technology in LongDong Oilfield, *J. Environmental Protection in Oilfield*, Vol. 18, No. 1, 2008, pp. 30–32 (in Chinese).
 5. Jiang Y. J., Guo F. T., Du H. T., Oily Sludge of DaQing Oilfield Continual Pyrolysis Treatment Technology, *J. Oil-Gasfield Surface Engineering*, Vol. 28, No. 1, 2009, pp. 8–10 (in Chinese).
 6. Xie S. X., Che M., Jiang G. C., *et al.*, Development and mechanism study of an additive for fuelization of oily sludge, *Chinese Journal of Environmental Engineering*, Vol. 5, No. 6, 2011, pp. 1351–1356 (in Chinese).
 7. A. Gezer Gorgec, G. Insel, N. Yagci, *et al.*, Comparison of energy efficiencies for advanced anaerobic digestion, incineration, and gasification processes in municipal sludge management, *Journal of Residuals Science & Technology*, Vol. 13, No. 1, 2016, pp. 57–64. <http://dx.doi.org/10.12783/issn.1544-8053/13/1/8>
 8. Wang Z. P., Ma Y. F., Oily sludge fluidization-suspension incineration technology and pollutant emission analysis, *Clean Coal Technology*, Vol. 21, No. 61, 2015, pp. 121–124 (in Chinese).
 9. Shi L. F., Pan L. X., Li Z. H., *et al.*, Treatment technologies and equipment for oil-containing sludge, *Environmental Engineering*, Vol. 33, 2015, pp. 526–534 (in Chinese).
 10. Yu L. L., Song J., Zheng K., *et al.*, Research on hot washing treatment process of oily sludge, *Science & Technology in Chemical Industry*, Vol. 22, No. 1, 2014, pp. 29–33 (in Chinese).
 11. A. Mendez, G. Gasco, M. M. A. Freitas., *et al.*, Preparation of carbon-based adsorbents from pyrolysis and activation of sewage sludges, *Chemical Engineering Journal*, Vol. 108, 2005, pp. 169–177. <http://dx.doi.org/10.1016/j.cej.2005.01.015>
 12. K. S. W. Sing., D. H. Everett., R. A. W. Haul., *et al.*, Reporting physiosorption data for gas/solid systems with special reference to the determination of surface area and porosity, *Pure & Appl. Chem.*, Vol. 57, No. 4, 1985, pp. 603–619. <http://dx.doi.org/10.1351/pac198557040603>
 13. Deng H., Wang R. S., Ren W., *et al.*, Study on adsorptive capacity of pyrolytic residues of oily sludge., *Environmental Protection of Oil & Gas Fields*, Vol. 20, No. 2, 2010, pp. 1–3 (in Chinese).
 14. B. Andrey., T. J. Bandosz., Efficient hydrogen sulfide adsorbents obtained by pyrolysis of sewage sludge derived fertilizer modified with spent mineral oil, *Environmental Science & Technology*, Vol. 38, No. 1, 2004, pp. 345–351. <http://dx.doi.org/10.1021/es0303438>
 15. Pei G. H., Yu F., Liu J. J., Feasibility study of individual treatments of desizing wastewater, *Journal of Residuals Science & Technology*, Vol. 12, S 1, 2015, pp. S85–S91. <http://dx.doi.org/10.12783/issn.1544-8053/12/S1/13>
 16. Tan F. X., Chen H. H., Wu D. J., *et al.*, Optimization of geosmin removal from drinking water using UV/H₂O₂, *Journal of Residuals Science & Technology*, Vol. 13, No.1, 2016, pp. 23–29. <http://dx.doi.org/10.12783/issn.1544-8053/13/1/4>
 17. Pang T. C., Zhong Q. P., Xiong Z., *et al.*, Extraction process optimization of saueda salsa polysaccharides by response surface methodology and analysis of its antioxidation activity, *Journal of Southern Agriculture*, Vol. 46, No. 7, 2015, pp. 1280–1286 (in Chinese).
 18. He Q. L., Liu W. B., Yang H. J., *et al.*, Isolation, identification of a p-tert-butylcatechol-degradaing strains and optimization for its degradation by response surface methodology, *Environmental Science*, Vol. 36, No. 7, 2015, pp. 2695–2705 (in Chinese).
 19. Yu L. L., Zhong Q., Preparation of activated carbon adsorbent made from sludge and its application, *Technology of Water Treatment*, Vol. 32, No. 5, 2006, pp. 61–64(in Chinese).

Changes in Nitrogen Form in Paper Mill Wastewater Treated by Ozone Oxidation

KE ZENG¹, TIANLI HAO², YIRAN LI¹, HONGCHAO ZHANG¹ and HONGYOU WAN^{1,*}

¹College of Water Conservancy & Environmental Engineering, Zhengzhou University, Zhengzhou 450001, China

²Zhengzhou Yu Lai Technology & Trade Co., Ltd, Zhengzhou 450002, China

ABSTRACT: Ozonizers will produce nitrogen oxides which can be dissolved into the wastewater as ozone is produced. This experiment, where ozonization process was employed as the post-treatment after the biological processes, aims to analyze the amount of nitrogen and its variation and transform rate in influents and effluents. Results showed that after ozonization process, the concentrations of total nitrogen in effluents were higher than the concentrations in influents (0.01~0.38 times higher). The concentrations of nitrate nitrogen in effluents were also higher than the concentrations in influents, and average increased rate of NO₃-N was 226.8%. Furthermore, the increase in the concentration of NO₃-N due to dissolution of NO_x was 47.10% of total increase in NO₃-N.

INTRODUCTION

As a strong oxidant, ozone is commonly used in the treatment process of water [1] and wastewater [2], and it also can be applied to a post-treatment after the biochemical processes in treating paper mill wastewater [3]. If air-fed ozone generators are employed, small amounts of by-products nitrogen oxides (NO_x) can be produced by ionization of the nitrogen in air [4]. However, the ionization potential of nitrogen from the air is 9.79 eV, which is far above the oxygen ionization potential 4.81 eV. Therefore, during the discharge process the probability of oxygen decomposition is higher than the ionization potential of nitrogen, which leads to only a small amount of nitrogen decomposed to form the NO_x [4]. The NO_x in ozonized gases as deleterious agents [5] would possibly influence the production of ozone [6].

The studies about NO_x generated by air discharge to produce ozone and their forms have been conducted all over the world. Some researchers thought the main form of NO_x in ozonized gas was NO₂ [7,8], and the range of proportion of NO_x in ozonized air was from 0.1–1.0% [9]. After the bio-chemical processes applied in treating organic wastewater, the nitrogen in organic matter will be transformed and become ammonia nitrogen (NH₃-N) and NO₃-N (NO₃-N) when ozone oxidation is used for advanced treatment [10,11]. However, there are only a few studies about dissolved transfor-

mation of NO_x and its influence factor, and the percentage of dissolved transformation of NO_x still remains unclear. The project that supports this paper used the air-fed ozone generator to treat the bio-chemical effluents of a paper mill wastewater by an air-water scrubber 6 m high, and the removal efficiencies of COD, UV₂₅₄ and chroma were tested. It is the first that this article studied the changes in the chemical forms of nitrogen and the corresponding amounts in the ozonized effluents together with ozone dosage and other factors, and the study discussed the transformation rate of dissolved NO_x in the ozonized effluents of paper mill wastewater.

MATERIAL AND METHODS

There is available information from a series of conducted pilot experiments [12], where air-fed ozone generators were employed to treat the effluents of biochemical processes in paper mill wastewater, to support this article. This experiment studied the removal efficiency of COD, chroma and UV₂₅₄ in ozonization process for treating the biochemically treated effluents, and the variations in the concentrations of total nitrogen (TN), NH₃-N and NO₃-N were also analyzed.

Experimental Apparatus and Materials

The ozonation process was performed in an air-water scrubber (height = 6000 mm, diameter = 500 mm) with an air distributor (aperture: 10 μm) installed in the

*Author to whom correspondence should be addressed. E-mail: hywan@zzu.edu.cn

lower part. Continuous feeds of the wastewater (450 L/h) and ozone (20~30 mg/L) with an air intake flow, 2.8 m³/h, of the ozonizer (Qingdao guolin industry co., ltd., Qingdao, China) were applied to the ozonation section. Ozone concentrations (gas and liquid respectively) were measured by online ozone monitors using UV spectrophotometry method [13], and the iodometry method was applied to calibrate the monitored results periodically.

The raw water applied in this experiment was collected from the aerobic biological treated effluent of the secondary sedimentation tanks in a pulp and paper mill factory. The parameters of the raw water quality during the period from July 2011 to February 2012 are shown in the Table 1.

Analytical Methods

All analyses regarding to the water parameters were according to the manual [14]. More precisely, TN was determined by using potassium persulfate oxidation UV spectrophotometry. NH₃-N was determined by using the Nessler's reagent spectrophotometry. NO₃-N was determined by using UV spectrophotometry. The values of pH were determined by a portable pH probe. And ozone concentration was determined in accordance with iodometry method. The spectrophotometer TU-1901, was made in Persee, Beijing, China.

Chemicals applied to the tests were analytical reagents except sodium hydroxide and hydrochloric acid which were guaranteed reagents.

VARIATIONS IN NITROGEN CONCENTRATION AND AMOUNT OF NO_x DISSOLVED INTO WASTEWATER

Variations in Nitrogen Concentration after Oxidation Treatment

Variations in concentration of TN and NO₃-N are seen in the Figures 1 and 2. Although the designated contact time and ozone dosage were set, concentrations of TN fluctuated in Figure 1 due to slight changes in contact time and ozone dosage during the operation plus variation of quality and quantity of influents [15]. Ozone dosage and retention time were obtained from Equations (1) and (2). See Equation (1).

$$D_o = (Q_{oi} \times C_{oi} / Q_{wi}) \quad (1)$$

where D_o is dose of ozone, mg/L, Q_{oi} is intake flow of

Table 1. Characterization of Experimental Raw Water.

Indicators	Unit	Range Value	Average Value
Temperature	°C	15–35	25
PH		7.2–8.5	7.9
COD	mg/L	170–400	285
UV ₂₅₄	cm ⁻¹	0.8–5.0	2.9
Chroma	time	100–500	300
TN	mg/L	4.9–11.5	8.2
NH ₃ -N	mg/L	1.0–5.5	3.3
NO ₃ -N	mg/L	0.0–5.8	2.9

ozone, C_{oi} is concentration of intake ozone, and Q_{wi} is flow of water influent. See Equation (2).

$$T_r = (A_s \times H_w / Q_{wt}) \quad (2)$$

where T_r is retention time, A_s is cross-sectional area of the scrubber, H_w is depth of water in the scrubber, and Q_{wt} is flow of water treated.

Data in figures and tables display variations in concentration of TN, NO₃-N, and NH₃-N during the oxidation process. It is clear concentration of TN, NO₃-N, and NH₃-N in effluents were higher than that found in influent (more data available in previous report) [15,16].

Seen in Figures 1 and 2, it is clear concentrations of TN and NO₃-N in effluents are larger than in influents after the oxidation process (0.01~0.38 times higher in TN). It is possible to speculate that the reason for the increase of TN in effluents is from inflow of extra source(s) nitrogen based on the law of mass conservation.

Amount of NO_x Dissolved into Wastewater

Compared with sewage, content of organic nitrogen in paper mill wastewater is low. Seen in Figure 2, the concentrations of NO₃-N in effluents were higher

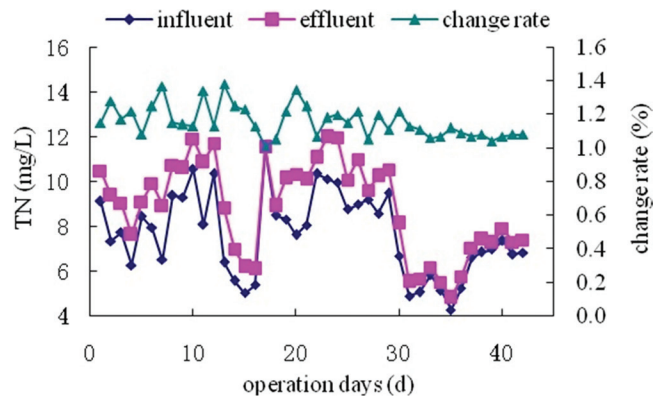


Figure 1. Variations in concentration of TN.

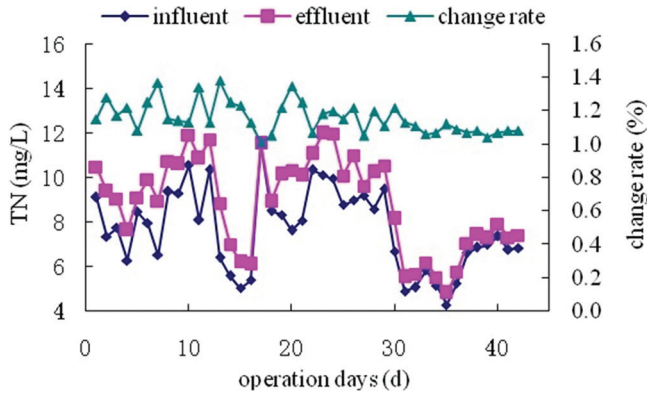


Figure 2. Variations in concentration of $\text{NO}_3\text{-N}$.

than that in influents, and the percentage of $\text{NO}_3\text{-N}$ increased ranged from 16.3–7575%. The reason why the percentages of $\text{NO}_3\text{-N}$ increased can reach to such high percentages is because an assumed concentration of $\text{NO}_3\text{-N}$ (0.08 mg/L, half of the detection limit) was applied to calculate those undetected samples. Apart from the undetected samples, the percentages of $\text{NO}_3\text{-N}$ increased in the effluent ranged from 36.0–2949%

with the average, 226.8%. Large increments in the concentrations of $\text{NO}_3\text{-N}$ in the effluent of the ozone process were observed, taking some values of the percentages of $\text{NO}_3\text{-N}$ increased (the concentration of $\text{NO}_3\text{-N}$ in influent, mg/L, the concentration of $\text{NO}_3\text{-N}$ in the effluent, mg/L) as examples, 271.6% (0.095, 0.353), 404.5% (0.110, 0.555), 240.8% (0.918, 3.128), 126.1% (0.440, 0.995), 136.8% (0.775, 1.835), 267.6% (1.080, 3.970), 163.1% (1.185, 3.118), 241.3% (1.270, 4.335), 208.9% (1.400, 4.325), 157.8% (1.830, 4.719) and 83.7% (2.020, 3.710) with the average, 209.3%. With the unusual increments mentioned above, there are questions that need to be addressed, “whether the increased $\text{NO}_3\text{-N}$ is due to the oxidation transformation of organic nitrogen and nitrite nitrogen or the dissolution of NO_x which were the by-products of the air-fed ozonizers”.

The analyzed concentrations of TN, $\text{NO}_3\text{-N}$ and $\text{NH}_3\text{-N}$ in the influents and effluents during the period from October 31st to December 5th are given in Table 2, and the reduction of organic nitrogen and calculated results are seen in the Table 3.

Table 2. Concentrations of TN, $\text{NH}_3\text{-N}$, and $\text{NO}_3\text{-N}$ in Influent and Effluents Treated by Ozonation.

TN (mg/L)		$\text{NH}_3\text{-N}$ (mg/L)		$\text{NO}_3\text{-N}$ (mg/L)		$\text{NH}_3\text{-N} + \text{NO}_3\text{-N}$ (mg/L)	
Influent	Effluent	Influent	Effluent	Influent	Effluent	Influent	Effluent
5.395	6.088	5.10	6.10	1.400	2.325	6.500	8.425
11.460	11.525	3.90	4.60	0.350	3.128	4.250	7.728
8.510	8.908	4.80	4.90	1.105	3.505	5.905	8.405
8.320	10.135	3.80	4.00	0.040	2.270	3.840	6.270
6.355	7.116	4.70	5.70	0.040	1.203	4.740	6.903
10.350	11.065	5.30	5.90	0.775	1.835	6.075	7.735
8.770	10.060	5.20	5.40	0.040	2.473	5.240	7.873
8.980	10.990	4.50	4.60	0.040	3.070	4.540	7.670
9.195	9.613	4.90	5.10	0.040	2.665	4.940	7.765
9.011	10.035	4.20	4.80	0.103	1.568	4.303	6.368
8.372	9.546	4.50	5.30	0.251	2.029	4.751	7.329
6.153	7.358	3.30	3.60	0.095	1.505	3.395	5.105
4.900	5.533	0.80	0.90	0.040	1.383	0.840	2.283
5.075	5.650	1.00	1.20	0.040	1.555	1.040	2.755
5.840	6.173	3.20	3.60	0.040	1.438	3.240	5.038
5.145	5.505	1.90	2.20	0.040	1.458	1.940	3.658
6.278	7.053	2.20	2.60	0.204	1.892	2.404	4.492
5.265	5.758	3.10	3.40	0.040	1.630	3.140	5.030
6.610	7.060	4.20	4.80	0.395	2.030	4.595	6.830
6.975	7.173	0.98	1.27	0.350	0.640	1.330	1.910
4.630	5.030	0.90	1.20	0.040	0.625	0.940	1.825
5.512	5.660	1.20	1.50	0.040	0.658	1.240	2.158
5.150	5.720	1.20	1.40	0.040	0.690	1.240	2.090
5.060	5.605	3.00	3.40	0.040	0.893	3.040	4.293
5.240	5.745	1.90	2.40	0.040	1.425	1.940	3.825
5.010	5.730	3.10	3.60	0.040	1.115	3.140	4.715

In Table 3, A, A – C and B – D mean the reduction of organic nitrogen, the amount of organic nitrogen oxidized to $\text{NO}_3\text{-N}$ and the amount of $\text{NO}_3\text{-N}$ dissolved respectively. The rates of generated $\text{NO}_3\text{-N}$ from oxidized organic nitrogen (55%) and the $\text{NH}_3\text{-N}$ (45%) were obtained by other research [17]. Particularly, B – D present the amount of dissolved NO_x generated by the air-fed ozonizers ranging from 0.065–2.010 mg/L.

Moderate values of E/B (from 2.34–87.60%, average: 47.10%) were obtained from this study, which could be related to the low concentration of organic nitrogen in the raw water.

NO_x TRANSFORMATION ESTIMATION

$\text{NO}_3\text{-N}$ concentration in effluent excluding that of influent is equal to the increment of $\text{NO}_3\text{-N}$. The $\text{NO}_3\text{-N}$ increment excluding the difference of the organic nitrogen decrease and the ammonium nitrogen increment is equal to the amount of NO_x dissolved into wastewater, which equals to the value of “B – D” in Table 3.

Some researches claimed that the volume of nitrogen oxide in the ozonized air ranged from 0.1–1% [8,9,18]. In this study, the value of the volume percentage (0.1%) was adapted together with ozone intake flow (2.8 m^3/h), ozone outlet pressure (0.1 MP) and the ozonized air temperature (25°C). The production of nitrogen dioxide generated by the ozonized air (10.36 g/h) was calculated according to Van Der Waals [19] and the parameters of the ozonized air. With an assumption that the nitrogen dioxides were dissolved completely, the amount of nitrogen oxide dissolved into the wastewater (3.15 g/h) were also obtained based on the volume of the wastewater treated and the theoretical concentration of nitrogen in the water (7.00 mg/L) [15].

“E/7” in Table 3 is equal to the value obtained from column E divided by 7.00 mg/L, which represents the percentages of NO_x dissolved into paper mill wastewater with a wide range (from 0.93–28.71%) and the average (12.33%). The maximum transformation rate of NO_x is 2.47% with 0.5% of nitrogen oxide in the ozonized air.

Seen in Figures 1 and 2, as well as in Table 2 and Table 3, concentrations of TN and $\text{NO}_3\text{-N}$ in effluent treated by the ozonation process were higher than in the influent suggesting gaseous NO_x dissolved in wastewater. Dissolved nitrogen produced during the ozonation process will remain in the effluent without final treatment where adsorption and ion exchange can be adopted after ozonation to remove the nitrogen.

DISCUSSION ABOUT FACTORS THAT INFLUENCE DISSOLVED TRANSFORMATION

Variations in concentrations of TN in influent and that in effluent with different ozone dosage (D_o) and different retention time (T_r) are displayed in Table 4 and Table 5, respectively.

Seen in Table 4 and 5, there is no significant relationship between ozone dosage and the percentage of increased TN whereas the amounts of TN increased are raised with the increase in the retention time. It is shown that the concentrations of TN in effluent were increased (0.04~0.13 times higher with different ozone dosage and 0.06~0.38 times higher with different retention time). With the possible reasons that slight variations in ozone dosage and retention time, we would like to find out the dominant reason contributing to the increment of the concentration of TN in the effluents.

However, the variations in the concentrations due to two potential factors were different. The percentages of TN increased could be significantly varied with slight variations in retention time, when the dosage changed. Also, the values of the effluent/influent in Table 4 were fluctuated while the values of that in Table 5 were changed steadily. For a better understanding, here shows an example based on the data from the second and third row in Table 4. With the increased dosage (from 65.11–72.15 mg/L), the concentration of TN was however reduced by 6.19%, which was because the retention time was reduced by 1.37%. But in Table 5, small variations in the dosage would not lead to large changes in the effluent/influent of TN increased with varied retention time. The reason why the concentration of dissolved NO_x were greatly affected by retention time instead of ozone dosage is that the variation in the amount of TN was caused by dissolution of NO_x generated by the air-fed ozonizers.

The increment of $\text{NO}_3\text{-N}$ in the wastewater can be affected by the raw water quality, its concentration, ozone dosage and retention time. Although temperature can also contribute to the increase, it can be neglected in this study based on the data shown above. However, the gas retention time, water depth that was presented by the water retention time, the pressure in the scrubber, dosage of ozone, cleanness of the diffuser, wastewater temperature and water quality can affect the variation in the amount of dissolved NO_x .

In this study, the main factors contributing to the variations in nitrogen contents can be retention time, ozone dosage, water types and its concentration (shown in a decreasing order). Specially, the retention time and

Table 3. Variations in Nitrogen Content in Influent and Effluents Treated by Ozonation.

Reduction of Organic Nitrogen	Increment of NO ₃ -N	Increment of NH ₃ -N	A – C	B – D	E/B	E/7
A (mg/L)	B (mg/L)	C (mg/L)	D (mg/L)	E (mg/L)	(%)	(%)
1.232	0.925	1.00	0.232	0.693	0.7492	0.0990
3.413	2.778	0.70	2.713	0.065	0.0234	0.0093
2.102	2.400	0.10	2.002	0.398	0.1658	0.0569
0.615	2.230	0.20	0.415	1.815	0.8139	0.2593
1.402	1.163	1.00	0.402	0.761	0.6543	0.1087
0.945	1.060	0.60	0.345	0.715	0.6745	0.1021
1.343	2.433	0.20	1.143	1.290	0.5302	0.1843
1.120	3.030	0.10	1.020	2.010	0.6634	0.2871
2.407	2.625	0.20	2.207	0.418	0.1592	0.0597
1.041	1.465	0.60	0.441	1.024	0.6990	0.1463
1.404	1.778	0.80	0.604	1.174	0.6603	0.1677
0.505	1.410	0.30	0.205	1.205	0.8546	0.1721
0.810	1.343	0.10	0.710	0.633	0.4713	0.0904
1.140	1.515	0.20	0.940	0.575	0.3795	0.0821
1.465	1.398	0.40	1.065	0.333	0.2382	0.0476
1.358	1.418	0.30	1.058	0.360	0.2539	0.0514
1.313	1.688	0.40	0.913	0.775	0.4591	0.1107
1.397	1.590	0.30	1.097	0.493	0.3101	0.0704
1.785	1.635	0.60	1.185	0.450	0.2752	0.0643
0.382	0.290	0.29	0.092	0.198	0.6828	0.0283
0.485	0.585	0.30	0.185	0.400	0.6838	0.0571
0.770	0.618	0.30	0.470	0.148	0.2395	0.0211
0.280	0.650	0.20	0.080	0.570	0.8769	0.0814
0.708	0.853	0.40	0.308	0.545	0.6389	0.0779
1.380	1.385	0.50	0.880	0.505	0.3646	0.0721
0.855	1.075	0.50	0.355	0.720	0.6698	0.1029

Notes:

^aA, “reduction of organic nitrogen”, is the difference of organic nitrogen concentration in the influent and effluent, A= [(concentration of TN in influent – sum of concentrations of NH₃-N and NO₃-N in influent) – (concentration of TN in effluent – sum of concentrations of NH₃-N and NO₃-N in effluent)],

^bA – C, “amount of organic nitrogen oxidized to NO₃-N”, difference of organic nitrogen reduction and concentration of NH₃-N,

^cB – D, “amount of NO₃-N dissolved”, difference of total increment of NO₃-N and amount of organic nitrogen oxidized to NO₃-N,

^dE/B is percentage of increased amount of dissolved NO₃-N accounted for total increment of NO₃-N, and

^eE/7 equals value calculated from B – D divided by 7 mg/L, theoretical concentration of nitrogen in water.

Table 4. Variations in Concentrations of TN in Influent and in Effluent with Different Ozone Dosage.

D _o , mg/L	TN, mg/L			T _r , hr
	influent	effluent	effluent/influent	
63.58	5.08	5.66	1.11	2.15
65.11	4.90	5.53	1.13	2.18
72.15	5.84	6.17	1.06	2.15
85.48	4.29	4.82	1.12	2.19
97.66	5.15	5.51	1.07	2.14
107.3	5.27	5.76	1.09	2.18
118.8	6.98	7.27	1.04	2.13
126.7	6.61	7.06	1.07	2.17
137.3	6.87	7.44	1.08	2.18
145.2	6.85	7.41	1.08	2.18
148.7	6.76	7.32	1.08	2.18
149.6	7.38	7.92	1.07	2.18

Table 5. Variations in Concentrations of TN in Influent and in Effluent with Different Retention Time.

T _r , hr	TN, mg/L			D _o , mg/L
	influent	effluent	effluent/influent	
0.62	10.4	10.98	1.06	245
1.09	8.77	10.06	1.15	250
1.31	8.58	10.25	1.20	250
1.54	6.70	8.14	1.22	245
1.96	8.09	10.86	1.34	206
2.18	7.64	10.32	1.35	240
2.40	6.40	8.82	1.38	222

ozone dosage affected the variations in nitrogen content directly, which were associated with the amount of dissolved nitrogen, raw water quality and its concentrations. Those factors can contribute to the variations in the amounts of nitrogen dissolved.

CONCLUSIONS

The concentrations of TN in the effluents treated by the ozonation process were higher than the concentrations in the influents (0.01~0.38 times higher). Together, the concentrations of NO₃-N in the effluents were also higher than the concentrations in the influents with the increased percentage ranging from 36.0–294.9% with the average, 226.8%.

NO_x by-products produced by air-fed ozonizers, could be dissolved into the wastewater during ozonation process to cause the increase in the concentrations of NO₃-N (0.065~2.010 mg/L) with the percentages of the total increment ranging from 2.34–87.60% and the average, 47.10%.

Using the experiment data facilitating with theoretical calculation, the transfer rates of NO_x dissolved were obtained (0.93~28.71%) with the average, 12.33%. And the transformation could be mainly affected by the retention time, ozone dosage, raw water quality and its concentration (listed in a decreasing order).

ACKNOWLEDGEMENTS

We would like to thank our supporters from the programme, Research and Demonstration of Key Technology on Advanced Purification and Reuse of Straw Pulping and Paper Mill Wastewater (No.2009ZX07210-002-001). This study is a sub-project of the National Science and Technology Major Project of the Eleventh Five-Year Plan in water pollution control and management technology.

REFERENCES

1. Tatianne Ferreira D. O., Olivier C., Benoit C., Henri F., Degradation kinetics of DEP in water by ozone/activated carbon process: Influence of pH, *Desalination*, Vol. 269, No. 1, 2011, pp. 271–275.
2. Yaal L., Hadas M., Ines Z., Dror A., Treating wastewater from a pharmaceutical formulation facility by biological process and ozone, *Water Research*, Vol. 47, No. 13, 2013, pp. 4349–4356. <http://dx.doi.org/10.1016/j.watres.2013.04.059>
3. Noemi M., Daphne H., Laura B., Luis C., Angeles B., Assessing the application of advanced oxidation processes, and their combination with biological treatment, to effluents from pulp and paper industry, *J. Hazardous Materials*, Vol. 262, No. 15, 2013, pp. 420–427.
4. Yagi S., Tanaka M., Mechanism of ozone generation in air-fed ozonizers, *J. Physics & Applied Physics*, Vol. 12, No. 9, 1979, pp. 1509–1520. <http://dx.doi.org/10.1088/0022-3727/12/9/013>
5. Fendel W., Mater D., Burtscher H., Schmidt-Ott A., Interaction between carbon or iron aerosol particles and ozone, *Atmosphere Environment*, Vol. 29, No. 9, 1995, pp. 967–973. [http://dx.doi.org/10.1016/1352-2310\(95\)00038-Z](http://dx.doi.org/10.1016/1352-2310(95)00038-Z)
6. Pekarek S., Rosenkranz J., Ozone and nitrogen oxides generation in gas flow enhanced hollow needle to plate discharge in air, *J. Ozone Science & Engineering*, Vol. 24, No. 3, 2002, pp. 221–226. <http://dx.doi.org/10.1080/01919510208901613>
7. Wu C. D., Zheng L. H., Chu J. Y., Research on ozone generation by discharge in Air, *High Voltage Engineering*, Vol. 30, No. 7, 2004, pp. 50–52.
8. Braun D., Kuchler U., Pietsch G., Behaviour of NO_x in air-fed ozonizers, *Pure & Applied Chemical*, Vol. 60, No. 5, 1988, pp. 741–746. <http://dx.doi.org/10.1351/pac198860050741>
9. Ge Z. L., Wu Y. R., Study on Technological improvement of industrial ozone generator, *High Voltage Engineering*, Vol. 25, No. 3, 1999, pp. 66–67.
10. Tripathi S., Pathak V., Tripathi D. M., Tripathi B. D., Application of ozone based treatments of secondary effluents, *Bioresource Technology*, Vol. 102, No. 3, 2011, pp. 2481–2486. <http://dx.doi.org/10.1016/j.biortech.2010.11.028>
11. Czerwionka K., Makinia J., Pagilla K. R., Stensel H. D., Characteristics and fate of organic nitrogen in municipal biological nutrient removal wastewater treatment plants, *Water Resource*, Vol. 46, No. 7, 2012, pp. 2057–2066. <http://dx.doi.org/10.1016/j.watres.2012.01.020>
12. Zeng K., Huang L. J., Hao T. L., Zhang H. C., Cui Y. P., Research of puny oxidation by ozone to the aerobic effluent of papering wastewater, *Environment Pollution & Control*, Vol. 36, No. 7, 2014, pp. 5–8.
13. Winter J., Dünnbier M., Schmidt-Bleker A., Meshchanov A., Reuter S., Weltmann K. D., Aspects of UV-absorption spectroscopy on ozone in effluents of plasma jets operated in air, *J. Physics & Applied Physics*, Vol. 45, No. 38, 2012, pp. 26–29. <http://dx.doi.org/10.1088/0022-3727/45/38/385201>
14. State environmental protection administration of China. 2002. *Monitoring and analytic methods of water and wastewater* (4th ed.), Beijing, Environmental Science Press of China.
15. Hao T. L. 2013. The experimental study of wheat straw pulp and paper wastewater secondary effluent by ozone oxidation, MS thesis, Zhengzhou University, Zhengzhou, China.
16. Zeng K., Cui Y. P., Hao T. L., Zhang H. C., Huang L. J., Nitrogen transformation in ozonation of effluent from a paper-mill wastewater treatment plant, *Environment Science & Technology*, Vol. 37, No. 12, 2014, pp. 209–213
17. Zhang K. S., Li J., Guo Z. H., Xin F., Zhang J. S., Influence of preozonation process on ammonia nitrogen in drinking water treatment, *China Water & Wastewater*, Vol. 21, No. 8, 2005, pp. 41–43.
18. Liu H. L., Wang X. W., Jiao R. Y., Li Z. J., Yang H., Cheng F. Q., Output and control of nitrogen oxides produced by household ozone generator as by-products, *J. Environment Health*, Vol. 26, No. 3, 2009, pp. 235–236.
19. Yang G., Xu X. W., Gao L. L., Li B. R., Characteristics of isovolumetric charging and releasing of high-pressure gas, *J. Lanzhou University Technology*, Vol.36, No. 3, 2010, pp. 42–46.

Pyrolysis and Carbocoal Characteristics for Biophysical Drying Sewage Sludge

TAO ZHU^{1,2,*}, XIAOYANG LI¹, WENJING ZHANG^{3,*}, WENJUAN ZHAO¹, NI XIA¹ and XIAOJIA WANG¹

¹School of Chemical & Environmental Engineering, China University of Mining & Technology (Beijing), Beijing 100083, China

²State Key Laboratory of Coal Resources and Safe Mining (CUMTB), Beijing 100083, China

³Chinese Academy for Environmental Planning, 100012 Beijing, China

ABSTRACT: With the sewage sludge yield increasing, the sludge treatment becomes a major problem in China. The pyrolysis technology is used to treat the sewage sludge, because of a lot of advantages, such as good economic returns, the less secondary pollution and the higher utilize value of pyrolysis products. And it is considered as one of the great potential thermo-chemical treatment technology. A series of experiments were carried out to study the biophysics of drying sludge and how to get the variation of production gas, oil and coke at the different pyrolysis temperatures. Also, how to obtain high-value pyrolysis products at optimum pyrolysis temperature. At the same time, by studying the biophysical drying sludge's char formation mechanisms and physico-chemical properties at the different pyrolysis temperature conditions, the indirect reference data for pyrolysis of sludge were provided. It is providing theoretical guidance for the safe disposal of sludge, through sequential extraction method of European Communities Bureau of Reference (BCR) exploring different forms of semi-coke in the enrichment of heavy metals.

INTRODUCTION

SLUDGE is the major by-product from urban sewage treatment plants. Mud cake has a high moisture content (80 wt%), high organic content, inorganic mineral and more compact structure, and so on [1]. There will be significant environmental risks if we cannot effectively deal with these solid wastes. Sludge amounts were increasing more than 10% every year in China which creates a significant problem for Chinese sewage treatment industry and municipal administration. Sludge pyrolysis is considered to be one of potential thermochemical treatment technology, because of its good economic returns, less secondary pollution, high use value of pyrolysis products, and so on. Sludge pyrolysis remains at the experimental stage in China.

Shen [2] got the pyrolysis temperatures, which were between 300–600°C obtaining the distribution of gas and oil production. The results showed that the maximum oil production rate was 30% at 525°C. When the temperature was higher than 450°C the cracking of heavy oil created a secondary decomposition reaction to become light oil. When the temperature was higher

than 525°C it formed more lightweight oil and gaseous hydrocarbons and gas production increased. Inguanze *et al.* [3] studied pyrolysis temperatures of 450°C, 650°C, and 850°C with heating rates of 5 K/min and 60 K/min. They found that heating rate was very important only for the lower pyrolysis final temperature such as 450°C. At higher pyrolysis temperatures (i.e., more than 650°C) the effects of heating rate would be neglected. At 450°C the improvement of heating rate made pyrolysis more efficient and more pyrolysis oil and pyrolysis gas would be produced.

Piskorz *et al.* [4] took use of fluidized bed reactor to do experiment of the sludge pyrolysis, at the conditions of the final pyrolysis temperature of 450°C, residence time of 0.3 s, 0.5 s, and 1 s. They found that the best time was 0.5 s, and the bio-oil yield was maximum (52 wt%) at this moment. Canadians Kim & Parker [5] studied the influence of different zeolite addition quantity on sludge pyrolysis. The final pyrolysis temperature was 500°C, the results showed when the zeolite addition amount was greater than 0.2 g/g dry sludge, the yield of coke decreased with catalytic amounts increasing, and the changes of tar yield were not obvious. Catalyst added into the reactor, is helpful for promoting the conversion from solid coke to gas, and producing more pyrolysis gas, but little effect on the tar.

*Authors to whom correspondence should be addressed.

E-mail: (Zhu) bamboozt@cumtb.edu.cn; (Zhang) zhangwj@caep.org.cn

About sludge pyrolysis mechanism, some researchers studied pyrolysis production (pyrolysis gas, tar, and coke). Dominguez *et al.* [6] studied the change of pyrolysis gas production in the range of 250–1000°C. They found pyrolysis gas production increased with the pyrolysis temperature increasing at the low temperature stage (< 700°C), and arrived at peak about 700–850°C, and then, reduced significantly along with the temperature rising (> 850°C). The final pyrolysis gases were mainly H₂, CO, CH₄ and the other gas composition of high calorific value. Lutz *et al.* [7] obtained the calorific value of tar which is 35–38 kJ/mol, dealing with sludge by the low temperature pyrolysis treatment. And the main compositions of tar were pentadecane and heptadecane, which belonged to heavy oil. Tay *et al.* [8] studied adsorption characteristics of phenol using sludge pyrolysis coke activated by ZnCl₂. They pointed out that absorbent BET surface area was 867.61 m²/g at 500°C for 2 hrs.

The current researches about the sludge pyrolysis mechanism are rare. In this paper, we adopt biophysical drying sludge to carry out a series of experiments in order to realize sludge harmless utilization and disposal. Our aims focuses on how to realize biophysics drying sludge to obtain high-value pyrolysis products at optimum pyrolysis temperature in the pyrolysis process, and how to decrease the environmental risk from heavy metal of the pyrolysis treatment of biophysics drying sludge.

MATERIALS AND METHODS

Experimental Materials

The pyrolytic raw material uses a biophysical drying sludge. Sludge, which is from Beijing Qinghe sewage treatment plant, is treated with in belt filter press processing. Sewage sludge was dried in 159L vertical tubular reactor (height of 1000 mm, inner diameter 450 mm) by short-term warming-intensified ventilation dehydrated biophysical drying effect. The physical and chemical properties of pyrolysis raw materials are send in Table 1 and Table 2.

Table 2. Thermal Drying Sludge and Biological Physics Drying Sludge Element Analysis.

Elemental Analysis (wt.%,d)	C	H	N	S	O
Biological and physical drying sludge	24.30	3.54	2.30	0.66	18.92

Experimental Apparatus and Instruments

The fast pyrolysis experiment device is shown in Figure 1. It mainly consists of the carrier gas systems, pyrolysis system, gas condensation system, the gas volume measurement and collection system. The carrier gas system includes cylinders and mass flowmeter, which fill the high purity nitrogen to provide an inert atmosphere. The pyrolysis system includes a horizontal tube resistance furnace, quartz tube and the console. The horizontal tube resistance furnace is controlled by the console, and its rated power is 4 kW and its maximum rated temperature is 1,000°C. Quartz tube is placed on the central axis in the furnace. When the temperature of the furnace achieves the established temperature, we immediately pushed the sample into the quartz tube by porcelain boat. The gas condensation system includes primary condenser (spherical condenser pipe), after-condenser (snakelike condenser pipe and cotton filter tube) and gas-washing bottle. Then the coke particles were removed by filtering and washing after the twice condensation for attaining purification pyrolysis gas. Gas volume metering and collection system includes electronic mass flowmeter and gas collection bag. The gas after purification was collected into this system to detect.

Experimental Methods

The 3.0 g biophysical drying sludge sample was put into the porcelain boat, and then the porcelain boat was put into the quartz tube. Bubbling into 30 ml/min high purity nitrogen, and purging 40 min to let air out in the experimental device for keeping inert atmosphere in the furnace. Adjusting the horizontal tube furnace, and letting the temperature increase to the preset temperature, we adjusted the high purity nitrogen flowing

Table 1. Biophysical Drying Sludge Industrial Analysis.

Proximate Analysis	Received Base Water (wt.%, d)	Volatiles (wt.%, d)	Ash Content (wt.%, d)	Fixed Carbon (wt.%, d)	Lower Calorific Value (kcal/kg, d)
Biological and physical drying sludge	4.56	43.09	48.47	3.89	2282.54

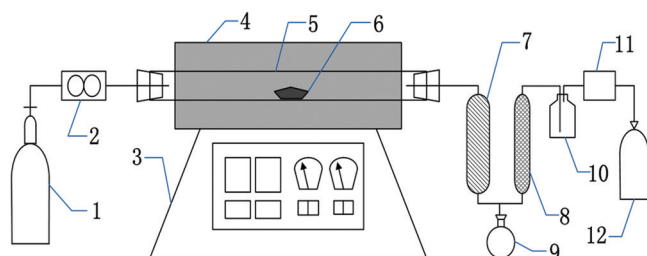


Figure 1. Pyrolysis experiment device. 1–Nitrogen gas cylinder; 2–Mass flowmeter; 3–Console; 4–Horizontal tube furnace; 5–Quartz tube; 6–Porcelain boat; 7–Primary condenser; 8–After-condenser; 9–Round-bottom flask; 10–Gas-washing bottle; 11–The gas flow totalizer; 12–Air pocket

down to 3 ml/min, and quickly put porcelain boat into the middle reaction area of tube furnace to pyrolysis. Then we continued to turn down nitrogen flowing to 0 ml/min. The reaction gaseous product volume was metered by electronic flowmeter. Next, we stopped heating after 20 min, and adjusted the high purity nitrogen flow to 30 ml/min, and kept on purging 40 min, and collecting purge gas at the same time. After cooling the reaction system, we took the porcelain boat and weighted it to obtain carbocoal quality by means of difference heavy method.

Pyrolysis gas is mainly composed of hydrogen, oxygen, methane, carbon dioxide, in addition to a certain amount of ethane, ethylene, propane, propylene and acetylene, etc. Gas quality is calculated according to the volume of gas and all kinds of gas composition contents. The yield of liquid tar is calculated by weighing the condensation system before and after the reaction, while the solid carbocoal is calculated according to the weight difference before and after the porcelain boat reaction.

ASAP2010 specific surface area and pore size analyzer from American Micrometrics Company was used to measure the coke pore structure parameters. The pore size measurement ranges from 1.7–300 nm, and the relative pressure P/P_0 ranges from 0.01–0.995. We used scanning electron microscope (SEM) to analyze the pyrolysis coke surface, so as to understand the volatile changes in the precipitation process and the pyrolysis coke pore structure.

RESULTS AND DISCUSSION

Influence of Temperature on Yield of Pyrolysis Products

The main pyrolysis products of biophysical drying sludge are divided into three parts: solid carbocoal, tar and pyrolysis gas. When pyrolysis temperature

changed, the output of three kinds of products changed. At relatively high pyrolysis temperature, macromolecular substances of the tar and solid carbocoal would decompose into small molecule gaseous products, so that the yields of semi-coke and tar decline and the gas products increase. For this reason, lower pyrolysis temperature is more appropriate for generating solid carbocoal [9]. The yields of gas, oil and coke of biophysical drying sludge with the change of temperature is seen in Figure 2.

Seen in Figure 2 along with the pyrolysis reaction temperature increasing, the yields of pyrolysis semi-coke of biophysical drying sludge decrease from 65.38–57.95 wt% at 850°C. When the temperature arrives at 900°C, the yields of semi-coke increase slightly. The yields of tar decrease significantly with the temperature increasing from 450–600°C. When the temperature is higher than 600°C, the yields of tar decline slightly. The yields of pyrolysis gas follow the same rule to tar yields, and the highest value of pyrolysis is 35.11% at 850°C. The above experimental phenomena described that organics and secondary pyrolysis for generating tar of biophysical drying sludge can be completely proceeded above 600°C. When the pyrolysis temperature is 450–600°C, the pyrolysis of sludge is not complete. Even if the reactions stop, there are still some organics for further decomposition in the solid carbocoal and tar. Thus, where there is the higher temperature there is the more gas production and less tar yield. When the reaction temperature surpasses 600°C, the increasing trends of gas production change slightly. It means when the pyrolysis temperature is

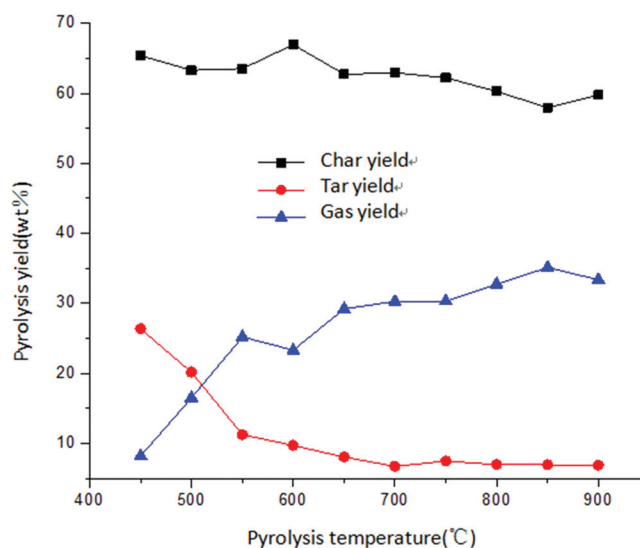


Figure 2. Pyrolysis products yield of biophysical drying sludge (wt %).

above 600°C, almost all the cleavable organic matter in semi-coke and tar involve in pyrolysis reaction, and the higher temperature will not improve the condition of the pyrolysis. However, at this time, the gas production increases and the yields of semi-coke and tar decline. The endothermic reaction between water, carbon dioxide in gas production and organics in tar and semi-coke strengthen with increasing temperature.

Evolutionary Changes of Surface Area, Pore Volume, and Pore Size of Semi-coke at Different Pyrolysis Temperatures

Semi-coke is a major media material to pyrolysis reaction and transformation process. In this experiment, the pyrolysis coke at temperatures 500°C, 600°C, 700°C, 800°C, and 900°C were detected and analyzed.

The Brunauer, Emmett, Teller's (BET) model was used to calculate the surface area of char in this experiment. ASAP 2010 was used to analyze the original sludge and the coke obtained at the pyrolysis temperature 500°C, 600°C, 700°C, 800°C, and 900°C, and IUPAU classification method was selected to analyze the hole. Table 3 includes information of BET specific surface area, the total pore volume and average pore size parameters of semi-coke. Taking the semi-coke particles and Biophysics drying sludge for comparison, it can be found that in general, the pyrolysis can effectively increase the pore volume and reduce the pore size. With the temperature increasing, the total pore volume of semi-coke increases. But when the temperature is changing from 500–900°C, the pore size remains almost stable, and this is related to the prior analysis of the mesopore's formation. In addition, it can be seen from Table 3 that the surface area of the char is small (3.105 m²/g under 500°C) at low temperatures. However the temperature rises to 800°C, the surface area grows up to a maximum of 30.503 m²/g. This may due to the release of gas. And when the temperature rises to 900°C, the surface area decreases to some extent.

Table 3. Parameters of Coke.

Sample	Specific Surface Area (m ² /g)	Pore Volume (cm ³ /g)	Pore Size (nm)
Original Sample	0.70	0.0034	16.03
500°C char	3.105	0.023	3.784
600°C char	19.187	0.034	3.828
700°C char	24.104	0.036	3.827
800°C char	30.503	0.049	3.829
900°C char	30.068	0.057	3.819

The specific surface area of semi-coke decreasing at 900°C, may be related to the phenomena of semi-coke compaction and melting.

Microstructure Analysis of Semi-coke

Figure 3 shows the SEM morphology photograph of pyrolysis coke particles from 300–900°C, and by the SEM images, we can be more intuitively understanding of the char pore structure characteristics. Figure 5 is a high magnification photo (×1000) of coke, it can be seen from these pictures that the pore size becomes larger, and the pore structure becomes complicated (identical to the BET model results anastomosis in previous section) with the pyrolysis temperature increasing. The coke surface changes from the beginning relatively flat layered structure to scattered particulate. Its surface becomes more rough and irregular, and the number of pits and round holes significantly increase. Especially at the temperature of 800–900°C, the molten or sintering phenomenon of semi-coke occurs. The channel and pits left during pyrolysis are much larger than that around the holes. There is a large amount of volatile gathering at some pyrolysis stage, and ultimately discharged in the form of bubbles [12]. Therefore, volatile take very irregular paths in the precipitation process to form irregular hole channels.

Elemental Qualitative Analysis of SEM Images for Semi-coke Surface

As the pyrolysis temperature gradually increased from 300–900°C, certain elements of coke have some regular changes. From Table 4, C element content decreases with the temperature increasing, while the O element content has an increasing trend. And Mg, Al, Fe, Ca contents all increase with the temperature increasing. This may be the result of relative increasing of the precipitation and volatile ash.

C, H, O, N, and S Elemental Variation at Different Temperatures

Figure 4 reflect the variation of five elements of C, H, O, N, S by CE-440 quantitative analysis at different temperatures.

Seen in Figure 4, the amounts of four elements of C, H, N, O have a decreasing trend with pyrolysis reaction temperature increasing. The hydrogen content is zero when the pyrolysis temperature is above 850°C. It indicates that, the existing form of semi-coke is basically

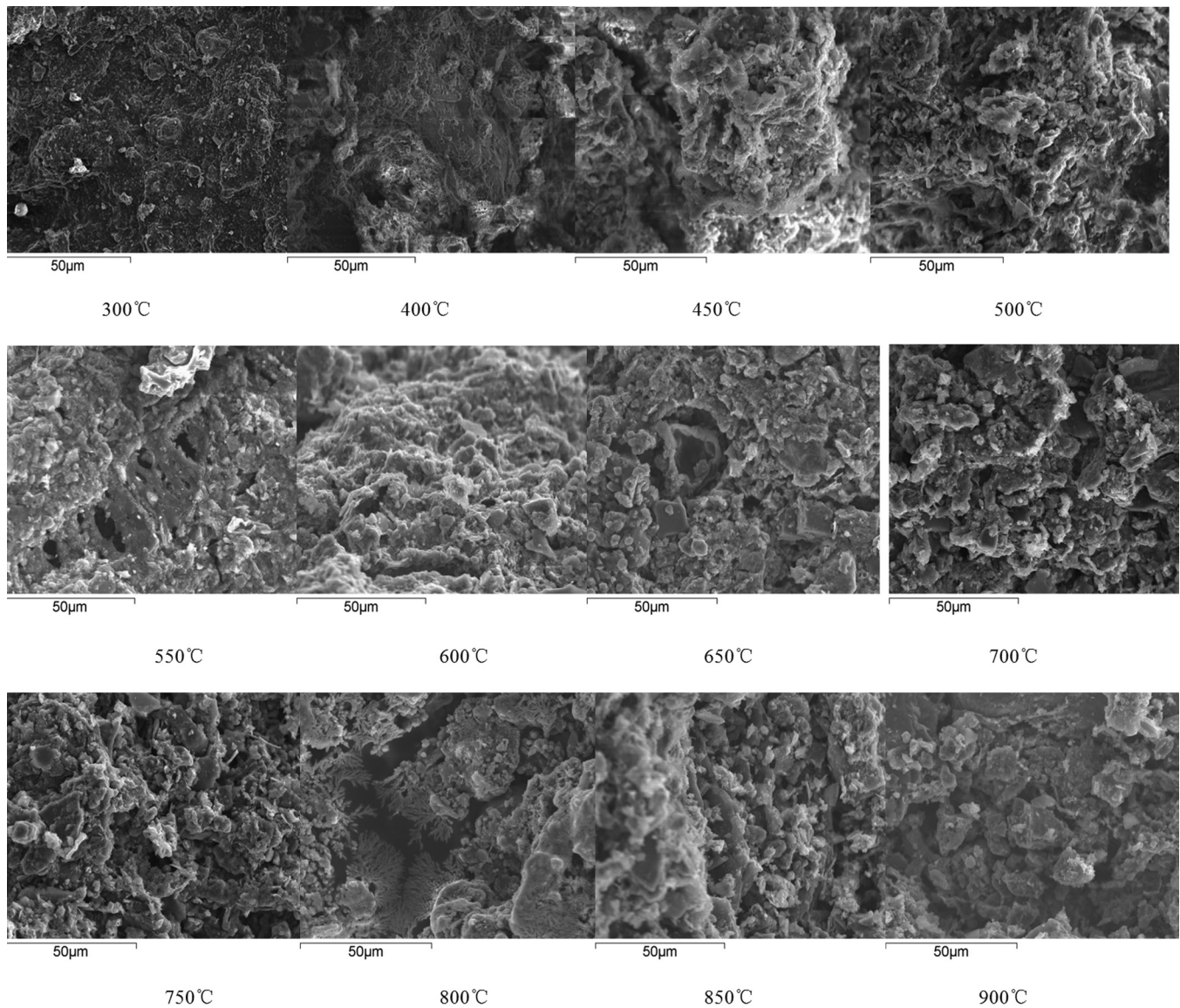


Figure 3. SEM scanning images at different temperatures.

carbon coke and the organic matter in the sludge pyrolysis completely at the pyrolysis reaction temperature of 850°C. Therefore, the ideal conditions for hydrogen production are the pyrolysis temperature above 800°C.

Nitrogen in inorganic substances in sludge mainly exists in the form of nitrate, but in the organic matter, it mainly presents in proteins and amino acids. In the pyrolysis process, the nitrogen is converted to ammonia, hydrogen cyanide, nitrogen oxides, nitrogen, and organic nitrogen. With the pyrolysis temperature increasing, nitrogen contents of the semi-coke decrease. It indicates that the protein, amino acids and other organic matter are fully decomposed at high temperatures.

Oxygen contents reduce with the pyrolysis temperature increasing. Because the pyrolysis reactions of tar,

aggravated carbocoal are more thorough at higher pyrolysis temperature.

Sulfur contents first increase and then decrease with the pyrolysis temperature increasing. This is because the pyrolysis reaction of sulfur-containing organic compounds becomes gradually strengthened with the pyrolysis temperature increasing, resulting in the decreasing of sulfur at lower pyrolysis temperature. When the pyrolysis temperature increases to a certain extent, the pyrolysis reaction can completely reacted and all the sulfur can be removed from the semi-coke. However, the gaseous products of coke and semi-coke can continuously react, so that the semi-coke yield will decrease with increasing temperature, resulting in slightly higher sulfur content.

Table 4. Surface Element Content of Semi-coke Under Three Different Pyrolysis Temperatures.

Temperature, °C	300°C	400°C	500°C	650°C	800°C	900°C
Element	Weight %					
C	55.1	48.42	34.05	36.03	26.01	30.97
O	25.47	29.87	35.76	31.47	36.51	31.39
Na	0.35	0	0	0.26	1.1	0.47
Mg	0.66	1.01	1.15	0.58	1.93	2.23
Al	1.75	2.25	3.44	2.69	5.22	5.25
Si	5.21	5.15	9.19	16.07	1.05	8.97
P	1.96	3.26	3.79	1.55	0.95	3.86
S	1.5	0.57	0.51	0.59	0.49	1.63
K	1.04	0.93	1.26	1.3	0.91	1.31
Ca	5.16	6.04	5.66	6.34	22.36	22.53
Fe	1.79	2.5	5.19	3.12	3.47	5.4
Total	100	100	100	100	100	100

Change Rules of Semi-coke Characteristic Functional Groups with Different Pyrolysis Temperature

Sludge pyrolysis follows the general rules of organic matters, that is, when the heating temperature rises to a certain level, the corresponding chemical bond will break, and the volatile gas precipitates. The kind of semi-coke group types of solid carbocoal at different temperatures is analyzed by FTIR spectra (Fourier Transform Infrared Spectrometer), in order to explore the reasons for pyrolysis effect change at different temperature, and the results are seen in Figure 5.

Vibration peaks at about wave number of $3,200\sim 3,600\text{ cm}^{-1}$ are the stretching vibration peaks of hydroxyl OH bond (alcohols, phenols), and amine hydrogen-nitrogen bond in semi-coke. Their height reflects the dehydrogenation effect during char pyrolysis. It can be seen that, the peak height decreases with the

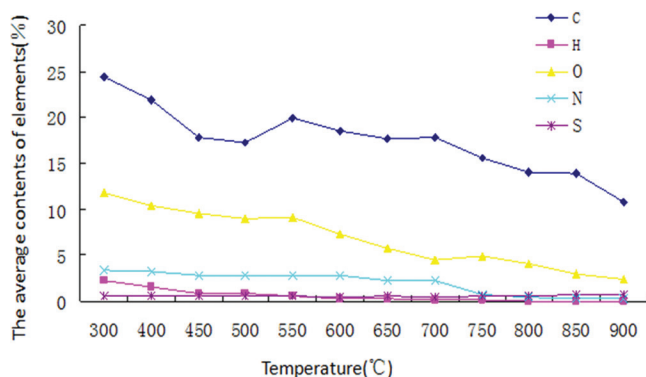


Figure 4. Different variations of elements in the semi-coke at different temperature.

temperature increasing. It means that dehydrogenation process of the biophysical dry sludge pyrolysis is strengthened with increasing temperature. It is obvious that high pyrolysis temperature is benefit to produce hydrogen.

Twin peaks at wavenumber of $2,800\sim 3,000\text{ cm}^{-1}$ are respectively the carbon-hydrogen bonds (alkanes) symmetric and asymmetric stretching vibration of methyl in semi-coke. The bimodal disappear when the pyrolysis reaction temperature is above 500°C , and the vibration intensity changed little when the pyrolysis reaction temperature is lower than 500°C . This phenomenon indicates that pyrolysis reaction of the organics is not violent below 500°C , even the methyl at the end of the carbon skeleton cannot be completely removed. This is further evidence of the fact that pyrolysis gas increases when the pyrolysis

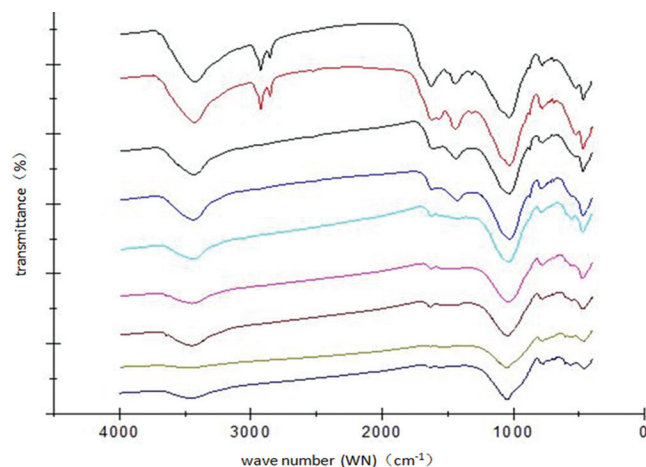


Figure 5. FTIR spectra pyrolysis char at different temperatures.

reactions are enhanced with the pyrolysis temperature increasing below 600°C.

The vibrational peaks at wavenumber of 1,400~1,450 cm^{-1} are the scissor vibration of carbon-hydrogen bonds on the secondary carbon, and the vibration is gradually decreased with the temperature increasing, and disappears when the pyrolysis temperature goes up to 700°C. It suggests that the pyrolysis of organic matter is more complete with the temperature increasing, and almost complete decomposition at 600~700°C, even the hydrogen in the middle of the carbon skeleton on the secondary carbon has been largely removed. This is further evidence that when the pyrolysis temperature is higher than 600°C, organic matter in solid carbocoal will pyrolysis entirely.

Regularity of Heavy Metal Enrichment

We take 0.5 g raw sludge and pyrolysis coke at 300°C, 400°C, 450°C, 500°C, 600°C, 650°C, 700°C, 750°C, 800°C, 900°C respectively, and select sequential extraction BCR process [13], which consists of the following three steps and one additional step [14] and the second step of the process is corrected. G. Rauret improved the BCR four steps, and used 0.5 mol/L of $\text{NH}_2\text{OH} \cdot \text{HCl}$ to substitute 0.1 mol/L of $\text{NH}_2\text{OH} \cdot \text{HCl}$ in the second step, and the acidity was adjusted to $\text{pH} = 1.5$. This method is called the modified BCR method [15].

Table 5 shows the original contents of heavy metals in sludge, and sludge samples contain relatively more Zn and Pb, and less Cu and Cr. Heavy metals in the sludge exist in four main forms [16]: exchangeable, reduction state, oxidation state and residuals, which are precisely corresponding to four samples of each step in BCR extraction system. According to BCR sequential extraction scheme, some representatives of the exchangeable section are metal in ionic form and combination of carbonate, such form of metal has strong ability of migration, and when the acidity of surrounding environment changes, the exchangeable sections quickly release into the environment and can be used by creatures. Some representatives of reduced state are iron and manganese oxides combined amorphous part

metal of hydroxides. Some representatives of the oxidation are combined organic matter and sulfide metal; these two forms may be indirectly used by plants. The representatives of residue are combine with silicate crystals, crystalline iron and part of the manganese oxides metals [14,16], which are difficult to be released under natural conditions, and are difficult to be used by organisms [16,17]. By exploring the amounts of Cr, Cu, Pb and Zn in semi-coke, we discussed the variation of different forms of heavy metals. With the above modified BCR sequential extraction process, the resulting data are uniformed and seen in Figure 6.

Seen in Figure 6(a), Zn in original sludge is mainly in oxidation states. Different forms of Zn in Pyrolysis coke change regularly with temperature changes. From 300–900°C, exchangeable states show a gradual decline, and reduction states show a trend from increasing to decreasing, which peek to a maximum at 600°C. The oxidation states decrease with increasing temperature, while the residuals gradually increase. It describes that there is the higher pyrolysis temperature, the better for Zn to be fixed.

From Figure 6(b), Pb in original sludge is mainly in oxidation states. The forms of Pb vary greatly in pyrolysis coke in different temperature. From 300–600°C, the residual states of Pb increase and oxidation state decrease, while the oxidation states increase and the residual states reduce from 600–900°C. For Pb fixed, the best pyrolysis temperature is 600°C. That could prevent Pb migrating into the environment and causing environmental harm.

In Figure 6(c), Cu in original sludge is mainly in oxidation states [18]. This may be related to the fact that Cu mainly exists on sulfides in nature. The main forms of Cu Pyrolysis carbocoal also change at different temperatures. From 300–500°C, the main forms of Cu are oxidation state, and the oxidation states of Cu increase with temperature increasing. From 500–900°C, the oxidation states of Cu become less, and the residues of Cu increase, and the exchangeable states of Cu increase. At temperature of 850°C, the main forms of Cu become residuals, and the various forms of Cu in coke are almost stabilized. This relates to that the organic matter and Cu can form a stable complex.

As shown in Figure 6(d), Cr in original sludge is mainly in oxidation state, and the forms of Cr changes greatly in the pyrolysis process. When the pyrolysis temperature changes from 300–900°C, the residual states of Cr have a trend from increasing to decreasing. At 750°C, the residuals of Cr in coke reach to the maximum. It indicates that the best pyrolysis temperature is

Table 3. Content of Heavy Metals in Sewage Sludge (mg/g).

Element	Cr	Cu	Pb	Zn
Content (mg/g)	0.060	0.091	0.726	0.768

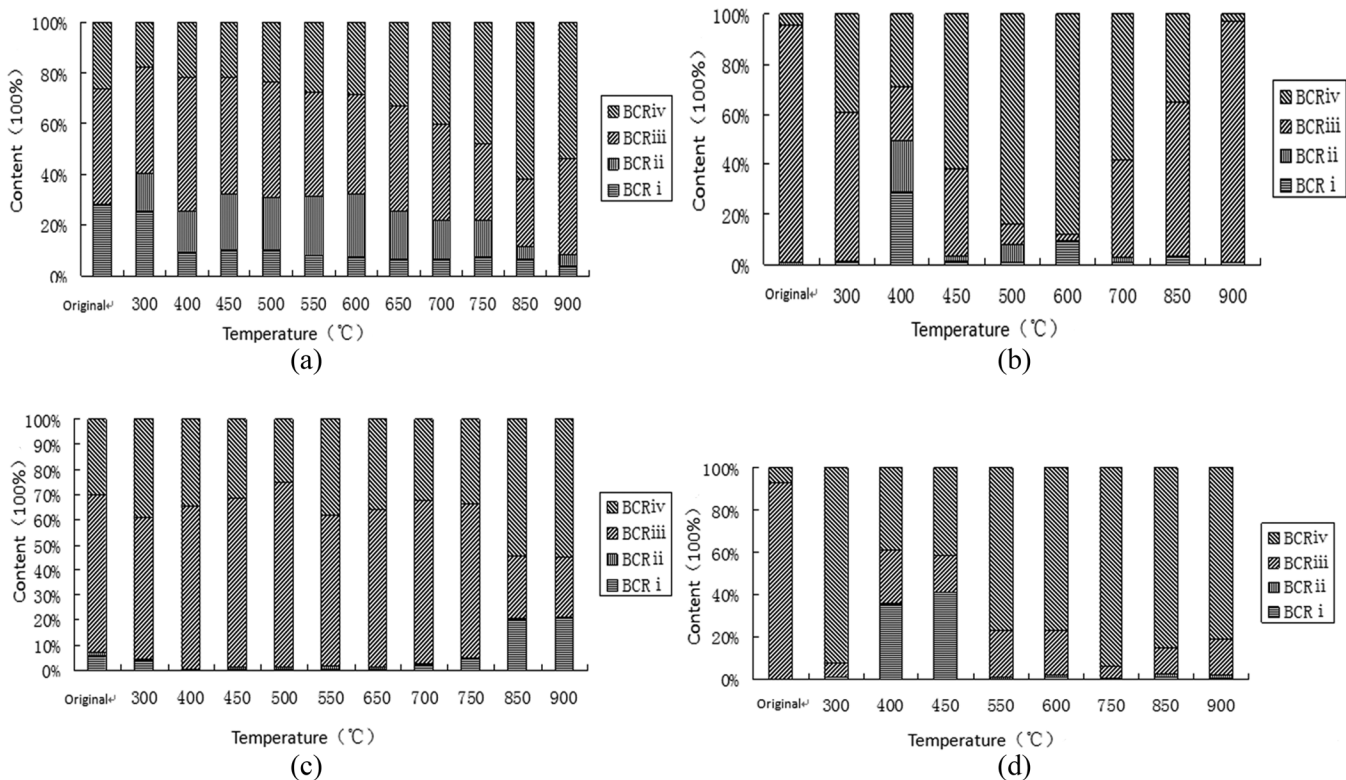


Figure 6. Different forms of heaven metals in char at different temperature. (a) zinc; (b) Pb; (c) Cu; (d) Cr.

750°C in order to avoid Cr contamination. So the higher the temperature is, the more effective for destructing the chemical bonds of Cr.

CONCLUSION

With the pyrolysis temperature increasing, the semi-coke yields decreased, and reached 57.95% at 850°C. When the pyrolysis temperature was 900°C, the semi-coke yields increased slightly. The yields of tar also tended to decreasing, while the pyrolysis gas increased with increasing temperature, and reached to the maximum value of 35.11% at 850°C. When pyrolysis temperature was 600°C almost all of the organics in sludge were involved in the pyrolysis reaction. Then, if kept on increasing the temperature and the energy consumption, the pyrolysis of organic matters were not increased. The original contents of heavy metals in sludge samples contained relatively more Zn and Pb, and less Cu and Cr. Heavy metals in the sludge existed in four main forms: exchangeable, reduction state, oxidation state and residuals. When pyrolysis temperature changed from 300–900°C, exchangeable states showed a gradual decline, and reduction states showed a trend from increasing to decreasing, which

peek to a maximum at 600°C. The oxidation states of Zn decreased with increasing temperature, while the residuals gradually increased. When pyrolysis temperature changed from 300–600°C, the residual states of Pb increased and oxidation state decreased. Then, the oxidation states of Pb increased and the residual states reduced from 600–900°C. For Pb fixed, the best pyrolysis temperature is 600°C. The main forms of Cu are oxidation state, and the oxidation states of Cu increase with temperature increasing from 300–500°C. The oxidation states of Cu become less, and the residues of Cu increased, and the exchangeable states of Cu increased from 500–900°C. At 850°C, the main forms of Cu become residuals, and the various forms of Cu in coke were stabilized. When the pyrolysis temperature changed from 300–900°C, the residual states of Cr had a trend from increasing to decreasing. At 750°C, the residuals of Cr in coke reached to the maximum value.

ACKNOWLEDGEMENTS

This work was supported by Program for New Century Excellent Talents in China (No. NCET120967), and Beijing outstanding talent training project (No. 2012ZG81), and Open Funds of State Key Laboratory

of Coal Resources and Safe Mining(CUMTB) (No. SKLCRSM16KFA04), and the Fundamental Research Funds for the Central Universities (No. 2009QH03). We would like to thank Dr. Annie Zeng at West Virginia University for providing language assistance.

ABBREVIATIONS

BCR – Communities Bureau of Reference
IUPAC – International Union of Pure and Applied Chemistry

ASAP – Automatic Physical Adsorption Instrument

SEM – Scanning Electron Microscope

BET – Brunauer, Emmett, Teller's

FTIR spectra – Fourier Transform Infrared Spectrometer

REFERENCES

- Fullana, J.A. Conesa. (2004) Formation and destruction of chlorinated pollutants during sewage sludge incineration. *Environmental Science and Technology*, 38: 2953–2958. <http://dx.doi.org/10.1021/es034896u>
- Shen L., Zhang D.K. (2003) An experimental study of oil recovery from sewage sludge by low-temperature pyrolysis in a fluidised-bed. *Fuel*, 82(4): 465–472. [http://dx.doi.org/10.1016/S0016-2361\(02\)00294-6](http://dx.doi.org/10.1016/S0016-2361(02)00294-6)
- Inguanzo M., Dominguez A., Menendez J.A. (2002) On the pyrolysis of sewage sludge: The influence of pyrolysis conditions on solid, liquid and gas fractions. *Journal of Analytical and Applied Pyrolysis*, 63(1): 209–222. [http://dx.doi.org/10.1016/S0165-2370\(01\)00155-3](http://dx.doi.org/10.1016/S0165-2370(01)00155-3)
- Piskorz J., Scott D.S., Westerberg I.B. (1986) Flash pyrolysis of sewage sludge. *Industrial & Engineering Chemistry Process Design and Development*, 25(1): 265–270. <http://dx.doi.org/10.1021/i200032a042>
- Kim Y., Parker W. (2008) A technical and economic evaluation of the pyrolysis of sewage sludge for the production of bio-oil. *Biore-source Technology*, 99(5): 1409–1416. <http://dx.doi.org/10.1016/j.biortech.2007.01.056>
- Dominguez A., Menendez J.A., Pis J.J. (2006) Hydrogen rich fuel gas production from the pyrolysis of wet sewage sludge at high temperature. *Journal of Analytical and Applied Pyrolysis*, 77(2): 127–132. <http://dx.doi.org/10.1016/j.jaap.2006.02.003>
- Lutz H., Romeiro G.A., Damasceno R.N. (2000) Low temperature conversion of some Brazilian municipal and industrial sludges. *Biore-source Technology*, 74(2): 103–107. [http://dx.doi.org/10.1016/S0960-8524\(00\)00011-0](http://dx.doi.org/10.1016/S0960-8524(00)00011-0)
- Tay J.H., Chen X.G., Jeyaseelan S. (2001) A comparative study of anaerobically digested and undigested sewage sludges in preparation of activated carbons. *Chemosphere*, 44(1): 53–57. [http://dx.doi.org/10.1016/S0045-6535\(00\)00384-2](http://dx.doi.org/10.1016/S0045-6535(00)00384-2)
- Balat M., Kirtay E., Balat H. (2009) Main routes for the thermo-conversion of biomass into fuels and chemicals. Part I: Pyrolysis systems. *Energy Conversion and Management*, 50: 3147–3157. <http://dx.doi.org/10.1016/j.enconman.2009.08.014>
- Zhixin Fu, Zhancheng Guo. (2007) Experimental study of pore structure of semi-coke temporal and spatial variation—changes in porosity specific surface area and pore size distribution. *Fuel Chemistry Journal*, 35(3): 273–279.
- Sing K.S.W., Everett D.H., Haul R.A.W. (1985) Reporting physisorption data for gas/solid systems, with special reference to the determination of surface area and porosity. *Pure and Applied Chemistry*, 57: 603–619. <http://dx.doi.org/10.1351/pac198557040603>
- Scott S.A., Davidson J.F., Dennis J.S. (2005) The rate of gasification by CO₂ of chars from waste. *Proceedings of the Combustion Institute*, 30(2): 2151–2159. <http://dx.doi.org/10.1016/j.proci.2004.08.061>
- He, Y. D., Zhai Y. B., Li, C. T., Yang F., Chen L., Fan X. P., Peng W.F. and Fu Z.M. (2010) The fate of Cu, Zn, Pb and Cd during the pyrolysis of sewage sludge at different temperatures, *Environmental Technology*, 31: 5, 567–574. <http://dx.doi.org/10.1080/09593330903514466>
- Ure A.M., Quevauviller P.H., Muntau H., and Griepink B. (1993) Speciation of heavy metals in soils and sediments. An account of the improvement and harmonization of extraction techniques undertaken under the auspices of the BCR of the Commission of European Communities. *Int. J. Environ. Anal. Chem.* 51: 135–151. <http://dx.doi.org/10.1080/03067319308027619>
- Rauret G., López-Sánchez J.F., Sahuquillo A. (1999) Improvement of the BCR three step sequential extraction procedure prior to the certification of new sediment and soil reference materials. *J. Environ. Monit. I*: 57–61. <http://dx.doi.org/10.1039/a807854h>
- Tiantian Liu T.T., He B., Wang Y.H. (2007) Improve BCR application in the heavy metal speciation analysis of activated sludge. *Analytical Laboratory*, 26(S1): 17–20.
- Zheng X.X., Cui C.H., Zhou L.X. (2007) The study of heavy metal content and form in the sludge of municipal sewage treatment plant in Jiangsu Province. *Agro-Environment Science*, 26(5): 1982–1987.
- Weisz M., Polyak K., and Hlavay J. (2000) Fractionation of elements in sediment samples collected in rivers and harbors at Lake Balaton and its catchment area, *Microchem. J.* 67: 207–217. [http://dx.doi.org/10.1016/S0026-265X\(00\)00064-3](http://dx.doi.org/10.1016/S0026-265X(00)00064-3)

A Three-Dimensional Model Coupled Mechanical Consolidation and Contaminant Transport

ZHIHONG ZHANG* and YUANFANG FANG

The Key Laboratory of Urban Security and Disaster Engineering of the Ministry of Education and Beijing, Beijing University of Technology, Beijing 100124, China

ABSTRACT: Contaminant transport is a common process for a waste disposal site, which is a practical concern in geo-environmental field. It is essential to study the contaminant transport behavior in impermeable clay liner. Considering the anisotropy of a clay barrier in permeability, a three-dimensional model coupled mechanical consolidation and contaminant transport is developed for simulation of contaminant transport through a deforming porous medium. This is based on the combination of Biot's theory and the theory of contaminant transport. Meanwhile, porosity is viewed as a coupling parameter. The influence of soil consolidation deformation and permeability anisotropy on contaminant transport can thus be determined reasonably. Transport equations are solved by using the finite-element software COMSOL Multiphysics. A parametric study has moreover been conducted to understand the influence of contaminant source types and adsorption modes, including constant contaminated source, attenuation contaminated source, linear adsorption, Freundlich adsorption, Langmuir adsorption. The simulation results indicate that the permeability anisotropy has a negligible effect on contaminant transport, adsorption modes have a significant impact on transport depth and range, and the concentration distribution of contaminant with different contaminated source types have showed a marked difference.

INTRODUCTION

CONTAMINANT contained in leachate can penetrate into the impermeable clay underneath the landfill and induce the pollution of surrounding soil and water which leads to serious negative economic and environment safety consequences. Therefore, it is of paramount importance to know the contaminant transport through clay layer, which can provide some useful advice to plan the remediation of contaminated land, predict the movement of polluted groundwater, design engineered landfills and evaluate the validity of impermeable clay. In order to protect the groundwater from pollution, it is important to understand how the contaminant osmosis conducts through clay and how the migration mechanism affects the contaminant transport. It is worth noting that, owing to the weight of the upper waste dump, the consolidation of soil at the bottom of waste yard can produce, which can lead to compression deformation. Therefore, how to accurately describe the contaminant transport through a deforming clay becomes significant importance.

Many efforts have been devoted to explore the transport of contaminant in a deforming porous medium. Based on a small and large strain analysis of a consolidating soil and conversation of contaminant mass, Smith *et al.* [1] developed a one-dimensional model of contaminant migration through a saturated deforming porous medium, which can be reduced to the familiar classical contaminant transport equation by a certain simplification and selection of suitable parameters. Fox [2,3], Arega [4] and Lewis [5] worked at the experimental and numerical investigation of the effect of clay consolidation on solute transport. In their effort, a one-dimensional mathematical model coupled large strain consolidation and contaminant transport was established based on the large strain consolidation theory. In the work of Fox [6,7], a model coupled large strain consolidation and solute transport is established, verified and simulated, in which the consolidation equation is set as one-dimensional form, and the transport equation is considered two-dimensional form, meanwhile, several transport mechanisms are taken into account, for instance, the convection, longitudinal and transverse dispersion, first-order decay reactions and linear equilibrium sorption. Xue *et al.* [8,9] proposed a gas-hydraulic-solid coupling model that can describe the

*Author to whom correspondence should be addressed.
E-mail: zhangzh2002@126.com

dynamic behavior of settlement and LFG flow in landfill, where after, four models were established of biological-thermo-hydro coupling model of landfill gas migration, hydro-biological-chemical coupling model of leachate migration and transformation in landfill under the effect of aerobe and anaerobe degradation, hydro-chemical coupling model of pollutant migration in composite liner system and thermo-hydro-mechanical coupling model on dry cracking of closure cover system of landfill under the effect of heat quantity changing and vapor migration. Li [10] presented a two-dimensional model of chemo-osmotic consolidation of clays in multi-dimensional domains, with volumetric strains induced by both changes in the chemistry and osmotically driven pore water flow considered. It was found that the consolidation process was dominated by osmotic consolidation in the early stages and subsequently by chemical consolidation. Huang [11] studied the influence of barrier consolidation on transport coefficients, and gave a three-dimensional transport model based on mixture theory for describing the liners that involve circular defects in the geomembrane. Fan *et al.* [12] draw a conclusion that the adsorption of heavy metals presented an order of $\text{Cu}^{2+} > \text{Pb}^{2+} > \text{Zn}^{2+} > \text{Cd}^{2+}$. According to large-scale three-dimensional numerical simulation, Wei [13] researched contaminant migration in groundwater and evaluated the scope of groundwater pollution.

Some progress has been made in coupled consolidation and contaminant transport model for simulating migration of contaminants through a deforming porous medium. Nevertheless, the study on coupled model is still incomplete. Permeability for example is assumed to be isotropy in most of multi-dimensional theoretical model, or the ratio of longitudinal permeability and transverse permeability is assumed to be a constant. Indeed, there appears to be an anisotropy character in natural soil due to the depositional history and develop environment, correspondingly the ratio of longitudinal permeability and transverse permeability will produce change with the soil consolidation. Hence the influence of permeability anisotropy on contaminant transport does not well recognized, and further work thus needs to be conducted.

The aim of the present investigation is to develop a three-dimensional model coupled consolidation and contaminant transport, taking the permeability anisotropy into account, and the porosity is viewed as the coupled parameter. The finite-element software COMSOL Multiphysics is employed to solve the transport equations. A parametric study has been conducted to

understand the influence of contaminant source types and adsorption modes, including constant source, attenuation source, linear adsorption, Freundlich adsorption, Langmuir adsorption.

THEORETICAL MECHANISMS FOR COUPLED MODEL

Basic Assumption

1. The soil is saturated, small deformation and linear elastic homogeneous continuum.
2. The soil particles and pore water are incompressible.
3. Seepage obeys the Darcy's law.
4. The main direction of seepage velocity keeps in line with coordinates.
5. The flow field is uniform and steady.

Biot's Consolidation Equation

According to the Biot's consolidation theory the following equations can be obtained.

$$\begin{cases} -G\nabla^2 w_x - \frac{G}{1-2\nu} \frac{\partial}{\partial x} \left(\frac{\partial w_x}{\partial x} + \frac{\partial w_y}{\partial y} + \frac{\partial w_z}{\partial z} \right) + \frac{\partial u}{\partial x} = 0 \\ -G\nabla^2 w_y - \frac{G}{1-2\nu} \frac{\partial}{\partial y} \left(\frac{\partial w_x}{\partial x} + \frac{\partial w_y}{\partial y} + \frac{\partial w_z}{\partial z} \right) + \frac{\partial u}{\partial y} = 0 \\ -G\nabla^2 w_z - \frac{G}{1-2\nu} \frac{\partial}{\partial z} \left(\frac{\partial w_x}{\partial x} + \frac{\partial w_y}{\partial y} + \frac{\partial w_z}{\partial z} \right) + \frac{\partial u}{\partial z} = \gamma' \end{cases} \quad (1)$$

where G means shear modulus of soil, kPa; ν is Poisson's ratio of soil; u is excess pore water pressure, kPa; γ' is the effective unit weight of soil, KN/m^3 ; ∇^2 is Laplace operator, $\nabla^2 = (\partial^2/\partial x^2) + (\partial^2/\partial y^2) + (\partial^2/\partial z^2)$; w_x , w_y , w_z , are the displacement of three direction x , y and z of soil separately, m .

Four unknowns w_x , w_y , w_z and u are contained in Equation (1). An equation is still needed to supplement in order to solve, the flow continuity equation thereby is used as supplementary equation. It can be written as

$$\frac{\partial \varepsilon_v}{\partial t} = -\frac{1}{\gamma_w} \left(k_x \frac{\partial^2 u}{\partial x^2} + \frac{\partial^2 u}{\partial y^2} + \frac{\partial^2 u}{\partial z^2} \right) \quad (2)$$

in which k_x , k_y , k_z are the permeability coefficient of

three directions x , y and z separately; γ_w is the unit weight of water; ε_v is the volumetric strain.

Thus the four unknowns can be determined by solving the equations set of Equation (1) and (2).

It is well known that when the soil undergo additional loading due to the waste, it can produce time-dependent deformation because of consolidation, moreover, the permeability coefficient will change with the consolidation deformation. In this investigation empirical formula [Equation (3)] given by Taylor is adopted, which has good applicability for clay soil [14].

$$k = k_0 \times 10^{\frac{e-e_0}{e_k}} \quad (3)$$

where k_0 means the initial permeability coefficient of soil, e is the void ratio of soil, e_0 is the initial void ratio of soil, e_k is the permeability index, $e_k = 0.5 e_0$.

The change of the soil volume is the change of the pore volume for saturated soil, under the assumption that the pore water and the soil particles cannot be compressed. Based on this the calculation formula of porosity can be expressed as following Equation (4), then the pore ratio can also be known by the relationship between porosity and void ratio, it has the form as Equation (5). Then the relational expression between permeability coefficient and pore water pressure can be determined through substituting Equations (4) and (5) into Equation (3).

$$n = 1 - \frac{1 - n_0}{1 - \frac{(p-u)(1-2\nu)}{2G(1-\nu)}} \quad (4)$$

$$e = \frac{n}{1-n} \quad (5)$$

in which n means porosity of soil, n_0 is the initial porosity of soil, p denotes the upper loading of impermeable layer.

Three-Dimensional Transport Equation of Contaminant in Deforming Soil

When the contaminant migrates through the clay liner beneath the landfill, here, it is assumed that the contaminant can be divided into two parts. One may adsorb onto the soil skeleton and be migrated with the soil particles as the soil consolidates, the other may transport within the pore passage of the soil. Based on the conversation of the whole contaminant mass, and considering the adsorption, a three-dimensional model

coupled mechanical consolidation and contaminant transport through clay barriers can be established.

$$\frac{\partial(nC)}{\partial t} + \frac{\partial[(1-n)\rho_s S]}{\partial t} = \nabla \cdot (n\mathbf{D} \cdot \nabla C - mvC) - \nabla \cdot [(1-n)\mathbf{v}_s \rho_s S] \quad (6)$$

$$\mathbf{v}_s = \frac{\partial \mathbf{w}}{\partial t} \quad (7)$$

$$\mathbf{D} = \mathbf{D}_m + \mathbf{D}_d \quad (8)$$

$$\mathbf{D}_m = \tau D_0 \quad (9)$$

$$\mathbf{D}_d = \alpha |\mathbf{v}_t| \quad (10)$$

where C is the concentration of contaminant in pore fluid; \mathbf{v}_s is the velocity of soil skeleton; \mathbf{D}_m is an effective diffusion coefficient tensor of contaminant in porous medium; D_0 is the diffusion coefficient for the contaminant in a free solution, which is a scalar and related to the type of contaminant; τ is the tortuosity factor for a soil and contaminant, which is defined as the ratio of distance between the actual movement distance of fluid particles with pore passage and straight-line distance, τ can be determined by the empirical formula [15], $\tau = (\tau_x, \tau_y, \tau_z)^T = (n^r, n^r, n^r)^T$. r is the empirical parameter; \mathbf{D}_d is the mechanical dispersion coefficient tensor; α is the dispersivity tensor; \mathbf{v}_t is the average velocity vector of fluid through the pore passage of porous medium; S is the mass of contaminant adsorbed within the soil particles per unit mass of solid phase; ρ_s is the density of soil particles.

Compared with the conventional pollutant transport model, the transport condition parameters of the adsorbed contaminant along with the soil particles are introduced in Equation (6). Besides that, permeability coefficient changes with the change of void ratio, the influence of soil deformation on contaminant transport consequently can be calculated. It is worth mentioning herein that, void ratio, hydrodynamic dispersion coefficient, Darcy velocity and deformed velocity of soil skeleton are all treated as variable, not constant, which are closely related to the consolidation pressure undergone.

Basic Theory of Permeability Anisotropy

The permeability anisotropy is usually defined as the ratio of the horizontal permeability coefficient to the vertical permeability coefficient, it can be expressed as

$$\frac{K_{\leftrightarrow}}{K_{\downarrow}} = r_K \quad (11)$$

where K_{\leftrightarrow} means the coefficient of permeability in horizontal direction, m/s; K_{\downarrow} is the coefficient of permeability in vertical direction, m/s; r_K is the coefficient of permeability anisotropy, ranging from 0.7–4 for homogeneous material, for cohesive material the value of r_K is 2.1 ± 0.5 , for no cohesive material the value of r_K is 1.6 ± 0.4 .

Then through Kozeny–Carman equation, the mathematical expression of permeability k can be written as

$$k = \frac{1}{C_K} \frac{1}{\tau^2} \frac{1}{S^2} \frac{e^3}{(1+e)} \quad (12)$$

in which C_K means the shape factor of Kozeny; S is the specific surface area; e is the void ratio.

Next the Kozeny–Carman equation is substituted into Equation (11), it can be obtained as

$$r_k = \frac{K_{\leftrightarrow}}{K_{\downarrow}} = \frac{\left(\frac{1}{C_{K_{\leftrightarrow}}} \frac{1}{\tau_{\leftrightarrow}^2} \frac{1}{S_{\leftrightarrow}^2} \frac{e_{\leftrightarrow}^3}{(1+e_{\leftrightarrow})} \frac{\gamma_f}{\mu_f} \right)}{\left(\frac{1}{C_{K_{\downarrow}}} \frac{1}{\tau_{\downarrow}^2} \frac{1}{S_{\downarrow}^2} \frac{e_{\downarrow}^3}{(1+e_{\downarrow})} \frac{\gamma_f}{\mu_f} \right)} = \left(\frac{\tau_{\downarrow}}{\tau_{\leftrightarrow}} \right)^2 \quad (13)$$

where γ_f is the unit weight of fluid; μ_f is the viscosity of fluid.

In most cases the void ratio will change with the consolidation deformation of soil, thus it is accepted that there is a functional relationship between tortuosity factor and void ratio. Through Scholes's work the following formula can be gotten [16].

$$r_k = r_0^2 \frac{1}{(1-\varepsilon)^2} \quad (14)$$

where r_0 indicates the ratio of initial tortuosity factor which is a constant. Especially, when the initial condition of soil keep isotropy before soil deformation, the value of r_0 is equal to one; ε is strain.

Equation (15) describes the relationship between linear strain and void ratio, which is substituted into Equation (14). Thereby the general relation Equation (16) of permeability anisotropy can be determined.

$$\varepsilon = 1 - \left(\frac{1+e}{1+e_0} \right) \quad (15)$$

$$r_K = \frac{K_{\leftrightarrow}}{K_{\downarrow}} = \left(\frac{1+e_0}{1+e} \right)^x \quad (16)$$

in which e is the void ratio at the strain of interest and e_0 is the initial void ratio where isotropy existed, x is the fitting factor that relates to the ratio of vertical to horizontal or axial to radial tortuosity.

It is to be noted that when the initial condition of soil is anisotropy, the permeability anisotropy coefficient r_K of soil can be expressed by the following Equation (17). It is an empirical equation that has a similar form to Equation (14), here using e_1 instead of e_0 as the basis for strain, and the fitting exponent x is renamed x^* .

$$r_K = r_1 \left(\frac{1+e_1}{1+e} \right)^{x^*} \quad (17)$$

where r_1 is the permeability ratio measured at void ratio e_1 , x^* is the fitting factor that relates to the ratio of vertical to horizontal or axial to radial tortuosity.

From Equation (17) it can be seen that the anisotropy is a function of void ratio, so the extent of anisotropy keeps changed, not a constant, as a result of an applied external force. Especially to be noticed here, the deformation in this study is primarily due to the particle arrangement rather than due to compression of the particles, when an additional loading is employed.

Then, Equation (17) is firstly substituted into flow continuity Equation (2), then combining three-dimensional Biot's consolidation Equation (1), meanwhile, considering the contaminant transport Equation (6) to solve simultaneously, as a result the concentration distribution of contaminant with time and space in permeability anisotropy soil will be determined.

Definite Solution Condition

A model is established in this investigation taking a simple landfill for example (Figure 1). The assumption is adopted that there are two axes of symmetry on the horizontal plane. Considering the symmetry of the concerned problem, the coordinate origin is located in the center of the landfill, then 1/4 of structural system is taken as the emphasis to study. The bottom width ① of landfill is set 50 m, the height of landfill is set 10 m, the slope of the lateral boundary ③ is 1:1, and the thickness of clay impermeable layer underneath the landfill is 4 m. The cross-section of landfill model is shown in Figure 3.

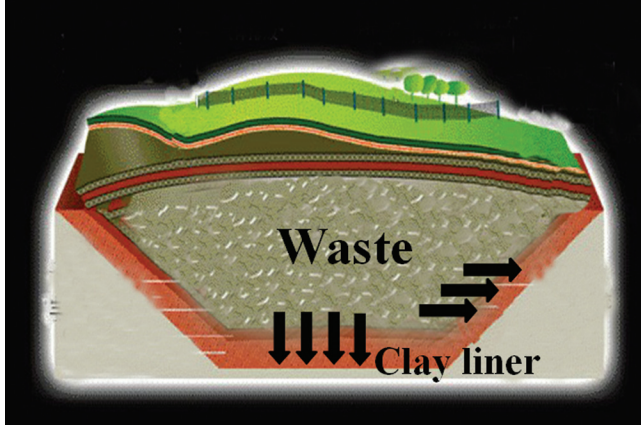


Figure 1. Simple waste landfill.

In this study several assumptions are adopted for obtaining the numerical solution of the proposed mode. (1) The bottom of waste is the natural clay liner; (2) the right boundary ④ and lower boundary ② of clay barrier are both rigid and permeable [17]; (3), p the additional loading imposes instantaneously, in this case, $(\partial\sigma)/(\partial t) = 0$; (4) the upper boundary ① and boundary ③ are permeable; (5) the background concentration of contaminant in soil is neglected. Hence the definite solution can be known according to the aforementioned assumption.

Three-dimensional consolidation

Table 1. Initial and Boundary Conditions of Consolidation Model.

Initial Condition	$u(x, y, z, 0) = p \quad ((x, y, z) \in \Omega)$
boundary ①	$u(x, y, H_2, t) = 0 \quad (t \geq 0)$
boundary ②	$u(x, y, 0, t) = 0 \quad (t \geq 0)$
boundary ③	$u(x, y, z, t) = 0 \quad (t \geq 0, L_1 \leq x \leq L_1 + L_3, H_2 \leq z \leq H_2 + H_1)$
boundary ④	$u(L_1 + L_2, y, z, t) = 0 \quad u(x, L_1 + L_2, z, t) = 0 \quad (t \geq 0)$

Three-dimensional transport model

Table 2. Initial and Boundary Conditions of Transport Model.

Initial Condition	$C(x, y, z, 0) = 0 \quad ((x, y, z) \in \Omega)$
boundary ①	$C(x, y, H_1, t) = c_0 \quad (t \geq 0, 0 \leq x \leq L_1)$
boundary ②	$\frac{\partial C(x, y, 0, t)}{\partial z} = 0 \quad (t \geq 0)$
boundary ③	$C(x, y, z, t) = C_0 \quad (t \geq 0, L_1 \leq x \leq L_1 + L_3, H_2 \leq z \leq H_2 + H_1)$
boundary ④	$\frac{\partial C(L_1 + L_2, y, z, t)}{\partial x} = 0 \quad \frac{\partial C(L_1 + L_2, y, z, t)}{\partial y} = 0 \quad (t \geq 0)$

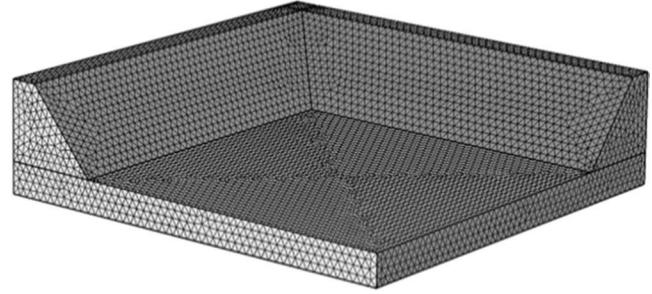


Figure 2. Geometry and finite element.

RESULTS AND ANALYSIS

During this work COMSOL Multiphysics, a multi-field coupled finite element software, was used to conduct numerical simulations. Based on the established model the numerical calculation aimed at a waste dump has been carried out.

Model Parameters

The type of simulated contaminant was chosen as ammonia nitrogen. Regarding the example considered here the parameters in Table 3 of clay liner are adopted.

In addition, the numerical simulation on contaminant transport under the different contaminant source and adsorption type has been conducted, with considering the consolidation of clay soil. The different source type and its parameters are shown in Table 4, and the different adsorption mode and its parameters are given in Table 5.

Simulation Results and Analysis

It can be found that permeability anisotropy is an important factor effected the process of contaminant transport, from the established coupled model in this work. At the first, when the soil has the character of permeability anisotropy, the permeability coefficient at any direction appears to be different. At the transport mechanism of contaminant, the advection mechanism is related closely to permeability coefficient. Secondly,

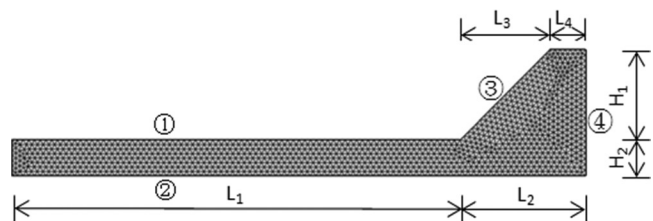


Figure 3. Cross-section of simple landfill model.

Table 3. Model Parameters of Clay Liner.

Parameters	Symbol	Value
Initial concentration of contaminant	C_0 (g/L)	0.5
Initial diffusion coefficient	D_0 (m ² /s)	6.76×10^{-9}
Empirical parameter	r	2.5
Thickness of natural clay liner	H (m)	4.0
Initial void ratio	e_0	0.8
Density	ρ_s (kg/m ³)	2.7×10^3
Poisson ratio	ν	0.3
Shear modulus	G (kPa)	2.6×10^3
Longitudinal dispersion	α_L (m)	0.5
Transverse dispersion	α_T (m)	0.05
Initial permeability coefficient	k_0 (m/s)	1.7×10^{-9}
Empirical coefficient	r_1	1.18*
index	x^*	1.3*

Note: the data with "*" was quoted from [14].

the hydrodynamic dispersion is also related to permeability coefficient. It can thereby be concluded that permeability anisotropy will have significant influence on contaminant transport, which has been verified through the following simulation results.

Contaminant Transport Results and Analysis: Constant Contaminated Source

It can be seen from Figure 4 and Figure 5 that the concentration distribution of contaminant exhibited similar tendency, whether the soil is permeability anisotropy. In other words, for a given transport time, the transport depth and horizontal distance reduce gradually and the concentration peak surface turn left with the consolidation pressure increase. Furthermore, the concentration peak curve gradually becomes sparse under different consolidation pressure with the increase of migration time, which show that the influence of consolidation pressure on contaminant transport increase gradually with the transport time.

As plotted in Figure 4, the transport depth of contaminant with permeability anisotropy is the same as that with permeability isotropy whether the transport time and consolidation pressure. Nevertheless, it can be noted from Figure 5 and Table 6 that the horizontal distance of contaminant transport with permeabil-

Table 4. Parameters of Different Source Type.

Contaminated Source Type	Expression	Parameter
Constant contaminated source	$C = C_0$	$C_0 = 0.5$ g/L
Attenuated contaminated source	$C = C_0 e^{-\eta t}$	$C_0 = 0.5$ g/L, $\eta = 0.4(1/\alpha)$

Table 5. Parameters of Different Adsorption Mode.

Adsorption Mode	Expression	Adsorption Parameter
Linear adsorption	$S = K_d C$	$K_d = 8.142 \times 10^{-4}$ kg/m ³
Freundlich adsorption	$S = K_f C^\beta$	$K_f = 8.142 \times 10^{-4}$ kg/m ³ , $\beta = 1.2$
Langmuir adsorption	$S = \frac{K_1 K_2}{1 + K_1 C} C$	$K_1 = 1$, $K_2 = 8.142 \times 10^{-4}$ kg/m ³

ity anisotropy are all higher than that of contaminant transport with permeability isotropy. Besides that, for a given transport time, the difference of contaminant transport distance along horizontal direction between permeability anisotropy and isotropy becomes more and more obvious, with the consolidation increase.

Under the consolidation pressure 200 kPa, the concentration distribution of contaminant with depth and horizontal distance of soil obtain under different adsorption, in which it is found that permeability anisotropy cannot affect contaminant transport with depth of soil whether any adsorption mode, this may be verified by coincidence of concentration curve with permeability anisotropy and isotropy. In addition, no matter what kind of adsorption mode, the transport distance of contaminant along horizontal direction with permeability anisotropy is higher than that of contaminant with permeability isotropy, furthermore, with the transport time increase, the difference of contaminant transport distance in horizontal direction between permeability anisotropy and isotropy becomes more and more obvious, this simulated results indicate that the influence of permeability anisotropy on contaminant transport in horizontal direction heighten gradually with the transport time increase.

Contaminant Transport Results and Analysis: Attenuation Contaminated Source

In this section the effects of permeability anisotropy on contaminant transport are determined with attenuation contaminated source under different consolidation pressure. Simple to say, the contaminant concentration of leachate attenuate with time, it is more in line with the practical situation, and the detailed parameter is shown in Table 4.

The profiles of concentration along the vertical and horizontal distance of soil are described in Figures 7 and 8. As can be seen, there exists a marked difference in concentration distribution form when the contaminated source is constant and attenuated. However, no matter how long the transport time is and how large

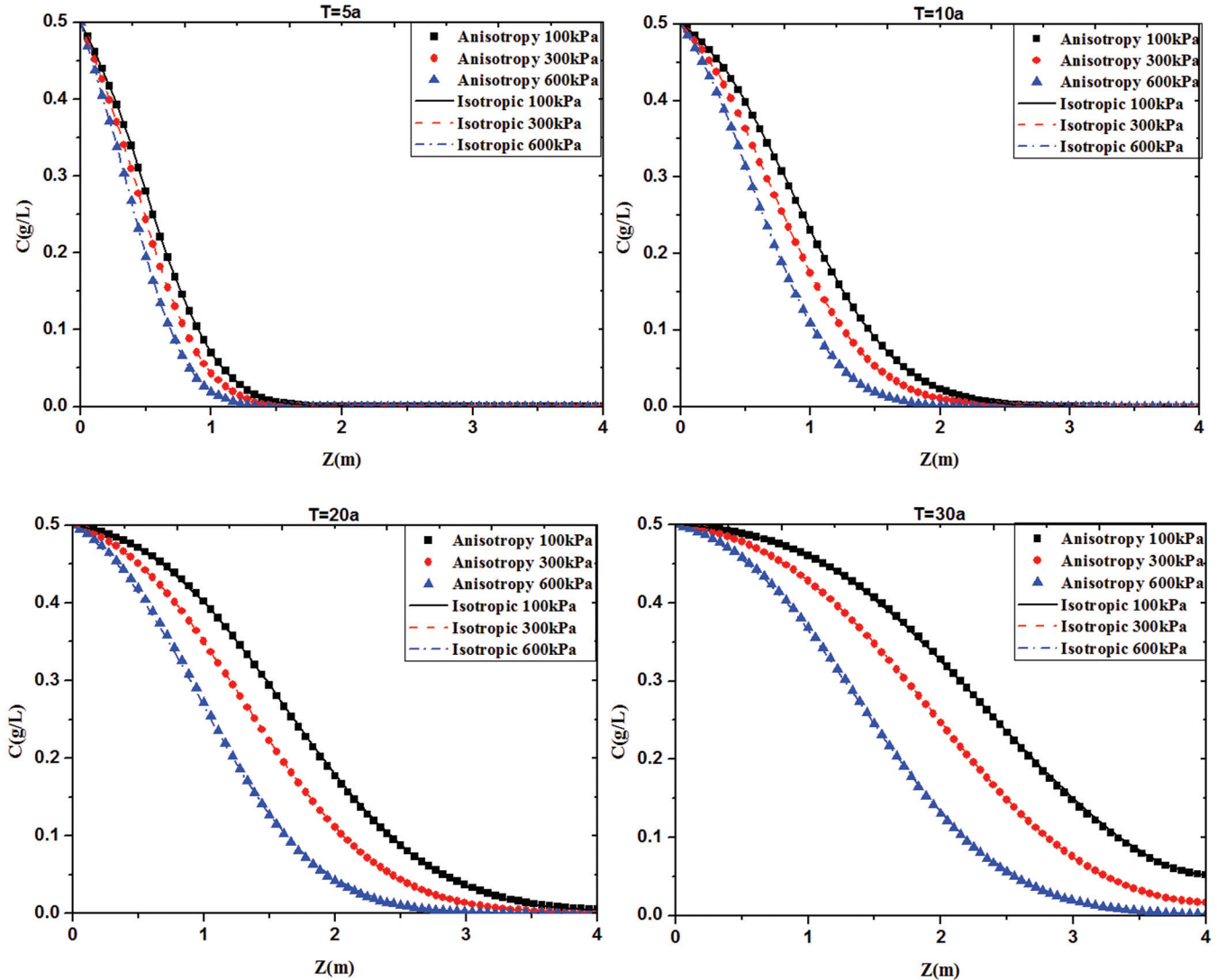


Figure 4. Contaminant concentration distribution with depth of soil layer under different consolidation pressures.

the consolidation pressure is, the transport depth of contaminant along vertical direction with permeability anisotropy and isotropy are same. It can be noticed that the transport distance in horizontal direction of contaminant with permeability anisotropy is greater than that of contaminant with permeability isotropy. And for a given transport time, the difference between the

transport distance of contaminant along the horizontal direction with permeability anisotropy and that of contaminant with permeability isotropy is more and more obvious, with the consolidation pressure increase, which can be seen clearly in Table 7.

Under the consolidation pressure 200 kPa, as the concentration of contaminated source is attenuated

Table 6. Horizontal Transport Distance of Contaminant Under Different Consolidation Pressures (m).

Time(a)	100 (kPa)			300 (kPa)			600 (kPa)		
	I	A	D	I	A	D	I	A	D
5	1.453	1.454	0.001	1.336	1.337	0.001	1.218	1.219	0.001
10	2.477	2.543	0.066	2.348	2.413	0.065	1.832	1.896	0.064
20	—	—	—	3.533	3.666	0.133	3.003	3.135	0.132
30	—	—	—	—	—	—	3.732	3.932	0.200

Note: I—Isotropy; A—Anisotropy; D—Horizontal distance differential value of contaminant transport with isotropic and anisotropy.

Table 7. Horizontal Distance of Contaminant Transport Under Different Consolidation Pressures (m).

Time(a)	100 (kPa)			300 (kPa)			600 (kPa)		
	I	A	D	I	A	D	I	A	D
5	1.453	1.454	0.001	1.336	1.337	0.001	1.218	1.219	0.001
10	2.347	2.413	0.066	2.087	2.152	0.065	1.768	1.832	0.064
20	3.732	3.865	0.133	3.201	3.334	0.133	2.607	2.739	0.132
30	—	—	—	—	—	—	3.333	3.533	0.200

Note: I—Isotropy; A—Anisotropy; D—Horizontal distance differential value of contaminant transport with isotropic and anisotropy.

which means the concentration of contaminant is a variable, not a constant. the concentration distribution of contaminant with depth and horizontal distance of soil obtain under different adsorption. As seen in Figure 9, no matter what kind of adsorption mode, the transport distance of contaminant along horizontal direction with permeability anisotropy is higher than that of contaminant with permeability isotropy,

furthermore, with the transport time increase, the difference of contaminant transport distance in horizontal direction between permeability anisotropy and isotropy becomes more and more obvious, this simulated results indicate that the influence of permeability anisotropy on contaminant transport in horizontal direction heighten gradually with the transport time increase.

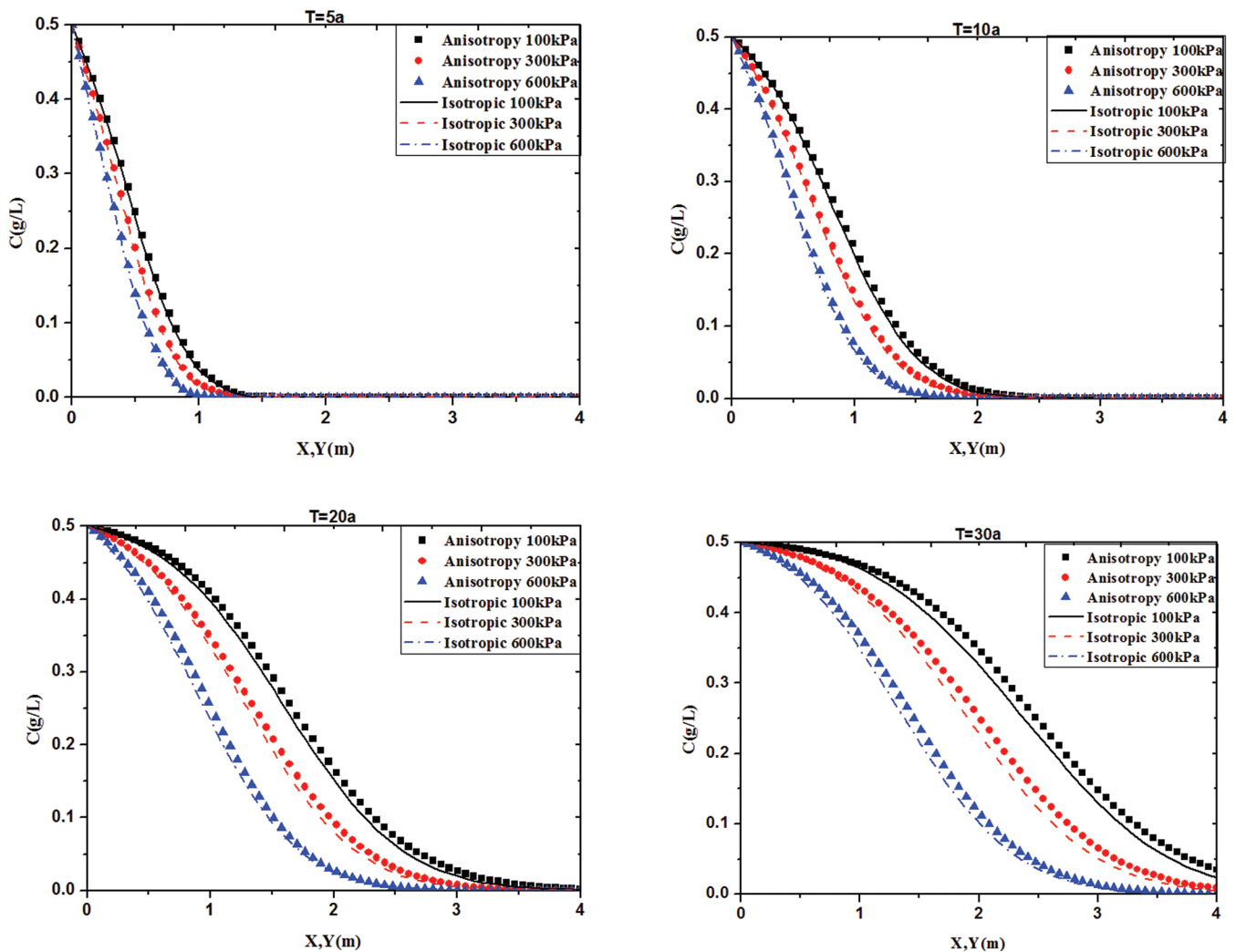


Figure 5. Contaminant concentration distribution with horizontal distance under different consolidation pressures.

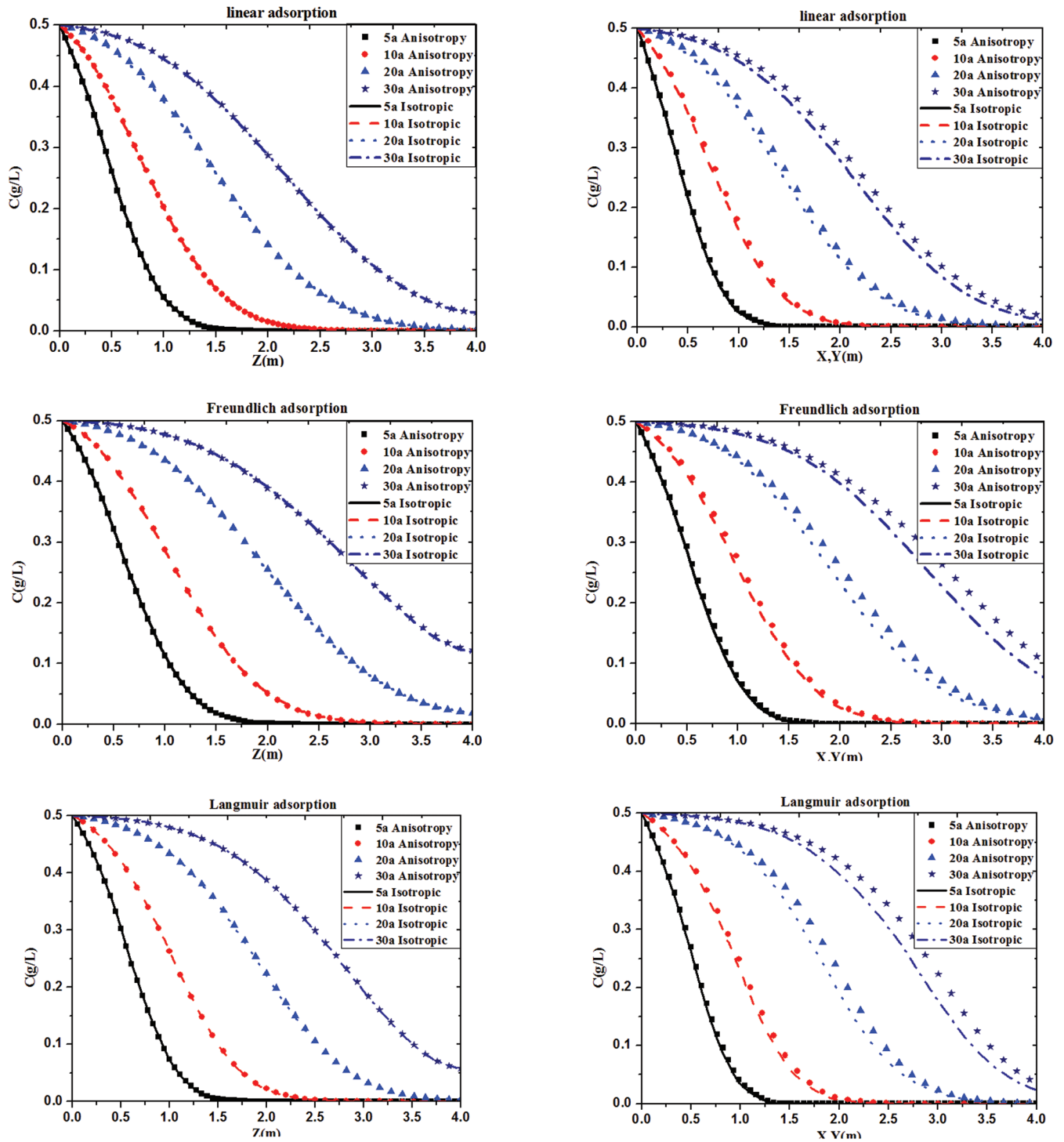


Figure 6. Contaminant concentration distribution at different times under different adsorption modes.

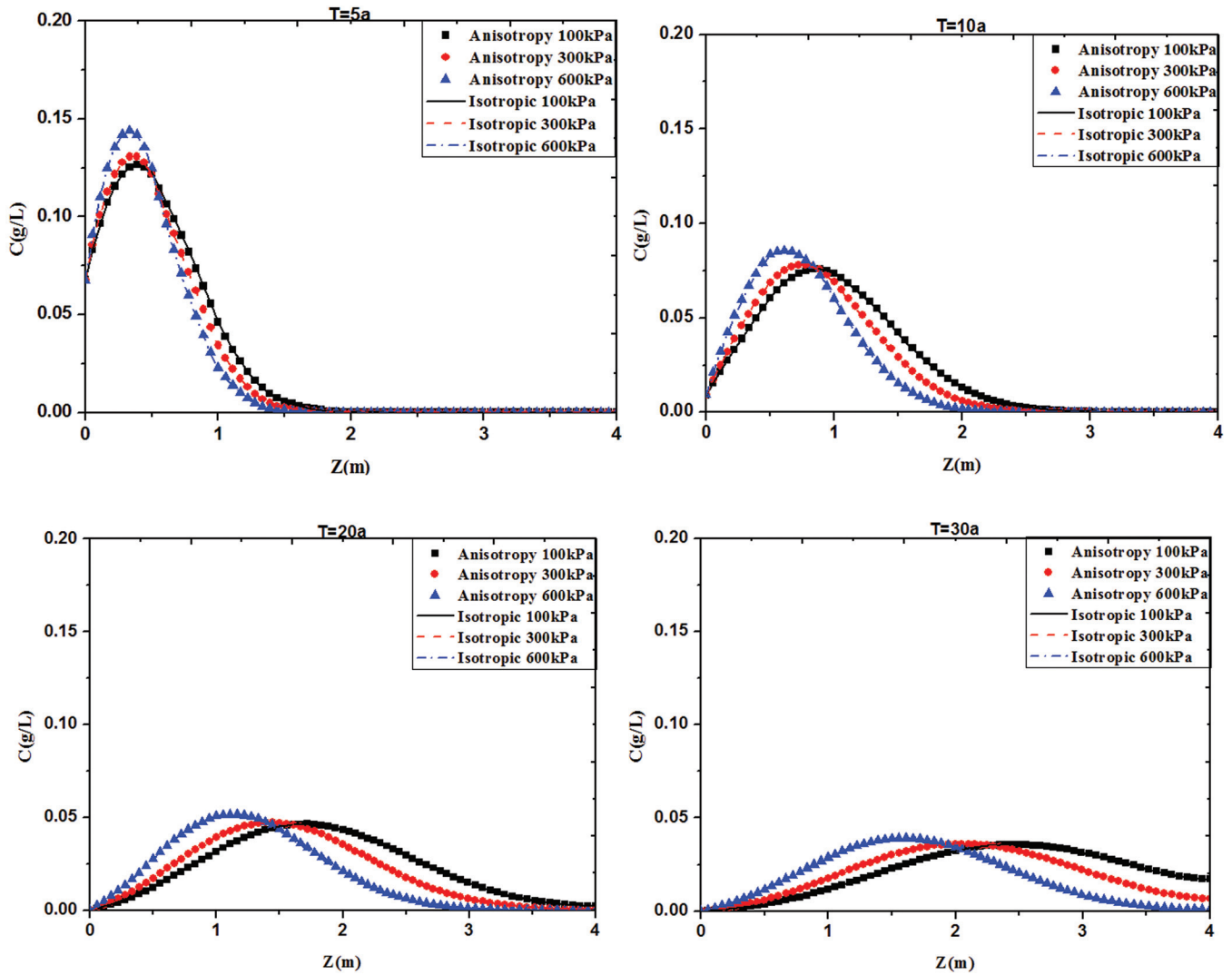


Figure 7. Contaminant concentration distribution with depth under different consolidation pressures.

CONCLUSIONS

In this study, a three-dimensional model coupled mechanical consolidation and contaminant transport with permeability anisotropy has been developed. The established coupled model can embody the influence of soil deformation and permeability anisotropy on contaminant transport. It should be emphasized that convection, hydrodynamic dispersion and flow continuity equation are fully related to permeability coefficient, thereby, it is of paramount importance that taking the permeability anisotropy of soil into account in determining the transport of contaminant through a deforming soil.

Taking the permeability anisotropy into account, a three-dimensional model coupled consolidation and contaminant transport has been developed, in which

the porosity is viewed as the coupled parameter. The presented model can not only consider the influence of soil deformation on transport parameters, but also embody the effect of permeability change on contaminant transport.

The numerical simulation has showed that consolidation deformation of soil and permeability anisotropy have a negligible influence on contaminant transport.

Compared to permeability isotropy, no matter the contaminated source is constant or attenuated, and no matter what kind of adsorption mode, the transport of contamination along vertical direction with permeability anisotropy keeps unchanged. However, for a given transport time, the transport distance of contaminant with permeability anisotropy along horizontal direction are all greater than that of contaminant with

permeability isotropy, furthermore, the difference between permeability anisotropy and isotropy becomes more and more clear. Within a migration period of 30 years the difference has even reached 200 mm.

For specific transport years, the difference with different adsorption mode appears to be not same of contaminant transport distance in horizontal direction with permeability anisotropy and isotropy, the difference is the biggest value with Freundlich adsorption, and the difference keep similar with linear adsorption and Langmuir adsorption.

ACKNOWLEDGEMENTS

Financial support for this work is provided by the National Natural Science Foundation of China (No. 51378035). Support is gratefully acknowledged.

REFERENCES

1. Smith, D. W., "One-dimensional contaminant transport through a deforming porous medium: theory and a solution for a quasi-steady-state problem", *J. International Journal for Numerical and Analytical Methods in Geomechanics*, Vol. 24, No. 8, 2000, pp. 693–722. [http://dx.doi.org/10.1002/1096-9853\(200007\)24:8<693::AID-NAG91>3.0.CO;2-E](http://dx.doi.org/10.1002/1096-9853(200007)24:8<693::AID-NAG91>3.0.CO;2-E)
2. Lee, J., Fox, P. J. and Lenhart, J. J., "Investigation of Consolidation-Induced Solute Transport. I: Effect of Consolidation on Transport Parameters", *J. Journal of Geotechnical and Geoenvironmental Engineering*, Vol. 135, 2009, pp. 1228–1238. [http://dx.doi.org/10.1061/\(ASCE\)GT.1943-5606.0000047](http://dx.doi.org/10.1061/(ASCE)GT.1943-5606.0000047)
3. Lee, J. and Fox P. J., "Investigation of Consolidation-Induced Solute Transport. II: Experimental and Numerical Results", *J. Journal of Geotechnical and Geoenvironmental Engineering*, Vol. 135, 2009, pp. 1239–1253. [http://dx.doi.org/10.1061/\(ASCE\)GT.1943-5606.0000048](http://dx.doi.org/10.1061/(ASCE)GT.1943-5606.0000048)
4. Arega, F. and Hayter, E., "Coupled consolidation and contaminant transport model for simulating migration of contaminants through the sediment and a cap", *J. Applied Mathematical Modeling*, Vol. 32, 2008, pp. 2413–2428. <http://dx.doi.org/10.1016/j.apm.2007.09.024>
5. Lewis, T. W., Pivonka, P., Fityus, S. G. and Smith, D.W., "Parametric sensitivity analysis of coupled mechanical consolidation and

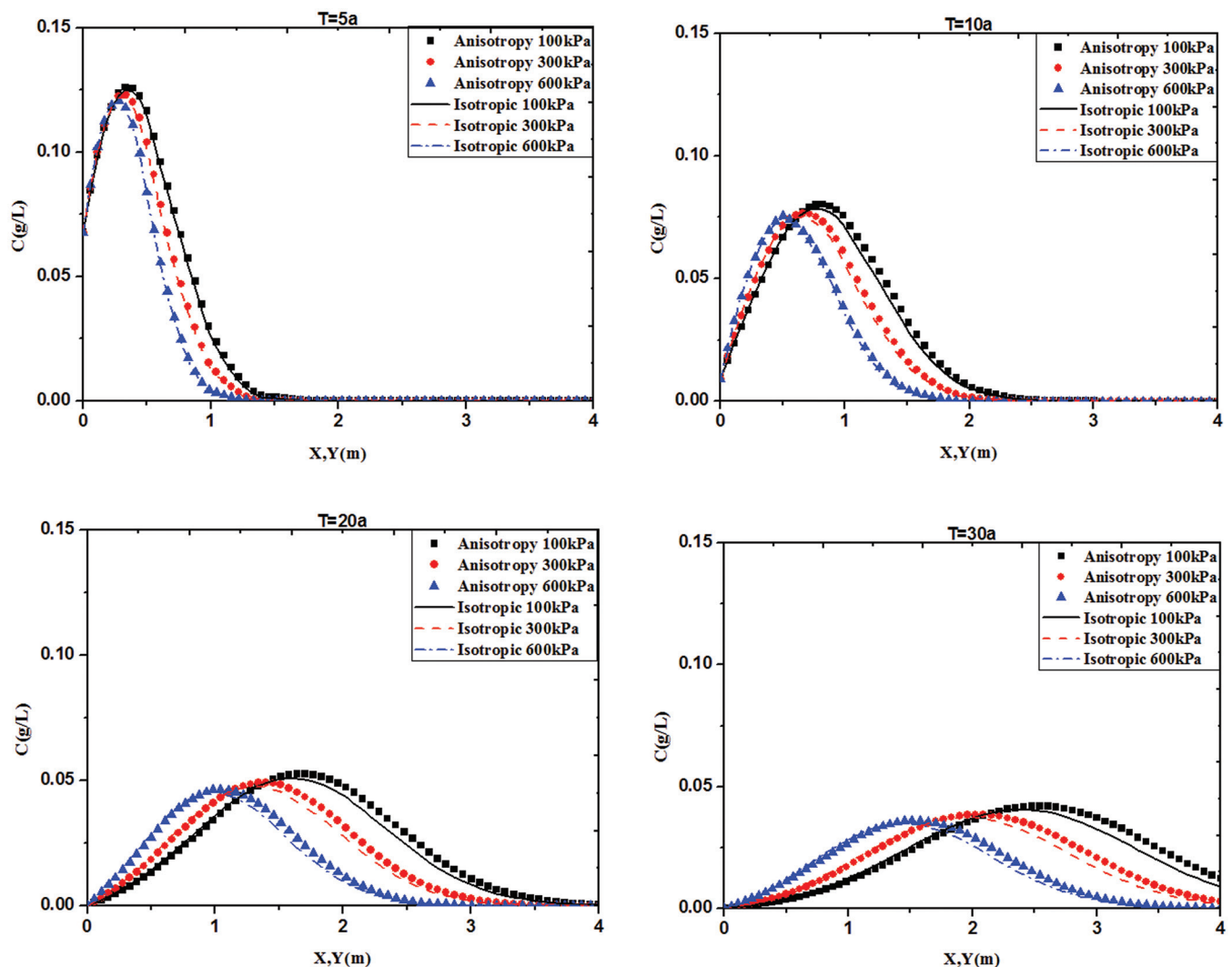


Figure 8. Contaminant concentration distribution with horizontal distance under different consolidation pressures.

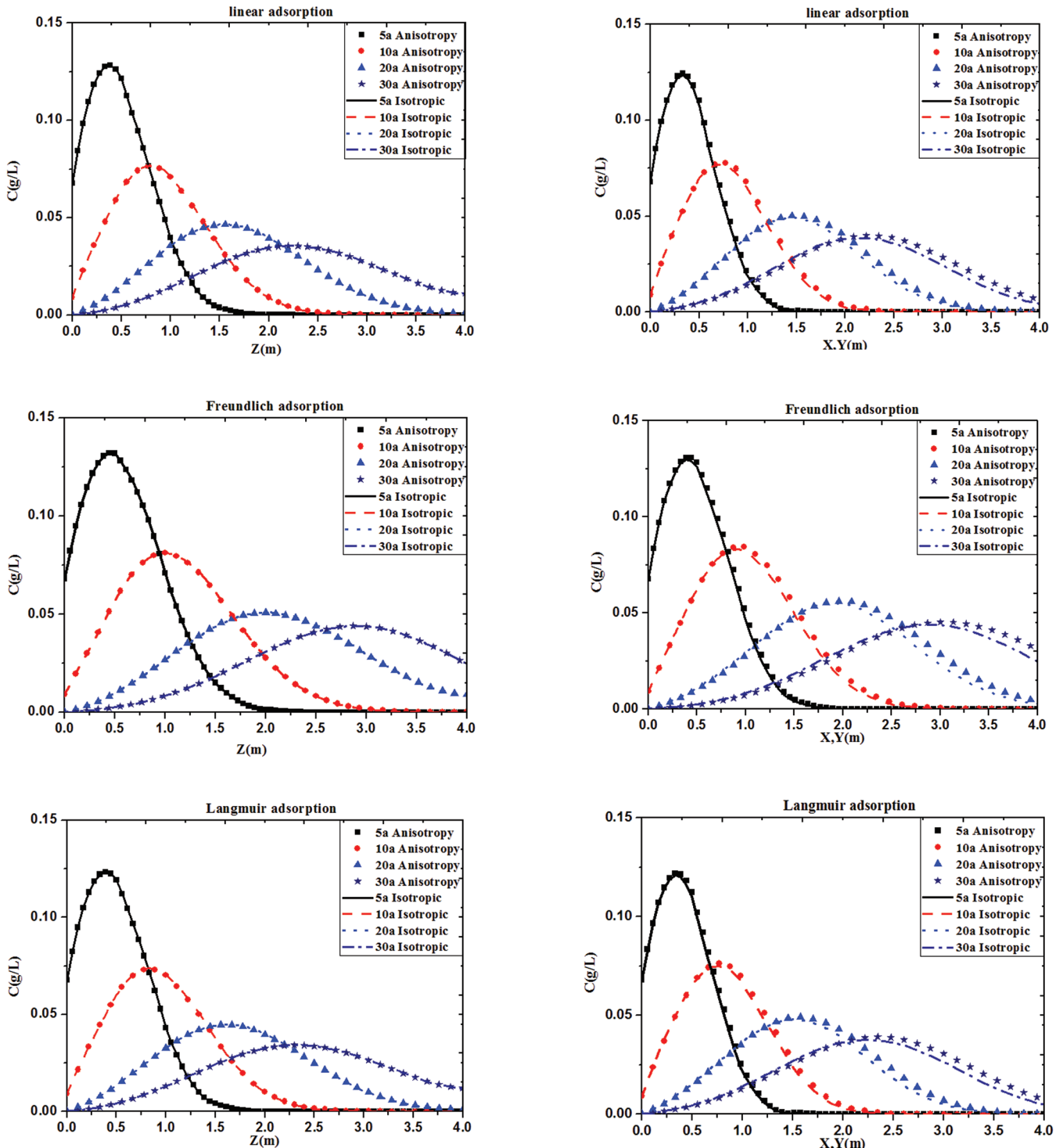


Figure 9. Contaminant concentration distribution at different times under different adsorption modes.

- contaminant transport through clay barriers”, *J. Computers and Geotechnics*, Vol. 36, 2009, pp. 31-40. <http://dx.doi.org/10.1016/j.compgeo.2008.04.003>
6. Fox, P. J., “Coupled large strain consolidation and solute transport. I: Model development”, *J. Journal of Geotechnical and Geoenvironmental Engineering*, Vol. 133, 2007, pp. 3-15. [http://dx.doi.org/10.1061/\(ASCE\)1090-0241\(2007\)133:1\(3\)](http://dx.doi.org/10.1061/(ASCE)1090-0241(2007)133:1(3))
 7. Fox, P. J., “Coupled large strain consolidation and solute transport. II: Model verification and simulation results”, *J. Journal of Geotechnical and Geoenvironmental Engineering*, Vol. 133, 2007, pp.16–29. [http://dx.doi.org/10.1061/\(ASCE\)1090-0241\(2007\)133:1\(16\)](http://dx.doi.org/10.1061/(ASCE)1090-0241(2007)133:1(16))
 8. Xue, Q., Liu, L., Liang, B., Zhao, Y. and Wang, Y. B., “A gas-hydraulic-solid coupling dynamics model under landfill settlement”, *J. Chinese Journal of Rock Mechanics and Engineering*, Vol. 26, Supp. 1, 2007, pp. 3473–3478.
 9. Xue, Q., Zhao, Y., Liu, L. and Lu, H. J., “Study of thermo-hydro-mechanical-chemical coupling effect of catastrophe process of landfill”, *J. Chinese Journal of Rock Mechanics and Engineering*, Vol. 30, No. 10, 2011, pp. 1970–1988.
 10. Li, Y. C., Cleall, P. J. and Thomas, H. R., “Multi-dimensional chemosmotic consolidation of clays”, *J. Computers and Geotechnics*, Vol. 38, No. 4, 2011, pp. 423–429. <http://dx.doi.org/10.1016/j.compgeo.2011.02.005>
 11. Huang, L., Zhao, C. G., Liu, Y. and Cai, G. Q., “3D contaminant migration model with consolidation dependent transport coefficients”, *J. Acta Mechanica Sinica*, Vol. 28, No. 1, 2012, pp. 151–163. <http://dx.doi.org/10.1007/s10409-012-0023-9>
 12. Fan, X. D. and Zhang, X. K., “Adsorption of heavy metal by adsorbents from food waste residue”, *J. Journal of Residuals Science and Technology*, Vol. 12, 2015, pp. 155–158. <http://dx.doi.org/10.12783/issn.1544-8053/12/S1/22>
 13. Wei, L. D., “Study on migration and pollution in shallow groundwater near a slag field”, *J. Journal of Residuals Science and Technology*, Vol. 12, No. 4, 2015, pp. 191–197. <http://dx.doi.org/10.12783/issn.1544-8053/12/4/1>
 14. Southeast University, Zhejiang University, Hunan University and Suzhou University of Science and Technology. 2005. *Soil mechanics*, Beijing, China Architecture & Building Press.
 15. Liu, J. G., Wang, H. T. and Nie, Y. F., “Fractal model for predicting effective diffusion coefficient of solute in porous media”, *J. Advances in Water Science*, Vol. 15, No. 4, 2004, pp. 458–462.
 16. Scholes, O. N., Clayton, S. A., Hoadley, A. F. A. and Tiu, C., “Permeability anisotropy due to consolidation of compressible porous media”, *J. Transport in Porous Media*, Vol. 68, No. 3, 2007, pp. 365–387. <http://dx.doi.org/10.1007/s11242-006-9048-5>
 17. Zhang, W. Q., Zhao, X. H. and Zai, J. M., “Finite layer analysis for layered and elastic half-space under arbitrary force systems”, *J. China Journal of Geotechnical Engineering*, Vol. 3, No. 2, 1981, pp. 27–42.

Synthesis and Mechanism of Flocculating-Decolorizing Agent PAD used for Polymer-Sulphonated Drilling Wastewater

QINGYANG LI¹, YAN LUO^{2,*}, BING HOU³ and ZIXUAN HAN³

¹State Key Laboratory of Oil and Gas Reservoir Geology and Exploitation, Southwest Petroleum University, Chengdu 610500, China

²Department of Sustainable Bioproducts, Mississippi State University, Mississippi State, MS 39762, United States

³State Key Laboratory of Petroleum Resources and Prospecting, China University of Petroleum, Beijing 102249, China

ABSTRACT: Cationic polyacrylamide (PAD) is synthesized and used as decolorizing agent for polymer-sulphonated drilling wastewater. Compared with other widely used decolorizing agents the wastewater processed by PAD results in a higher decolorization speed, lower chromaticity, and less flocs. It also adapts to polymer-sulphonated drilling wastewater with different salinity. Used for on-site wastewater, it is both efficient and pleiotropic. It reduced the chromaticity to lower than 50 times while the COD is reduced to 100 mg/L and even much lower than 100 mg/L. Meanwhile, the suspended solids content is lower than 40 mg/L and the flocs content is very low. Therefore, the processing results may greatly help the following treatment. Fourier transform infrared spectroscopy (FTIR) and a scanning electron microscope (SEM) are used to analyze interaction between functional groups of PAD with the polymer-sulphonated drilling wastewater and decolorizing mechanism. The decolorizing mechanism is mainly a union of ionic bonds, charge neutralization, and adsorption bridging between PAD and polymer-sulphonated additives.

INTRODUCTION

THE polymer-sulphonated drilling fluid system is stable under high temperature conditions and much cheaper than other drilling fluid systems used for deep wells. It is widely used for wells deeper than 3,000 m. According to a survey, about 300 m³ drilling fluid is abandoned after a 3,000–4,000 m well is completed [1]. When the waste drilling fluid is combined with rainfall and other drilling wastewater much more waste polymer-sulphonated drilling wastewater is formed. Additionally, with the consistently increasing difficulty in oil and gas exploitation many more wells deeper than 3,000 m will be drilled which will further generate a large amount of waste polymer-sulphonated drilling fluid [2].

Methods of solidification and solid-liquid separation are most widely applied on-site for treatment of drilling wastewater. Normally the chromaticity of most water-based drilling fluid can meet the national standard after it is treated by the methods of solidification and solid-liquid separation. However, for the waste

polymer-sulphonated drilling fluid, the chromaticity of effluent after solid-liquid separation and lixivium from solidification is more than 1,000 times and difficult to treat for the reasons that conventional sulfonated additives have better water-soluble properties and much higher chromaticity. Therefore, the waste polymer-sulphonated drilling fluid needs further treatment to meet the national standard. There are some ways such as oxidation and electrolytic process to meet state regulations but are difficult to apply on-site for high costs or unproven technology [4–7]. Though some agents are effective for the chromaticity, most of them decolorize with bulky flocs left and limited COD removal effect. It is essential to find a more effective agent to further decrease the chromaticity of preliminarily treated waste polymer-sulphonated drilling fluid [8–11]. Based on knowledge of the additives of the polymer-sulphonated drilling fluid cationic polyacrylamide is found very effective in decolorizing the drilling wastewater. First, cationic polyacrylamide may combine with the anionic polymer additives which makes a greater contribution to the chromaticity of drilling wastewater. Second, cationic polyacrylamide may be used as a decolorizing agent for polymer-sulphonated drilling wastewater as it also has an ability to deposit the colored material [12–15].

*Author to whom correspondence should be addressed.

Department of Sustainable Bioproducts, Mississippi State University, Mississippi State, MS 39762, United States. E-mail address: luohaiyanabc@163.com

MATERIALS AND METHODS

Chemicals and Materials

Methacryloyloxyethyl trimethyl ammonium chloride (DMC, 78 wt% in water; industrial grade) and acrylamide (AM, 99%; industrial grade) were obtained from Beijing Aoli Chemicals Co., Ltd. Sodium sulfite, potassium persulfate, ethanol, sulfuric acid, and acetone of analytical grade were purchased from Beijing Aoli Chemicals Co., Ltd. Drilling fluid additives (industrial grade) were provided by CNPC Offshore Engineering Co., Ltd. All chemicals and aforementioned materials were used directly without purification. Several decolorizing agents such as CW-08, SHQN, and QTRY (industrial grade) were purchased from Yixing Cleanwater Chemicals co., Ltd, and YH-3 was provided by Jiangsu Oilfield of SINOPEC.

Synthesis and Characterization of PAD

To find the cationic polyacrylamide with the most suitable cationic degree and molecular chain for polymer-sulphonated drilling wastewater single factor experiments were made and finally the decolorizing agent (PAD) was synthesized by 10 g acrylamide (AM) and 37.5 g acryloyloxyethyl trimethyl ammonium chloride (DMC) with 0.05 g Na₂SO₃ and 0.05 g K₂S₂O₈ as initiators in 52.5 g aqueous solution. The whole reaction was performed at 45°C for 4.5 h under nitrogen atmosphere and 0.3 g EDTA was used as cross-linking agent. FTIR spectra were characterized by the Nicolet iS50 FTIR spectrometer (KBr pellets). SEM images were obtained using the Quanta250 SEM under environmental scan mode. Zeta potential and particle size in treated wastewater were determined using the ZETASIZER NANOZ and MASTERSIZER2000, respectively.

Preparation of Wastewater used for Experiment

Polymer-sulphonated drilling fluid was prepared according to the methods of Xinjiang Oilfield, Sichuan Oilfield, and offshore oilfield of Chinese National Petroleum Corp.

Preparation of polymer-sulphonated drilling fluid: 4% Bentonite + 0.1% Sodiumhydroxide (NaOH) + 0.05% Sodiumcarbonate (NaCO₃) + 0.5% Fluid loss agent (BDF-100S) + 3% Sulphonated phenolic resin (SMP) + 2% Sulfonated lignite (SPNH) + 3% Anticollapse agent (BDSC-300L) + Stabilizer for borehole wall (Asphalt) + 1% Lubricant (BDLU-100L) + 1% Potassiumchloride (KCl) + 350 g Barite.

Then, the prepared drilling fluid was hot rolled for 16 h at 150°C to simulate the used drilling fluid. After that, the drilling fluid was centrifuged for 20 min at 3,500 rpm. The upper liquid was diluted 100 times. The diluted water was used as the wastewater for further treatment. The chromaticity and the COD of the wastewater are 1,200 times and 916 mg/L, respectively.

Evaluation of Decolorization Rate

The 0.5 wt% PAD solution in water was prepared. Under certain condition, a specified volume of 0.5 wt% PAD solution was added into the beakers containing 100 ml polymer-sulphonated drilling wastewater. The chromaticity was tested by the platinum-cobalt methods and the dilution multiple method. When the chromaticity was higher than 70 times, the upper liquid was diluted to less than 70 times before tested by the platinum-cobalt method. While the chromaticity was lower than 70 times, the upper liquid was tested directly by the platinum-cobalt method. Regarding Equation (1),

$$\text{Decolorization rate (\%)} = (1 - C_N/C_0) \times 100\% \quad (1)$$

where C_N and C_0 represent the chromaticity of decolorized wastewater and the chromaticity of original wastewater, respectively.

Analysis of the Main Materials Responsible for the Chromaticity

The component of polymer-sulphonated drilling fluid was analyzed to find out the additives most responsible for chromaticity. Organic additives were prepared as a solution according to their dosage in drilling fluid, respectively. The chromaticity of each organic additive is seen in Table.1.

Table 1. Chromaticity of Each Organic Additive.

Additives	BDF-100S	SMP	SPNH	BDLU-100L	BDSC-300L	Asphalt
Dosage (wt%)	0.5	3	2	1	3	0.5
Chromaticity (times)	colorless	120800	709000	milky	colorless	284

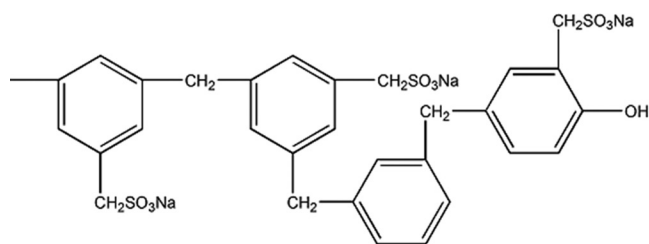


Figure 1. Sulphonated phenolic resin.

Sulphonated phenolic resin and sulphonated lignite which have high chromaticity and most widely used at present were found to mainly affect chromaticity of wastewater. The main structures of sulphonated phenolic resin and sulphonated lignite are seen in Figures 1 and 2, respectively.

RESULTS AND DISCUSSION

Effect of PAD Dosage on Decolorization Rate

First, the pH of wastewater was adjusted to 5 to destroy the stability of waste drilling fluid because drilling fluid is more stable in alkaline condition. Then, a certain amount of PAD solution was added into the beakers containing 100 ml polymer-sulphonated drilling wastewater. The decolorization effect, zeta potential, and flocs are seen in Figures 3 and 4.

Seen in Figure 3 decolorization rate increases with increasing PAD dosage from 0.25–0.35 g/L and then decolorization effect decreases with further increase in dosage level to 0.50 g/L. This suggests the sulphonated phenolic resin and sulfonated lignite are removed at the optimal dosage of 0.35 g/L. Also, at this optimal dosage the flocs are the least and the zeta potential approaches 0 mV as seen in Figure 4 which indicates that electrostatic interaction was responsible for decolorization. When added into drilling wastewater PAD absorbs on the chain of additives. At low dosage levels of PAD the system of wastewater does not lose stability completely and the flocs are negatively charged because of excessive anionic additives. Anionic additives with high chromaticity may still dissolve in wastewater or adsorb

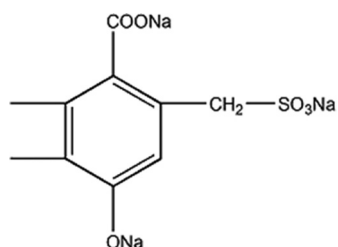


Figure 2. Sulfonated lignite.

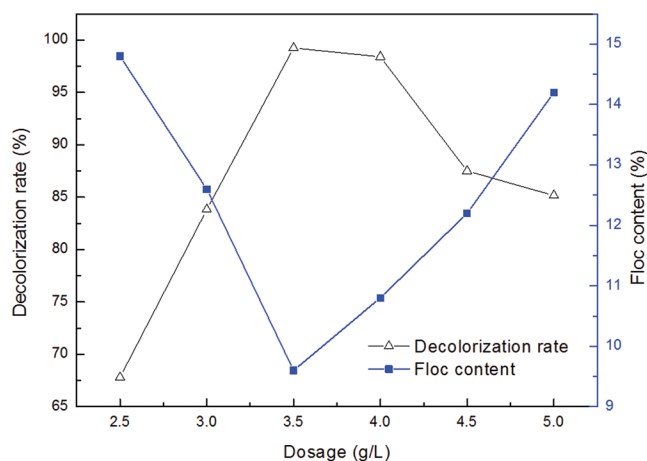


Figure 3. Effect of dosage on decolorization rate.

on flocs which would cause flocs to be dispersed. This is due to the electrostatic repulsive interaction between the flocs. As the dosage of PAD increased the stability of wastewater and charge density of the flocs decreased which caused a decrease in stability of the flocs. Also, more dissolved anionic additives are combined. Residual color of the sample as a result became lighter and flocs became compact. When PAD is over-dosed the flocs are positively charged. Dispersion stability of compactness of flocs increased due to a higher positive charge density [16–18].

Effect of pH of Wastewater on Decolorization Rate

The pH of wastewater plays an important role in the decolorization process. Normally, the pH of polymer-sulphonated drilling wastewater is about 9 which caused the system to be fairly steady. To break stability of the wastewater the pH of wastewater was adjusted to become acidic. Decolorization rate at different pH

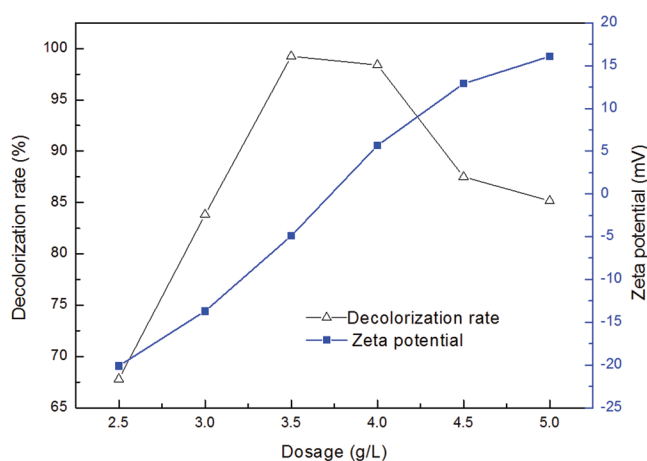


Figure 4. Influence of dosage on zeta potential.

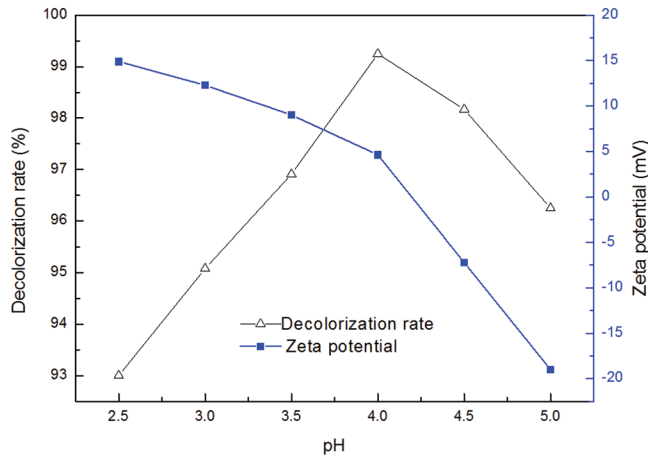


Figure 5. Effect of pH of wastewater on decolorization rate.

levels using a 0.35 g/L dosage level is displayed in Figure 5.

When the pH of wastewater is higher than 4.0 the decolorization rate and zeta potential increase with an increase of H^+ concentration. When the pH of wastewater is lower than 4.0 the decolorization rate reduces and zeta potential continuously rises with the increase of H^+ . The studied wastewater has the best decolorization rate at a wastewater pH of 4.0 and zeta potential of approximately zero. The system loses its stability with an increase in concentration of H^+ which is supported by the changing trend of Zeta potential [19, 20]. Too much H^+ screens the opposite charges of anionic additives and decreased both decolorization rate and the bonding between anionic additive and PAD. Furthermore, the structure of PAD may be destroyed under mild acidity. The system has the worst stability. However, PAD would work most efficiently at a wastewater pH of 4.0.

Effect of Stirring Rate and Stirring Time on Decolorization Rate

Stirring rate and stirring time have a great effect on the decolorization rate. To find the best stirring rate and stirring time corresponding experiments were performed at the dosage level of 0.35 g/L and a wastewater pH of 4.0. After the optimal string rate and stirring time were determined the laser particle analyzer (Mastersizer2000) was used for analyzing the phenomenon and testing the size of particles remaining in the wastewater. Results are seen in Figure 6 (stirring rate) and in Figure 7 (stirring time).

Figures 6 and 7 show variations in decolorization rate and $D_{0.5}$ with stirring rate and stirring time, re-

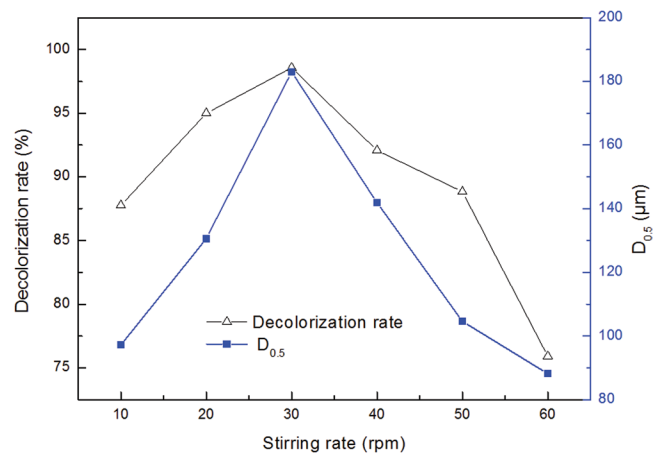


Figure 6. Effect of stirring rate on decolorization rate.

spectively, at room temperature. An appropriate stirring rate and time may be propitious to execute the PAD function, accelerate the decolorization process, and enhance the decolorization effect. When stirring rate is too rapid and stirring time is too long the PAD chain is cut too short to form large flocs and precipitated large flocs may be broken down into small particles that cannot be precipitated. Decolorization effect decreases as a result. However, when the stirring rate is too slow and the stirring time is too short the PAD cannot be dispersed well in the polymer-sulphonated drilling wastewater [21]. The PAD cannot completely react with sulphonated phenolic resin and sulfonated lignite and thereby resulting in failure of colored particles in the waste drilling water attaching to each other and the PAD reacts with more particles. Figures 6 and 7 display that the decolorization rate first increased and then decreased with an increase in stirring rate and time. The decolorization rate reached a maximum at

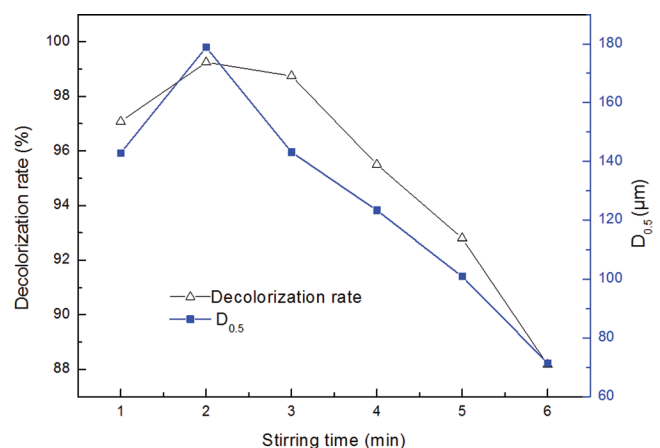


Figure 7. Effect of stirring time on decolorization rate.

a stirring rate of 30 rpm and a stirring time of 2 min. Decolorization rate is in agreement with the $D_{0.5}$ of effluent because the $D_{0.5}$ is bigger and the little particles are less [22].

Comparison with Several Decolorizing Agents

Performance of PAD was compared with several decolorizers on the market. These agents include SHQN, QTRY, CW-08, and YH-3. To compare them fairly the best dosage, pH, string time, and string speed of the four agents was found, respectively. The best decolorization rate of each was determined, respectively.

Comparison of Decolorization Rate, COD Removal Rate, and Volume of Flocs

The decolorization rate, COD removal rate, and volume of flocs are seen in Table 2.

As seen in Table 2, CW-08, QTRY, SHQN, and YH-3 possess the ability to decolorize. However, the COD removal rate of each is poor and the leftover flocs is even twice that of PAD. Compared with agents mentioned above, PAD decolorized the wastewater most accompanied with a high COD removal rate and less flocs leftover. Therefore, PAD is considered as a strong and effective decolorizing agent for polymer-sulphonated drilling wastewater.

Table 2. Comparison of Decolorization Rate, COD Removal Rate, and Volume of Flocs.

Decolorizing Agent	Decolorization Rate (%)	COD Removal Rate (%)	Volume of Flocs (%)
CW-08	98.8	2.0	17.3
QTRY	99.0	11.6	17.8
SHQN	99.1	2.4	16.7
PAD	99.1	94.0	8.9
YH-3	97.7	44.7	11.5

Comparison of Decolorizing Speed

To compare decolorizing speed visually, the decolorizing processes of YH-3, QTRY, CW-08, SHQN, and PAD were each photographed at time intervals of 5 min, 10 min, 1 h, 4 h, 8 h, and 24 h. Measuring cylinder from left to right of each picture contains wastewater disposed by YH-3, QTRY, CW-08, SHQN, nothing, and PAD (Figure 8).

Figure 8 suggests that PAD has the fastest decolorizing speed. It has an obvious effect at 5 min and the water is nearly clear one hour later. At the 4 h time interval the flocs settle to the bottom of the measuring cylinder. This may be that the decolorizing speed is too fast to squeeze out the water in the flocs at the beginning of decolorizing process causing the relatively large volume and relatively small density of

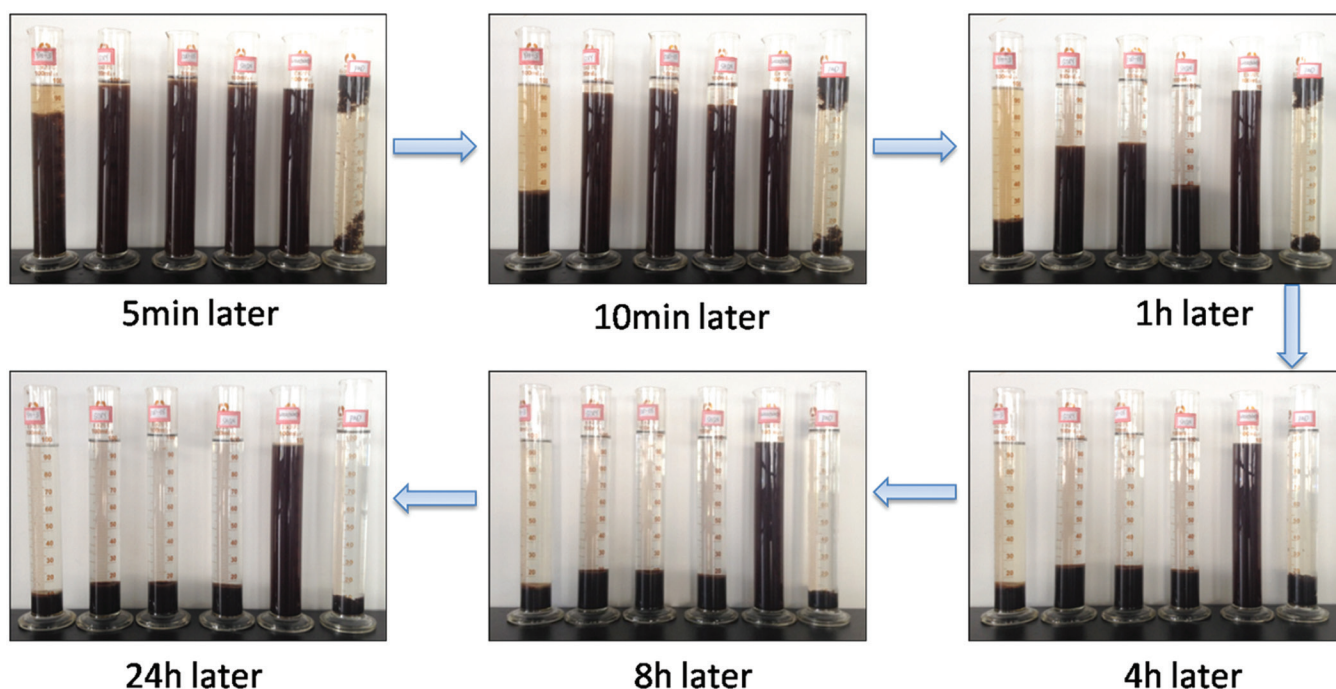


Figure 8. Decolorizing processes.

Table 3. Influence of NaCl and Ca₂Cl on Decolorizing Effect.

NaCl		Ca ₂ Cl		NaCl + Ca ₂ Cl	
Dosage (%)	Chromaticity (times)	Dosage (%)	Chromaticity (times)	Dosage (% +%)	Chromaticity (times)
1.00	250	0.05	65	1+0.05	60
2.00	128	0.10	40	2+0.10	55
3.00	104	0.15	100	3+0.15	130
4.00	75	0.20	115	4+0.20	140
5.00	75	0.25	140	5+0.25	150
6.00	100	0.30	140	6+0.30	150

flocs. Eight hours later the flocs become tight fibrous. The decolorizing process of PAD is completed while the decolorizing process of other agents continues and flocs look like sand.

Influence of Salinity on Decolorizing Effect

Salinity varies in different drilling wastewater. Therefore, to decolorize the well in-site it is significant to study influence of salinity on decolorization. First, the pH of polymer-sulphonated drilling wastewater was adjusted to 4. Then, a different dosage of NaCl and Ca₂Cl was added. Finally, it is mixed for 2 min at the stirring rate of 30 rpm after a decolorizing agent was added at a dosage of 3.0 g/L.

Seen in Table 3 both NaCl and Ca₂Cl have great influence on decolorization. When the dosage of decolorization agent is not enough a small quantity of mineral salt has a positive effect on decolorization for the reason that the mineral salt can neutralize the electronegativity of polymer-sulphonated agent. However, when the mineral salt is in excess it has a negative effect for the reason that the excess cation will hinder the connection of the decolorization agent and polymer-sulphonated agent. Therefore, the dosage of the decolorization agent should be adjusted according to the salinity in the lab before its used on-site.

Treatment of On-Site Drilling Wastewater

Drilling wastewater from Jiangsu oilfield, Southwest Oil & Gas field and Tarim Oilfield was decolorized, respectively. Results are seen in Table 4.

Seen in Table 4 the chromaticity of treated wastewater from the three oilfields can meet the primary standard of China. Meanwhile, the decolorizer has the extra effect of decreasing suspended solids content and COD which reduces suspended solids content under the primary standard of China and the COD under the secondary standard at least. Results indicate that the decolorizer is efficient and multifunctional helping to reduce the subsequent difficulty of treatment.

FTIR and SEM Analysis

To investigate chemical interaction between PAD and wastewater, the PAD wastewater and flocs were dried and pressed into pellets together with dried potassium bromide (KBr) for FTIR studies. The FTIR spectra are seen in Figure 9.

FTIR band at 954.09 cm⁻¹, representing quaternary ammonium of PAD, weakens in intensity and slightly shifts to 952.65 cm⁻¹ in the formed flocs. Within the FTIR spectrum of dried wastewater, bands at 1,043.06 cm⁻¹, 1,126.89 cm⁻¹ and 1,186.67 cm⁻¹ represent sul-

Table 4. Result of Treating On-site Drilling Wastewater.

Source of Wastewater	Condition	Chromaticity (times)	COD (mg/L)	Suspended Solids Content (mg/L)	Flocs Content (%)
Jiangsu Oilfield	before treatment	2500	1024	456	—
	treated	33	101	16	50
Southwest Oil & Gas Field	before treatment	1600	1100	1240	—
	treated	25	84	33	33
Tarim Oilfield	before treatment	2600	654	1121	—
	treated	15	54	12	13

fonic group. FTIR spectrum of flocs shows that the peak at $1,043.06\text{ cm}^{-1}$ broadens and shifts to $1,030.27\text{ cm}^{-1}$ while the peak at $1,126.89\text{ cm}^{-1}$ disappears and the peak at $1,186.67\text{ cm}^{-1}$ weakens and shifts to $1,176.00\text{ cm}^{-1}$. These changes indicate sulfonic groups in additive molecules of wastewater react with quaternary ammonium of PAD and form products like $-\text{N}^+(\text{CH}_3)_3\text{SO}_3^-$ in aqueous solution [23,24]. Additionally, the band at $3,415.75\text{ cm}^{-1}$ representing $-\text{NH}_2$ becomes boarder and shifts to $3,301.54\text{ cm}^{-1}$ while the peak of $\text{C}=\text{O}$ at $1,669.46\text{ cm}^{-1}$ disappears in flocs. These changes indicate that PAD may show good adsorbability by amide group.

SEM was used to interpret the mechanism of decolorization intuitively and to further verify the FTIR results. The SEM images of PAD in 0.5% aqueous solution and flocs under different magnification are seen in Figure 10.

The structure of PAD in aqueous solution looks like a spider web. The spider web is three-dimensional and possesses a definite range of strength. When the decolorizing agent acts on the drilling wastewater the spider lines become thicker and the space truss is filled with

other substances. This makes the whole flocs look like a braid. On one hand the attraction of the negatively charged material (e.g., sulfonated enolic resin and sulfonated lignite) combine with positively charged functional groups on spider web coarsening the spider web. However, on the other hand through the combination of hydrogen bonding and nucleic reaction other water-soluble additives are wrapped into the spider web making the space trusses of the decolorizing agent tight [25].

CONCLUSION

The decolorizing agent, PAD, synthesized by acrylamide (AM) and methacryloyloxyethyl trimethyl ammonium chloride (DMC) using the solution polymerization method was found to be very effective in decolorizing polymer-sulfonated drilling wastewater. Based on electric charge interaction and adsorption PAD can break the structure of the wastewater and act on anionic additives. For polymer-sulfonated drilling wastewater prepared in lab the optimal PAD dosage, pH of wastewater, stirring rate, stirring time are 0.35

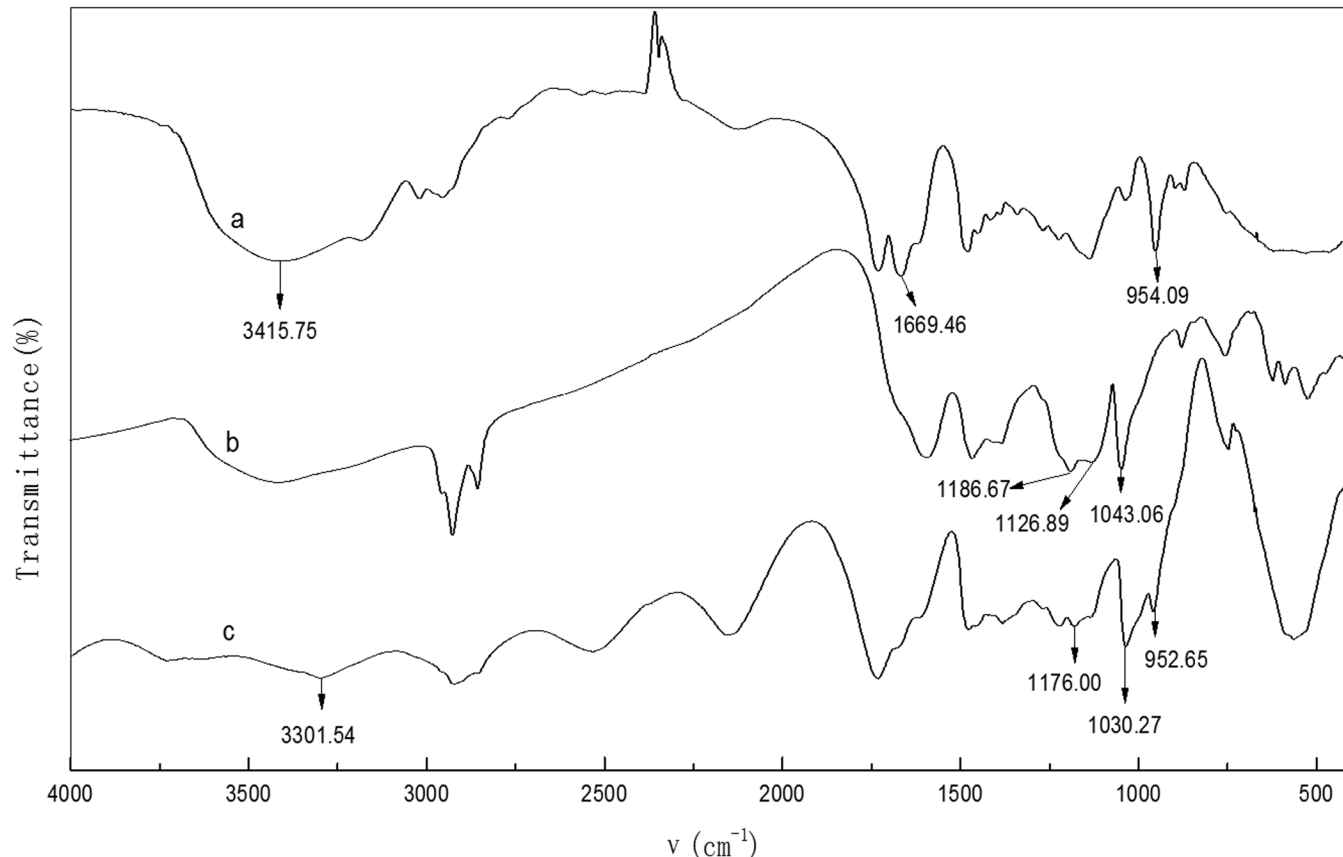


Figure 9. FTIR spectra of (a) PAD, (b) dried wastewater, and (c) flocs.

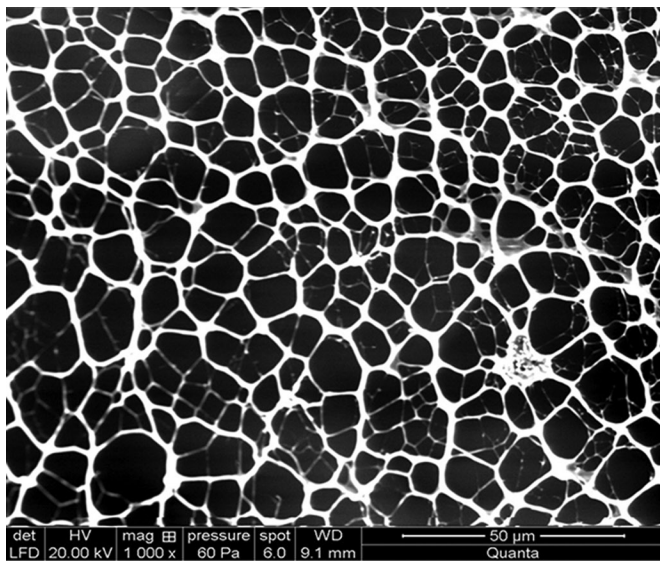
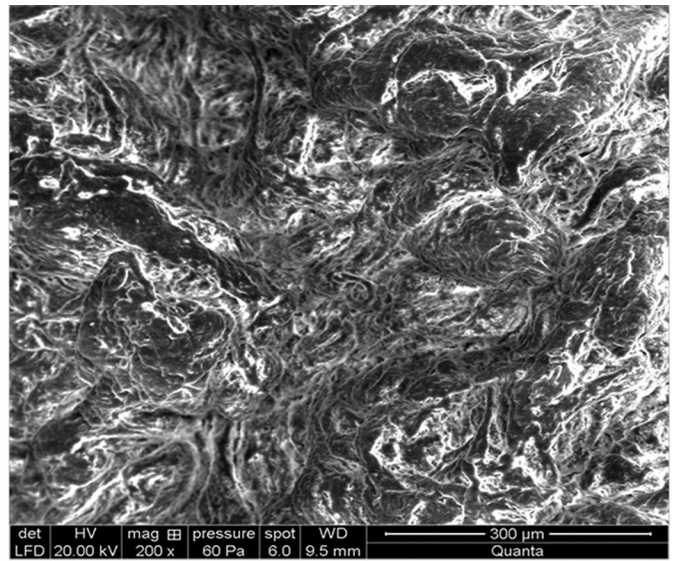
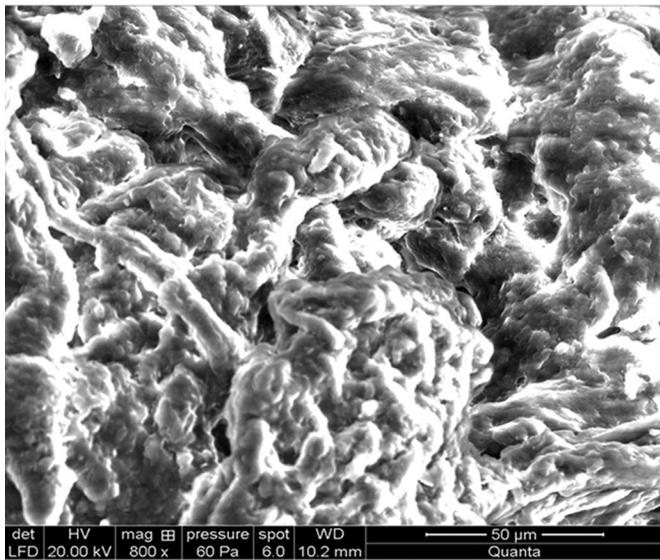
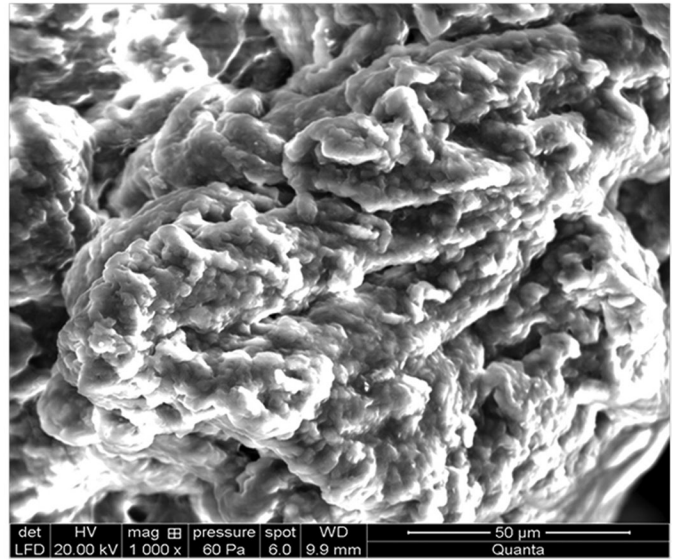
0.5% PAD in water $\times 1000$ Flocs $\times 200$ Flocs $\times 800$ Flocs $\times 1000$

Figure 10. SEM images of PAD and flocs.

g/L, 4, 30 rpm, and 2 min, respectively. This resulted in a decolorization rate up to 99.1%. Additionally, compared with other chemical agents mostly used for polymer-sulfonated drilling wastewater, PAD created less flocs and higher COD removal ability. Compared with electric coagulation and catalysis the method barely needs power and additional equipments. PAD is also suitable for polymer-sulfonated drilling wastewater with different salinity and shows good effectiveness for oilfield wastewater. Though the specific ingredients of different polymer-sulfonated drilling fluids changed a lot the decolorization processing principles are simi-

lar. Therefore, before the polymer-sulfonated drilling wastewater is decolorized further some related laboratory tests might be required to obtain the most spot effects.

ACKNOWLEDGEMENTS

This work was supported by the National Science and Technology Major Project titled "Study of Harmless Treatment Technology of Drilling Waste" (2011ZX05021-004). I would like to express my gratitude to Professors Rongsha Wang and Dr. Shuixiang

Xie for their valuable scientific insight, comments, and suggestions.

REFERENCES

- Ismail, Z., Kong, K.K., Othman, S.Z., Law, K.H., Khoo, S.Y., Ong, Z.C., and Shirazi, S.M., "Evaluating accidents in the offshore drilling of petroleum: Regional picture and reducing impact", *Measurement*, Vol. 51, 2014, pp. 18–33. <http://dx.doi.org/10.1016/j.measurement.2014.01.027>
- Ghazi, M., Quaranta, G., Duplay, J., Hadjamor, R., Khodja, M., Amar, H.A., and Kessaissia, Z., "Life-cycle impact assessment of oil drilling mud system in Algerian arid area", *Resources Conservation and Recycling*, Vol. 55, No. 12, 2011, pp. 1222–1231. <http://dx.doi.org/10.1016/j.resconrec.2011.05.016>
- Badani, Z., Amar, H.A., and Salah, A.S., "The inhibitive effect of lead concentration on the biological treatment of wastewater of oil well drillings", *Desalination*, Vol. 206, No. 1-3, 2007, pp. 295–299. <http://dx.doi.org/10.1016/j.desal.2006.03.571>
- Zou, J., Zhu, H., Wang, F.H., Sui, H.Y., and Fan, J.T., "Preparation of a new inorganic-organic composite flocculant used in solid-liquid separation for waste drilling fluid", *Chemical Engineering Journal*, Vol. 171, No. 1, 2011, pp. 350–356. <http://dx.doi.org/10.1016/j.cej.2011.03.100>
- Fersi, C., Gzara, L., and Dhabbi, M., "Treatment of textile effluents by membrane technologies", *Desalination*, Vol. 185, No. 1–3, 2005, pp. 399–409. <http://dx.doi.org/10.1016/j.desal.2005.03.087>
- Chen, Y.X., Liu, S.Y., and Wang, G.Y., "A kinetic investigation of cationic starch adsorption and flocculation in kaolin suspension", *Chemical Engineering Journal*, Vol. 133, No. 1–3, 2007, pp. 325–333. <http://dx.doi.org/10.1016/j.cej.2007.02.019>
- Tong, K., Zhang, Y.H., Fu, D., Meng, X.H., An, Q., and Chu, P.K., "Removal of organic pollutants from super heavy oil wastewater by lignite activated coke", *Colloids and Surfaces A: Physicochemical and Engineering Aspects*, Vol. 447, 2014, pp. 120–130. <http://dx.doi.org/10.1016/j.colsurfa.2014.01.062>
- Wang, J.H., Han, X.J., Ma, H.R., Ji, Y.F., and Bi, L.J., "Adsorptive removal of humic acid from aqueous solution on polyaniline/attapulgite composite", *Chemical Engineering Journal*, Vol. 173, No. 1, 2011, pp. 171–177. <http://dx.doi.org/10.1016/j.cej.2011.07.065>
- Yang, Z.L., Gao, B.Y., Wang, Y., Liu, X.X., and Yue, Q.Y., "Synthesis and application of polyferric chloride-poly (epichlorohydrin-dimethylamine) composites using different crosslinkers", *Chemical Engineering Journal*, Vol. 213, 2012, pp. 8–15. <http://dx.doi.org/10.1016/j.cej.2012.09.120>
- Wang, Y.F., Gao, B.Y., Yue, Q.Y., Wang, Y., and Yang, Z.L., "Removal of acid and direct dye by epichlorohydrin-dimethylamine: flocculation performance and floc aggregation properties", *Bioresource Technology*, Vol. 113, 2012, pp. 265–271. <http://dx.doi.org/10.1016/j.biortech.2011.11.106>
- Shen, J.J., Ren, L.L., and Zhuang, Y.Y., "Interaction between anionic dyes and cationic flocculant P(AM-DMC) in synthetic solutions", *J. Hazardous Materials*, Vol. 136, No. 3, 2006, pp. 809–815. <http://dx.doi.org/10.1016/j.jhazmat.2006.01.013>
- Khouni, I., Marrot, B., Moulin, P., and Amar, R.B., "Decolourization of the reconstituted textile effluent by different process treatments: Enzymatic catalysis, coagulation/flocculation and nanofiltration processes", *Desalination*, Vol. 268, No. 1–3, 2011, pp. 27–37. <http://dx.doi.org/10.1016/j.desal.2010.09.046>
- Kang, Q., Gao, B.Y., Yue, Q.Y., Zhou, W.Z., and Shen, D.Z., "Residual color profiles of reactive dyes mixture during a chemical flocculation process", *Colloids and Surfaces A: Physicochemical and Engineering Aspects*, Vol. 299, No. 1–3, 2007, pp. 45–53. <http://dx.doi.org/10.1016/j.colsurfa.2006.11.021>
- Kang, Q., "Residual color profiles of simulated reactive dyes wastewater in flocculation processes by polydiallyldimethylammoniumchloride", *Separation and Purification Technology*, Vol. 57, No. 2, 2007, pp. 356–365. <http://dx.doi.org/10.1016/j.seppur.2007.04.018>
- Joo, D.J., Shin, W.S., Choi, J.H., Choi, S.J., Kim, M.C., Han, M.H., Had, T.W., and Kim, Y.H., "Decolorization of reactive dyes using inorganic coagulants and synthetic polymer", *Dyes Pigments*, Vol. 73, No. 2, 2007, pp. 59–64. <http://dx.doi.org/10.1016/j.dyepig.2005.10.011>
- Gupta, V.K., and Suhas., "Application of low-cost adsorbents for dye removal—A review", *J. Environmental Management*, Vol. 90, No. 8, 2009, pp. 2313–2342. <http://dx.doi.org/10.1016/j.jenvman.2008.11.017>
- Forgacs, E., Cserhati, T., and Oros, G., "Removal of synthetic dyes from wastewaters": A review, *Environment International*, Vol. 30, No. 7, 2004, pp. 953–971. <http://dx.doi.org/10.1016/j.envint.2004.02.001>
- Chen, D.N., Liu, X.G., Yue, Y.M., Zhang, W.D., and Wang, P.X., "Dispersion copolymerization of acrylamide with quaternary ammonium cationic monomer in aqueous salts solution", *European Polymer Journal*, Vol. 42, No. 7, 2006, pp. 1284–1297. <http://dx.doi.org/10.1016/j.eurpolymj.2005.12.007>
- Ali, I., Asim, M., and Khan, T.A., "Low cost adsorbents for the removal of organic pollutants from wastewater", *J. Environmental Management*, Vol. 113, 2012, pp. 170–183. <http://dx.doi.org/10.1016/j.jenvman.2012.08.028>
- Marcucci, M., Nosenzo, G., Ciabatti, L., Corrieri, D., and Ciardelli, G., "Treatment and reuse of textile effluents based on new ultrafiltration and other membrane technologies", *Desalination*, Vol. 138, No. 1–3, 2001, pp. 75–82. [http://dx.doi.org/10.1016/S0011-9164\(01\)00247-8](http://dx.doi.org/10.1016/S0011-9164(01)00247-8)
- Hou, B., Liang, C., Deng, H., Xie, S.X., Chen, M., and Wang, R.S., "Oil removing technology of residues from waste oil-based drilling fluid treated by solid-liquid separation", *Journal of Residuals Science & Technology*, Vol. 9, No. 4, 2012, pp. 143–150.
- Kuan, W.H., and Hu, C.Y., "Chemical evidences for the optimal coagulant dosage and pH adjustment of silica removal from chemical mechanical polishing (CMP) wastewater", *Colloids and Surfaces A: Physicochemical and Engineering Aspects*, Vol. 342, No. 1–3, 2009, pp. 1–7. <http://dx.doi.org/10.1016/j.colsurfa.2009.03.019>
- Harrelkas, F., Azizi, A., Yaacoubi, A., Benhammou, A., and Pons, M.N., "Treatment of textile dye effluents using coagulation-flocculation coupled with membrane processes or adsorption on powdered activated carbon", *Desalination*, Vol. 235, No. 1–3, 2009, pp. 330–339. <http://dx.doi.org/10.1016/j.desal.2008.02.012>
- Yang, Z., Wu, H., Yuan, B., Huang, M., Yang, H., Li, A., Bai, J.f., and Cheng, R.S., "Synthesis of amoteric starch-based grafting flocculants for flocculation of both positively and negatively charged colloidal contaminants from water", *Chemical Engineering Journal*, Vol. 244, 2014, pp. 209–217. <http://dx.doi.org/10.1016/j.cej.2014.01.083>
- Hou, B., Li, Q.Y., and Luo, Y., "Synthesis and mechanism of a novel organosilicone used as a selective plugging agent", *Journal of Residuals Science & Technology*, Vol. 12, No. 3, 2015, pp. 149–156. <http://dx.doi.org/10.12783/issn.1544-8053/12/3/5>

A Positional Method for Accidental Chemical Oxygen Demand to Determine a River's Pollution Source

LIU YING, LI YONG, OUYANG FENG and CHEN YU*

Faculty of Geosciences and Environmental Engineering, Southwest Jiaotong University, Chengdu 610031, P.R.China

ABSTRACT: This study stems from a current lack of technology to assess pollutant sources along rivers located in China. A positive water quality distribution model for pollution sources was established, which applies reverse tracing to investigate the likely source of pollution, and a positional method of accidental chemical oxygen demand (COD, analyzed using the dichromate method GB11914-89, the COD in this paper therefore refers to COD_{cr}) of the pollution source in a river was proposed. This method is based on the COD degradation principle in a natural water body, where the variation in the concentration of pollutants in the controlling cross sections was calculated by establishing a mathematical model. A set of calculated values for the controlling cross sections were determined by making educated assumptions about each accidental outlet. The calculated value and the monitored value in the same cross sections were then matched, and the outlets with calculated values that were closer to the monitored value are likely to be the sources of accidental pollution. On this basis, the probability values of these matching outlets were calculated by error sequence.

INTRODUCTION

INDUSTRIAL enterprises in China are mainly located along rivers. The wastewater produced by industrial facilities is treated to satisfy the relevant standards [1,2], and then discharged into the rivers. Restricted by technology and economic conditions, daily online monitoring of the water quality in the outlet area is not practical [3]. When a pollution accident occurs in a river basin, the examination of just one water sample from each outlet, using emergency monitoring equipment, requires a large amount of time. It takes 2 h for the current COD (chemical oxygen demand) emergency monitoring equipment to analyze one sample, and only one sample can be prepared at a time. This kind of expensive monitoring equipment cannot possibly be equipped, therefore, manual checking of the outlets, one by one, is standard working procedure [4,5]. When pollution accidents occur in a river basin, the accidental pollution source is mostly unknown and the determination of the source takes a long time, through repetitive work, and often the pollution source is not determined rapidly enough. If the pollution source cannot be determined and controlled, the amount of pollution will likely increase. This may in turn lead to citizens having a lack of confidence in their government.

*Author to whom correspondence should be addressed.
Tel: 008613880727070. Email: 273620202@qq.com.

METHODS

Practical Considerations for Accidental Pollution Source Positioning

Currently, there are 119 automatic river water quality monitoring stations working and under construction in China. All stations are located at the entrance or exit of the important administrative areas along the main rivers. These monitoring stations can be seen as the first line of defense in water quality warning systems. When pollution incidents occur, the variation of water quality indexes can be captured by the automatic monitoring stations in the river basin. The location in the river where the first automatic monitoring station detects the pollutant will be referred to as the controlling cross section. The first cross section upstream from the controlling cross section, which is not polluted, will be used for comparison, and the river section between them will be referred to as the controlling river section (the polluted section).

Following initial discharge into the river, the pollutants will become diluted and degrade over time. Therefore, if pollutants beyond the normal level are discharged by different outlets, the water quality index in the controlling cross section will be different. The untreated industrial wastewater discharged directly by an outlet will be seen as the produced amount, while

the wastewater discharged by other outlets will be seen as the discharged amount. Based on this, we hypothesize that each pollutant discharge cross section is the accidental pollution source in sequence, then predict the COD value on the controlling section. By analyzing the water quality index on the controlling cross section, the position of the accidental pollution source in the controlling section of the river can be located.

Establishment of a Positioning Model to Predict the Source of Accidental Pollution

The existing water quality model involves a number of variables and can be conducted in many different ways. According to spatial distribution characteristics of water quality variation, the water quality model can be seen as zero-dimensional, one-dimensional, two-dimensional, and three-dimensional. According to the variation of water quality against time the water quality model can be divided into a stable model and a dynamic model. According to variables used in the model it can be divided into a single component model and a multiple component model. According to the mathematic characteristics of the solution to the model it can be divided into a deterministic model and a random model. According to reaction dynamics characteristics it can be divided into a net migration model, a pure reaction model, a migration and reaction model, and an ecological model [6–9]. There are far too many input parameters for these models and the analytical work involved is overwhelming [10–13]. It is not a practical method for predicting the source of pollution accidents which is why a reasonable pollutant transmission model to simulate the impact of pollutants on water quality is required.

The online monitoring location of each political area is only set at the entrance and exit of each administrative area. Therefore, the length of the river that contains the source of accidental pollution is quite expansive. The pollutant can be seen as mixed even when it reaches the downstream monitoring cross section [14–17]. Therefore, the variables studied herein include upstream background input, the secondary river input, the industrial pollution input, the central municipal wastewater outlet, the area source input, the river section output, and the density variation in the vertical direction (i.e., water flow direction).

Pick a river section, A, between two neighboring pollution sources. The location of pollution source 1 is cross section I and the location of pollution source 2 is cross section II. Daily COD discharge in cross sec-

tion I is Q_{COD1} and in cross section II the daily COD discharge is Q_{COD2} . The length of the river section is L (km), the area source input of the river section is $q \cdot L$ in which q is the area source input in a unit section length (kg/km·d), and Q_{COD0} is the background input of the upper stream. Assuming the total area source input in cross section I is Q_{COD1} , then $Q_{COD1} = Q_{COD0} + Q_{COD1}$.

COD is a nonpersistent substance. It will degrade due to chemical or bio-reactions in the environment. Degradation follows the rule of first class reaction dynamics. It also depends on flow distance and degradation of the substance. Neglecting the discrete action the COD amount in any position, x , of the river section can be described follows in Equation (1):

$$\frac{dQ_{COD}}{dx} = q - k^* Q_{COD} \quad (1)$$

Boundary condition: when $x = 0$, $Q_{COD} = Q_{COD1}$ such that the integral of Equation (1) along distance x should be as follows in Equation (2):

$$Q_{CODx} = Q_{COD1}e^{-k^*x} + \frac{q}{k^*}(1 - e^{-k^*x}) \quad (2)$$

If x is equal to the length of river section L , then the output COD in the end cross section of the river section is as follows in Equation (3):

$$Q_{CODL} = Q_{COD1}e^{-k^*L} + \frac{q}{k^*}(1 - e^{-k^*L}) \quad (3)$$

Therefore the pollutant output amount in cross section II is as follows in Equation (4):

$$Q_{CODII} = (Q_{COD0} + Q_{COD1})\exp(-k^*L) + \frac{q}{k^*}[1 - \exp(-k^*L)] \quad (4)$$

Since pollution source 2 enters the river at the exit of river section A it has no contribution to pollution in river section A and only impacts the following river section. It will thus be seen as an input in the downstream river section.

If there is a river section similar to river section A on the downstream side of cross section II (i.e., there's a third pollution source downstream of pollution source 2), then the output amount Q_{CODIII} of river section B can be described according to Equation (4). According to the position of pollution source the river section can be divided into several sections $L_1, L_2, L_3 \dots L_m$. The

output of the sub-section can be seen as the input of the next sub-section. Then, the output of each sub-section can be obtained and Equation (5) for calculating the output of n number of sections is:

$$Q_{COD} = \left[\begin{aligned} & (Q_{COD0} + Q_{COD1}) \exp(-k^* L) \\ & + \sum_{i=2}^n [Q_{CODi} \exp(-k^* \sum_{j=i}^n L_j)] \\ & + \frac{q}{k^*} - \frac{q}{k^*} \exp(-k^* L) \end{aligned} \right] \quad (5)$$

The upper stream background input Q_{COD0} , the pollution load of each source or sub-section of the fixed river section Q_{CODi} , the distance from each pollution source to the controlling section L_j , the pollution load of the areal pollution source per unit river section per unit time q , and the decreasing rate k^* of the pollutants are parameters. After Equation (5) if all these parameters are known the pollution load Q_{COD} of the controlling cross section or the terminal of the polluted river section can be calculated using Equation (6):

$$C'_{CODi} = \frac{\left[\begin{aligned} & Q_{COD0} \exp(-k^* L) \\ & + \sum_{i=1}^n [Q_{CODi} \exp(-k^* \sum_{j=i}^n L_j)] \\ & + \frac{q}{k^*} - \frac{q}{k^*} \exp(-k^* L) \end{aligned} \right]}{864 \times u} \quad (6)$$

Based on the previously mentioned positional method of locating the accidental pollution source the first special condition is that there might be more than one pollutant outlet in any cross section in the polluted river section. This means there can be more than one outlet contributing to the pollution discharge cross section that is established according to the pollution outlet position. Under this condition, the C'_{CODi} which is calculated from the above method needs to be adjusted (i.e., when there are r number of outlets in some cross section a_i , where >1) and then total COD, Q_{CODi} , is the aggregate COD of each outlet. When calculating the possible COD amount of this cross section under the accidental condition the COD amount of the cross section is calculated by assuming each outlet as the produced amount and other outlets as the discharged amount in sequence. This means in the above method, the i th pollution discharge cross section, a_i , has r number of polluted outlets in sequence. Thus, there would

be r number of datapoints $Q_{CODi(y)}$ for the total COD in the i th pollution discharge cross section Q_{CODi} , $y = 1, 2, \dots, r$, and Equation (7):

$$Q_{CODi(y)} = Q_{CODiy} + \sum_{x \neq y}^r Q_{CODix}$$

where Q_{CODiy} is the COD produced by the y th outlet, which is the supposed accidental pollution source (kg/d) obtained from the local environmental protection department. $Q_{CODi(x)}$ is the COD discharged from other outlets contributing to the i pollution discharge cross section (kg/d) obtained from the local environmental protection department.

Another special condition is where the outlets in a river section are located very close to each other. Under this condition if one cross section is built for each outlet there would be too many cross sections and the distance between two neighboring sections would be too short. The inspection period would take too long and have an adverse effect on precision. Under these circumstances the outlets located close to each other are merged into one outlet according to the *Environmental Impact Assessment Technical Specification – Surface Water Environment* (HJ/T2.3) regulations such that all outlets are separated into different cross sections. Then, the location of each discharge cross section (a_i , $i = 1, 2, \dots, n$) in the polluted river section and the distance (l_i , where $i = 1, 2, \dots, n$) between a_i and the control cross section is determined. Therefore, where there is more than one outlet in a certain discharge cross section the above mentioned method can be used to finish the calculated prediction.

APPLICATION

The Yangtze River section in Yibin City has third-level quality surface water in which the upper limit COD is 20 mg/L. The COD pollution accident chosen for this study is an industrial center along the Yangtze River section in Yibin City. When the industrial unit was under maintenance and no pollution was discharged this is taken as the normal condition. When it starts to work and discharge, it is presumed to be a COD pollution accident. The basic information on the pollution source provided by the local environmental protection department is seen in Table 1 where all the outlets that are very close to each other are merged. After analysis 15 discharge cross sections were confirmed as a_1, a_2, \dots, a_{15} . The basic data of the controlling section is seen in Table 2.

Assume cross sections $\alpha_1, \alpha_2, \alpha_3 \dots \alpha_{15}$ are the accidental pollution source cross sections in sequence and for each cross section assume Qn is the pollution outlet. According to Equations (6) and (7) the predicted COD value of the related controlling cross section C'_{CODi} , $i = 1, 2, \dots n$ is seen in Table 3.

By comparing calculated results in Table 3 and the C_{COD} value (11.88 mg/L) of the controlling cross section it shows that the value of cross section α_6 (11.87 mg/L) is most similar to the controlling cross section. Upon practical examination the predicted result fits reality.

Table 1. Pollution Sources and Data of Discharge Cross Section α_i .

Cross Section α_i	Pollution Source	Distance from Cross Section (α_i) to the Controlling Section, I_j (km)	COD Generation (t/a)	COD Discharge (t/a)
α_1	Q1	83.3	100419.20	28691.20
	Q2	83.3	3.15	0.90
	Q3	83.3	15.05	4.30
	Q4	83.3	700.00	200.00
	Q5	83.3	137690.00	39340.00
	Q6	83.3	63.00	9.00
	Q7	83.3	214.90	30.70
	Q8	83.3	35.00	5.00
	Q9	83.3	44.80	6.40
α_2	Q1	82.3	15000.00	600.00
	Q2	82.3	1.40	0.20
	Q3	82.3	224.00	32.00
	Q4	82.3	32557.50	1302.30
α_3	Q1	81.3	4154.60	4154.60
	Q2	81.3	1344.00	192.00
	Q3	81.3	56.00	8.00
	Q4	81.3	212.80	30.40
	Q5	81.3	256.20	36.60
α_4	Q1	80.3	147224.00	21032.00
α_5	Q1	79.3	540540.00	54054.00
α_6	Q1	77	107020.00	0
α_7	Q1	61	8662.50	346.50
α_8	Q1	61	2250.00	90.00
α_9	Q1	56.1	4935.00	493.50
α_{10}	Q1	42.3	1890.00	270.00
α_{11}	Q1	40.2	7.00	1.00
	Q2	40.2	10066.70	10066.70
	Q3	40.2	210.00	30.00
	Q4	40.2	3.50	0.50
	Q5	40.2	55.65	15.90
	Q6	40.2	138.25	39.50
	Q7	40.2	126.00	36.00
	Q8	40.2	1504.00	188.00
	Q9	40.2	842.50	33.70
	Q10	40.2	2270.10	324.30
	Q11	40.2	63000.00	9000.00
	Q12	40.2	240.00	9.60
α_{12}	Q1	38	36000.00	1440.00
α_{13}	Q1	22.8	4102.70	4102.70
α_{14}	Q1	19.6	70000.00	10000.00
α_{15}	Q1	5.5	27828.00	2319.00
	Q2	5.5	3000.00	250.00

Table 2. Basic Data of the Controlling River Section.

C_{COD0} (mg/L)	Q_{COD0} (kg/d)	C_{COD} (mg/L)	L (km)	q [16] (kg/km·d)	u (m ³ /s)	v (m/s)	k^* [18] (1/km)
11.74	4595.40	11.88	86	11792.60	4530.45	0.94	0.00246

DISCUSSION

Since there are some parameter and calculation errors in the simulation and there might be several matching values in the simulation, the information acquired is just a probability value. Define a binary unit $A(a_i, Q_j)$ in which $a_i, i = 1, \dots, n$ refers to the i th discharge cross section, $Q_j, j = 1, \dots, m$ and refers to the j th pollution discharge outlet, and $A(a_i, Q_j)$ refers to the j th pollution discharge outlet in the i th cross section. It is thus observed that $A(a_i, Q_j)$ can refer to only one pollution discharge outlet.

Suppose one discharge outlet $A(a_i, Q_j)$ is the accidental pollution source, calculate the COD value (C'_{CODi}) of the monitored cross section downstream that is the controlling cross section with Equation (3). There the calculated COD value (C'_{CODi}) is marked as $C'_{COD}(a_i, Q_j)$. The monitored COD value from the controlling cross section is C_{COD} . Let the deviation be the difference of the calculated and tested COD value, marked as:

$$COD, i = 1, \dots, n, j = 1, \dots, m$$

And let Equation (8) be

$$m(a_i, Q_1) = \frac{MAX(r(a_i, Q_1))}{r(a_i, Q_1)} \tag{8}$$

j can be calculated [Equation (9)]:

$$P^0(a_i, Q_1) = \frac{m(a_i, Q_1)}{\sum_{i,j} m(a_i, Q_1)} = \frac{1}{r(a_i, Q_1) \sum_{i,j} r(a_i, Q_1)} \tag{9}$$

The deviation and probability for a pollution source is provided. Results are seen in Table 4.

CONCLUSION

When sudden pollution accidents occur in a drainage area the method proposed herein can be used alongside a basic database for each outlet provided by the local environmental department. This method involves comparison of monitoring data from river

Table 3. Calculated COD Value.

Cross Section α_i	Pollution Source	Predicted COD Value of Related Controlling Cross Section, C'_{CODi} (mg/L)
α_1	Q1	11.65
	Q2	11.23
	Q3	11.23
	Q4	11.23
	Q5	11.81
	Q6	11.23
	Q7	11.23
	Q8	11.23
	Q9	11.23
α_2	Q1	11.31
	Q2	11.23
	Q3	11.23
	Q4	11.41
α_3	Q1	11.23
	Q2	11.24
	Q3	11.23
	Q4	11.23
	Q5	11.23
α_4	Q1	11.98
α_5	Q1	14.13
α_6	Q1	11.87
α_7	Q1	11.28
α_8	Q1	11.24
α_9	Q1	11.26
α_{10}	Q1	11.24
	Q1	11.23
	Q2	11.23
	Q3	11.23
	Q4	11.23
	Q5	11.23
	Q6	11.23
	Q7	11.23
	Q8	11.24
	Q9	11.23
	Q10	11.24
	Q11	11.58
Q12	11.23	
α_{12}	Q1	11.45
α_{13}	Q1	11.23
α_{14}	Q1	11.63
α_{15}	Q1	11.41
	Q2	11.25

Table 4. Deviation and Probability of Pollution Source.

Cross Section α_i	Pollution Source	$r(a_p, Q_j)$	$P^0(a_p, Q_j)$
α_1	Q1	0.23	2.25
	Q2	0.65	0.80
	Q3	0.65	0.80
	Q4	0.65	0.80
	Q5	0.07	7.41
	Q6	0.65	0.80
	Q7	0.65	0.80
	Q8	0.65	0.80
	Q9	0.65	0.80
α_2	Q1	0.57	0.91
	Q2	0.65	0.80
	Q3	0.65	0.80
	Q4	0.47	1.10
α_3	Q1	0.65	0.80
	Q2	0.64	0.81
	Q3	0.65	0.80
	Q4	0.65	0.80
	Q5	0.65	0.80
α_4	Q1	0.10	5.19
α_5	Q1	2.25	0.23
α_6	Q1	0.01	51.86
α_7	Q1	0.60	0.86
α_8	Q1	0.64	0.81
α_9	Q1	0.62	0.84
α_{10}	Q1	0.64	0.81
α_{11}	Q1	0.65	0.80
	Q2	0.65	0.80
	Q3	0.65	0.80
	Q4	0.65	0.80
	Q5	0.65	0.80
	Q6	0.65	0.80
	Q7	0.65	0.80
	Q8	0.64	0.81
	Q9	0.65	0.80
	Q10	0.64	0.81
	Q11	0.30	1.73
	Q12	0.65	0.80
α_{12}	Q1	0.43	1.21
α_{13}	Q1	0.65	0.80
α_{14}	Q1	0.25	2.07
α_{15}	Q1	0.47	1.10
	Q2	0.63	0.82

cross sections to a control cross section. Through calculation the accidental pollution source can be located relatively quickly. This reduces the need to retrieve and analyze samples from each outlet. The monitoring location in China is usually set at the entrance and exit of

a political area the distance between which is hundreds of kilometers. Therefore, there may be many suspected pollution outlets if pollution accidents take place. Under these conditions the proposed method can shorten the period of time taken to locate the pollution source or significantly narrow the pollution source area or focus. Thus, the amount of work involved is significantly decreased, the scale of pollution can be lowered, the recovery period for the environment can be shortened, and costs can be decreased.

ACKNOWLEDGMENTS

We acknowledge the support of the National Natural Science Foundation of China (grant number: 51209178) and the China scholarship council Foundation.

REFERENCES

1. Yu Z.H., Xia J.X., Ren H.T. 2014. "Water Pollution Accident Emergency Response and Early-Warning Model in Gansu-Ningxia-Inner Mongolia Section of the Yellow River", *Yellow River*, 36(4):37-40.
2. Li L.Z., Qian Y., Zhang Y.C. 2011. "Forecasting and Warning the Accidental Water Pollution and Warning the Accidental Water Pollution Effect Based on the EFDC and WASP", *Resources and Environment in the Yangtze Basin*, 20(8):2010-2016.
3. Sun H.L., Li J.F., Zhu Y.Y. 2009. "Development and Prospect of Water Quality On-line Monitoring System in China", *China Environmental Protection Industry*, 2:12-16.
4. Li F.. 2012. Rapid Determination of Chemical Oxygen Demand based on Micro-spectrometer. Master's thesis, Chongqing University, Chongqing, China.
5. Liu Q., Cheng J.B. 2012. "The Research on Flow Injection Technology in COD Online Monitoring", *Environmental Monitoring and Forecasting*, 4:20-23.
6. Wang, L. 2006. An application study on common water quality model in environmental impact assessment. Master's thesis, Lanzhou University, Lanzhou, China.
7. Miao, H.B. 2004. Contamination two-dimensional water quality model study of surrounding area of drainage outlet of city rivers. Master's thesis, Sichuan University, Chengdu, China.
8. Shi, Z. 2009. The research of water environmental capacity based on uncertainty model of xiangjiang river section in chang-zhu-tan. Master's thesis, Hunan University, Changsha, China.
9. Xu, J. 2007. Research on mass transfer theory for 2-D stochastic water quality model. Master's thesis, Chongqing University, Chongqing, China.
10. Dou M., Ma J., Xie D.Y., et al. 2007. "Numerical simulation on Cadmium pollution in North River", *Journal of Zhen zhou University (Engineering Science)*, 28(28) :117-120.
11. He Q., Peng S.J., Zhai J. 2011. "Development and application of a water pollution emergency response system for the Three Gorges Reservoir in the Yangtze River China", *Journal of Environmental Sciences*. 23(4):595-600. [http://dx.doi.org/10.1016/S1001-0742\(10\)60424-X](http://dx.doi.org/10.1016/S1001-0742(10)60424-X)
12. Manel G., Gabriel J., Manuel E., et al. 2011. "A management system for accidental water pollution risk in a harbour: The Barcelona case study", *Journal of Marine Systems*, 88(1): 60-73. <http://dx.doi.org/10.1016/j.jmarsys.2011.02.014>
13. Liu, Y.G., Yang, Y.X., Xu, C.D.. 2015. "Risk Evaluation of Water Pollution in the Middle Catchments of Weihe River", *Journal of Residuals*

- Science & Technology*, 12(S1):1544–8053. <http://dx.doi.org/10.12783/issn.1544-8053/12/s1/19>
14. Chen L.P., Jiang J.C., Yin L. 2007. "Numerical simulation water pollution diffusions for sudden hazardous chemical", *Journal of Hydrodynamics*, 22(6):500–504.
 15. Cao, L.L., Huang, C.G., Wang, J.H.. 2014. "Pollution Status of Selected Metals in Surface Sediments of the Pearl River Estuary and Daya Bay, South China Sea", *Journal of Residuals Science & Technology*, 11(4): 119–130.
 16. Wang Q.G., Zhao X.H., Wu W.J.. 2008. "Advection-diffusion models establishment of water-pollution accident in middle and lower reaches of Hanjiang River", *Advances in Water Science*, 19(4):500-504.
 17. Tao Y., Ren H.T., XIA J.X.. 2013. "Effect Analysis of Different Emergency Measures for Accidental Water Pollution", *Journal of Basic Science & Engineering*, 21(2):203–213.
 18. Zhang, B.H., Wang, L.J. and Guo, B. 2009. "Load of Non-Point source pollutants from upstream rivers into Three Gorges Reservoir", *Research of Environmental Sciences*, 22(2): 127–129.

Biosolids Application for Barley Production

AKRUM H. TAMIMI^{1,*}, B. ATHAMNEH², C. P. GERBA¹ and W. SULEIMAN²

¹Department of Soil, Water and Environmental Science, University of Arizona, Tucson, AZ

²Water and Environment Center, Royal Scientific Society, Amman, Jordan

ABSTRACT: Biosolids with different loading rates were applied to soil planted with rain-fed barley to study the effects of applying biosolids on soil and on barley's straws and grains yield. Randomized Complete Block experimental design was employed with 5 treatments. This included a control and four replicates to test the null hypothesis which states that there is no significant difference between treatment means on crop and soil parameters vs. the research hypothesis which states applying biosolids to land planted with rain-fed barley affects both soil and crop parameters. Biosolids loading rates were 0 as a control, 2, 4, 6, and 8 metric tons/ha.

Soil at the testing site had a high clay content in the sub-soil and relatively lower clay content on the surface, probably due to wind erosion. The soil was slightly calcareous with lime content increasing with depth and with a slight alkalinity. Organic matter and phosphorus contents of soil were low with colors that varied from reddish brown to yellowish brown.

At harvesting time, there was no significant differences in grain yields at different biosolids loading rates with a *p*-value of 0.52. Average grain yields of 2.86, 3.37, 3.4, 3.57, and 3.20 tons/ha were measured at biosolids loading rates of 0, 2, 4, 6, and 8 tons/ha, respectively. Average grain yield of 3.00 for a recommended inorganic fertilizer rate of diammonium phosphate and Urea traditionally applied at rates of 90 kg/ha and 20 kg/ha, respectively, showed a yield higher than the 0 biosolids loading rate. However, it was lower than all other biosolids loading rates.

It was determined that applying biosolids to soils planted with rain-fed barley significantly increased straw yield and straw protein content. No significant increase in grain yield or in grain protein content was measured. It was also determined that a statistical significant decrease in the thousand grain weight occurs as biosolids loading rates increased with a *p*-value < 0.000001. This has negative effects on barley's grain quality.

No significant increase in heavy metals in the crop or the soil was observed in the biosolids treated plots. However, increases in soil organic carbon, total Kjeldahl nitrogen and salt concentrations were increased with increasing biosolids loading rates.

The null hypothesis tested in this study showed that applying biosolids to soils planted with rain-fed barley had positive effects on the crop with no effects on the soil in comparison with no application of biosolids and the application of inorganic fertilizer.

OBJECTIVE

THE objectives of this study were to determine effects of applying biosolids to soils planted with rain-fed barley on the soil and the crop and to determine the optimized biosolids loading rate that generates ultimate biological yield.

BACKGROUND

Wastewater management policy issued by Jordan Ministry of Water and Irrigation (MWI) addresses the management of wastewater as a water resource in-

cluding development, collection, treatment, and reuse. Among the specific policies and aspects emphasized are the beneficial reuse of treated effluent and biosolids. While the use of biosolids for agricultural production is now commonplace in many countries around the world, this resource is not currently utilized in Jordan. Generated biosolids are currently disposed of at landfills or are stored in wastewater treatment plants (Suleiman *et al.*, 2010). However, (Skjelhaugen, 1999) showed that proper reuse of biosolids can alleviate pollution problems and health hazards. A sustainable and acceptable option for the long-term management of biosolids must be environmentally friendly, economically viable, and socially acceptable (Wang *et al.*, 2008). There is general consensus among sanitary en-

*Author to whom correspondence should be addressed.
Email: akrumt@email.arizona.edu.

gineering professionals that municipal wastewater and biosolids are not a “waste”, but a location of valuable resources (State of Science Report: Energy and Resource Recovery from Sludge, 2008). Leblanc *et al.*, 2003 stated that biosolids must be regarded as a recyclable resource that can be put to beneficial reuse. Although there are different biosolids beneficial reuse options, application of biosolids to agricultural land is of primary importance and has been widely practiced in different countries for many years (Magesan and Wang 2003; Cartmell 2006; González *et al.*, 2008). Amajiri-onwu *et al.*, 2008 studied the impact of stakeholder participation in the management of biosolids in Ireland and found that 81% of stakeholders believed that local and regional sustainable development indicators due to participatory biosolids management as either ‘useful’ or ‘very useful’. The indicators addressed all the domains of biosolids management namely, production, quality, cost, legislation, regulation, training, research, recycling and disposal. The stakeholder approach is recognition that no effective indicator set can be developed without the input of stakeholders.

Biosolids have direct effects on soil physical properties such as soil aggregation, soil encrustation, tilt, aeration, temperature and microbial activities. Oudeh *et al.* (2002) reported that biosolids can replenish organic matter levels with beneficial effects on physical and biological conditions. Moreover, addition of biosolids to a fine-textured clay soil can make soil more friable and can increase the pore space available for root growth and entry of water and air into the soil (González *et al.*, 2008). Zebarth *et al.* (1999), indicated that application of biosolids to soils significantly increased soil water content and water holding capacity. Mays *et al.* (1973) stated that the incorporation of composted biosolids at a rate of 327 metric tons/ha over a two-year period significantly increased moisture holding capacity from 11.1–15.3% at 1/3 bar and decreased bulk density from 1.37–1.12 gm/cm³. Soil organic matter is a major determinant of soil fertility, water holding capacity, and biological activity as well as diversity both below and above ground. Loss of organic matter can lead to soil erosion and loss of fertility. Consequently, using biosolids for agricultural production has an important role in replacing losses that can arise from intensive arable farming. Pu *et al.* (2004), found that the optimized biosolids application rate of 7 tons/ha for aerobically digested biosolids and 10 tons/ha for anaerobically digested biosolids for growing forage sorghum. They also determined that excessive application rates of biosolids that are above the optimized values did not

show further increases in dry mass of forage sorghum production and resulted in significant increases in soil residue nitrate and phosphorous, which in the cases of heavy rainfall and irrigation could result in losses through leaching and runoff respectively. Mantovi *et al.*, 2004 applied dewatered biosolids at the loading rate of 5 and 10 tons/ha on winter wheat-maize-sugar beet rotation and found that Biosolids gave crop yields similar to the highest mineral fertilizer application. Biosolids increased organic matter, total nitrogen, and available phosphorus in the soil while reducing soil alkalinity, especially at loading rate of 10 tons/ha. Significant accumulations of total zinc and copper were detected in amended top soils, but other heavy metals remained well below the hazard limits. Biosolids applications significantly increased the content of nitrogen, phosphorus, zinc and copper in wheat grain, nitrogen and copper in sugar beet roots, and only copper in maize grains. Kresse and Naylor (1983) reported that biosolids treated plots produced corn yields equivalent to those to which commercial fertilizers were applied. Reuse of biosolids in agricultural production increases supply of macro and micro-nutrients to the plant and hence improves agricultural productivity (Werheim *et al.*, 2000, Athamneh, 2003). Rusan and Athamneh (2009), reported that application of biosolids to calcareous soil improved soil organic matter, available phosphorous and micro-nutrients as well as plant growth.

Biosolids appropriate loading rate is one that maximizes yield while ensuring protection of the environment (Avnimelech *et al.*, 1990). However, loading rate of biosolids has commonly been based on nitrogen content and nitrogen requirement of the crop (Barbarick and Lppolioto, 2000). Schroder *et al.* (2008) studied the effects of long-term annual application of biosolids on soil properties, phosphorus, and metals. They found that repeated long-term application of biosolids above the nitrogen agronomic rate should be avoided and application should be based on other criteria such as an agronomic phosphorus threshold. Jin *et al.*, 2011 studied the effects of biosolids application rate on soil potential carbon and nitrogen mineralization in the lab. They applied 0, 22, 25, 45, and 67 tons/ha Class B biosolids for several years. They found that biosolids addition enhanced organic carbon by 32–92%, total nitrogen by 30–157%; and that high loading rates of biosolids might increase the risk of off-site nutrient transport. Lagae *et al.* (2009) determined that using biosolids as a soil amendment can have positive economic benefits. Lomontea *et al.*, 2010 investigated the potential of phytoremediation of Mercury contaminat-

ed biosolids by nine plant species (*Atriplex condonocarpa*, *Atriplex semibaccata*, *Australodanthonia caespitosa*, *Brassica juncea*, *Brassica napus*, *Gypsophila paniculata*, *Sorghum bicolor*, *Themeda triandra* and *Trifolium subterraneum*). They found that *Atriplex condonocarpa* and *Australodanthonia caespitosa* to be the most suitable candidates for mercury phytoextraction because of their ability to translocate mercury from roots to the above-ground tissues.

METHODS AND MATERIALS

Experimental Site Description

The Ramtha Regional Experimental Center was selected as the experimental study site. The Ramtha Center is located in the middle of 264 hectares that are farmed with rain-fed cereal crops, especially barley that is used as a fodder crop. Barley grains are mostly used in raising meat producing animals such as sheep and lambs due to the grain's high content of protein; while barley straws are used to feed sheep and lambs but is also used to feed work animals such as donkeys, mules and horses. Ramtha Center is located five Kilometers to the North of Wadi Hassan Waste Water Treatment Plant (WWTP) and about 70 Kilometers to the North of the Jordan Capital, Amman, with an altitude of 590 meters above sea level. The climate is represented by cold winters and hot summers with average temperatures ranging from 5° Celsius in January to 35° Celsius in August with an average annual rainfall of 235 mm/year occurring between November and March.

Initial Soil Characterization

Initial soil characteristics shown in Table 1 were determined by collecting composite samples at three soil depths prior to applying biosolids. The samples were tested for general physical, chemical and microbial characteristics using United States Environmental Protection Agency (U.S. EPA) standard methods.

Biosolids Characterization

Tamimi *et al.* (2007) characterized biosolids generated at Wadi Hassan WWTP and found it to be of Class B quality based on the U.S. EPA 503 rule (U.S. EPA, 1993a and U.S. EPA, 1993b). Biosolids obtained from Wadi Hassan WWTP was characterized prior to applying it to the experimental site and was found to be of Class B quality. Table 2 shows biosolids characteristics

Table 1. Experimental Site Initial Soil Characteristics.

Parameter	Unit	Sampling Depths (cm)			
		0–15	15–30	30–60	
Soil Texture:	Sand	%	9	8	6
	Silt	%	40	36	35
	Clay	%	51	55	59
Texture			Clay	Clay	Clay
pH 1:1			8.38	8.38	8.52
EC 1:1	dS/m	0.359	0.368	0.925	
Organic Matter	%	1.58	1.26	1.62	
TKN	mg/kg D.W.*	853	678	476	
NH ₄ -N	mg/kg D.W.	5.01	4.47	4.01	
NO ₃ -N	mg/kg D.W.	11.1	13.3	11.3	
available-P	mg/kg D.W.	11.83	5.90	2.63	
CaCO ₃	%	9.67	11.00	11.33	
available-K	mg/kg D.W.	817	587	406	
available-Na	mg/kg D.W.	105	167	392	
available-Mg	mg/kg D.W.	816	1009	1186	
available-Ca	mg/kg D.W.	7790	7441	6974	
As	mg/kg D.W.	N.D.	N.D.	N.D.	
Cd	mg/kg D.W.	N.D.	N.D.	N.D.	
Cr	mg/kg D.W.	42	32	22	
Cu	mg/kg D.W.	13	11	7	
Pb	mg/kg D.W.	45	36	22	
Hg	mg/kg D.W.	30	33	N.D.	
Mo	mg/kg D.W.	N.D.	N.D.	N.D.	
Ni	mg/kg D.W.	32	20	18	
Se	mg/kg D.W.	N.D.	N.D.	N.D.	
Zn	mg/kg D.W.	58	61	61	
Co	mg/kg D.W.	28	33	28	
Salmonella	MPN/g	N.D.	N.D.	N.D.	
coliforms	MPN/g	N.D.	N.D.	N.D.	
IPN***	Eggs/g	N.D.	N.D.	N.D.	

*D.W.: Dry Weight

**N.D.: Not Detected

***IPN: Intestinal Pathogenic Nematodes

obtained during the current study and those found by Tamimi *et al.* (2007).

United States Environmental Protection Agency microbial analytical laboratory methods were used in the detection of *Salmonella*, fecal coliforms and Helminth (*Ascaris*) ova (EPA/625/R-92-013).

Experimental Design

After characterizing the soil profile at the study area and biosolids intended to be applied, the experimental field was divided into plots based on a randomized complete block experimental design with 4-treatments. A control and 4-replicates comprising 20 plots of 6 m by 4 m with a buffer of 2 m between plots were used. The treatments represented loading rates of zero tons/

Table 2. Biosolids Characteristics of Wadi Hassan Wastewater Treatment Facility.

Parameter	Unit	Tamimi et al. (2007)			
		Current Study (Prior to Application)	Arithmetic Mean	95% Confidence Interval	
				Lower Limit	Upper Limit
TS	%	88	85.44	82.19	88.70
TVS	% of TS	53	45.22	43.46	46.99
TKN	%	3.20	3.81	3.66	3.95
NH ₄	%	0.03	0.14	0.10	0.18
T-P	%	0.39	1.05	0.79	1.30
K	mg/kg DW*	3299	4159	3887	4431
As	mg/kg DW	<4.5	ND**	ND	ND
Cd	mg/kg DW	2.71	3.21	2.99	3.43
Cr	mg/kg DW	50.73	49.8	46.6	53.0
Cu	mg/kg DW	95.66	73.8	68.3	79.3
Pb	mg/kg DW	56.4	23.3	20.8	25.8
Hg	mg/kg DW	<2.82	ND	ND	ND
Mo	mg/kg DW	<11.3	18.7	15.7	21.7
Ni	mg/kg DW	38.30	41.1	39.5	42.7
Se	mg/kg DW	<6.8	ND	ND	ND
Zn	mg/kg DW	1001	792	733	852
Co	mg/kg DW	<1.12	ND	ND	ND
<i>Salmonella</i>	MPN/10 g	Absent	Absent	Absent	Absent
fecal coliforms	MPN / g	9.30 × 10 ⁴	2.0 × 10 ⁵	2.7 × 10 ³	3.7 × 10 ⁵
Helminth (<i>Ascaris</i>) Ova	Eggs/g	ND	ND	ND	ND

*D.W.: Dry Weight

**N.D.: Not Detected

ha for the control, 2, 4, 6, and 8 tons/ha. Loading rates were assigned to the plots randomly and the plots were labeled accordingly.

Barley Seeding

Soil at the experimental site was ploughed to a depth of approximately 110 mm before the rainy season. A few days after the major first rain storm, a second plough was performed during which furrows were formed. Biosolids were incorporated uniformly with soil to a depth of 8 cm according to the experimental design and barley (Rum variety popular in Jordan for growing under stress conditions) was sowed using sowing machinery with a seeding rate of 100 kg/ha.

Crop Sampling

At the end of the growing season, plant samples were collected from representative areas of one squared meter in each plot and the grain and straw were separated. Samples were transferred directly after collection to the laboratories in sterile sealed bags and then analyzed for microbiological parameters following

the World Health Organization (1989) and Manual of Food Quality Control (1992). For chemical analysis, samples were dried at 68° Celsius to stop enzymatic reaction; then samples were grinded using laboratory mill with 0.5 mm sieve size to obtain suitable and homogeneous samples for laboratory analysis. Samples then were kept in sealed jars and analyzed for total nitrogen, protein content, total phosphorus, total potassium, and trace metals.

Soil Sampling

At the harvesting stage, soil samples were collected at two depths: 0–15 cm and 15–30 cm. A total of 40 random composite samples were collected from the 20 experimental plots at two depths and were analyzed for chemical parameters.

Analysis of Variance (Ott and Longnecker, 2001) was performed for each parameter measured during the study to determine if there is a significantly measured statistical difference between the treatments and the control on the measured parameters; and hence infer the effects of applying biosolids on the crop and the soil.

All statistical significant tests conducted here use an upper-tail value of the F statistic corresponding to a rejection area of $\alpha = 0.05$ representing the probability of type I error: rejecting the null hypothesis when it is true (Ott and Longnecker, 2001).

RESULTS AND DISCUSSION

Biosolids Effects on Crop Yield

Four yield parameters were measured at the end of the growing season: total biological yield, grain yield, straw yield and thousand kernel count. In addition, percent protein content in straw and grain were measured and statistical analysis of variance was performed. Total biological yield for cereal crops is defined as the total above ground biomass (total dry matter) produced by the plant. Grain and straw yield is the weight of grain and straw in tons per hectare. The thousand kernel or grain weight, however, is a measurement of the weight in grams of 1,000 seeds of a grain random sample and is an indication of the size of the individual grain. The weight varies from one variety to another and from one crop type to another. In fact, the thousand grain weight of a single variety will vary from year to year and from field to field.

The null hypotheses being tested for the total biological yield parameter states that the arithmetic means of the total biological yield measured for the different treatment plots are identical and there is no difference between them. This implies that there is no effect of applying biosolids on total biological yield. The analysis of variance concludes though that one should reject the null hypothesis inferring that there is a difference in total biological yield with a p -value = 0.035 between the different treatments. Figure 1 shows the trend of in-

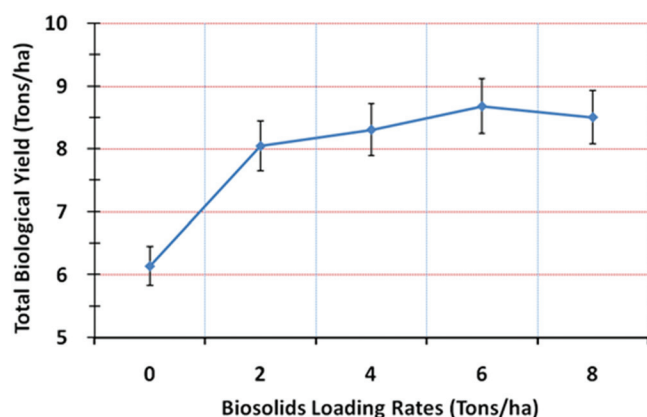


Figure 1. Relationship between total biological yield and biosolids loading rate.

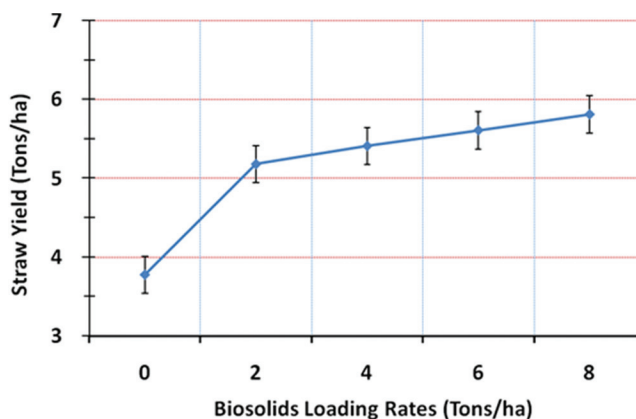


Figure 2. Effect of biosolids loading rate on straw yield.

creasing total biological yield with increasing biosolids loading rate to a peak of 8.68 tons/ha at biosolids loading rate of 6 tons/ha. Applying more biosolids than the 6 tons/ha reduces the total biological yield.

There was no significant change in grain yield due to the application of biosolids. The analysis of variance test indicates that the difference between the arithmetic means of the treatments is statistically insignificant with a p -value = 0.52.

There was however a significant effect on straw yield while increasing biosolids loading rate (p -value = 0.0013). Figure 2 shows the increasing trend of straw yield when biosolids loading rate is increased.

Figure 3 shows a significant (p -value < 0.000001) decreasing trend of the thousand grain weight with increasing biosolids loading rates with a minimum thousand grain weight of 32.6 grams, which corresponds to a biosolids loading rate of 8 tons/ha compared to a 38.8 grams for the control plots.

Percent straw protein content and the analysis of variance indicated that there was a statistical significant difference amongst the treatment means with p -value = 0.00004. Figure 4 shows an increase in per-

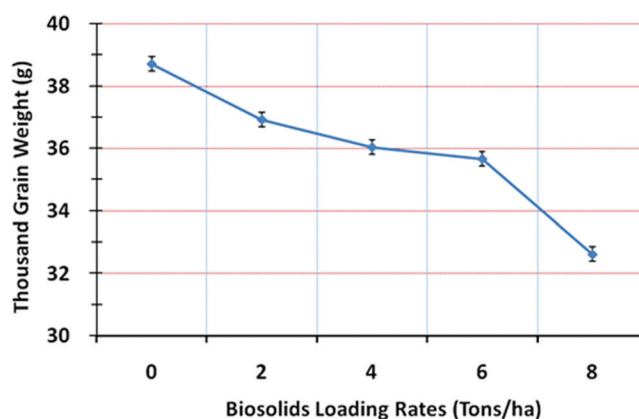


Figure 3. Effect of biosolids loading rate and thousand grain weight.

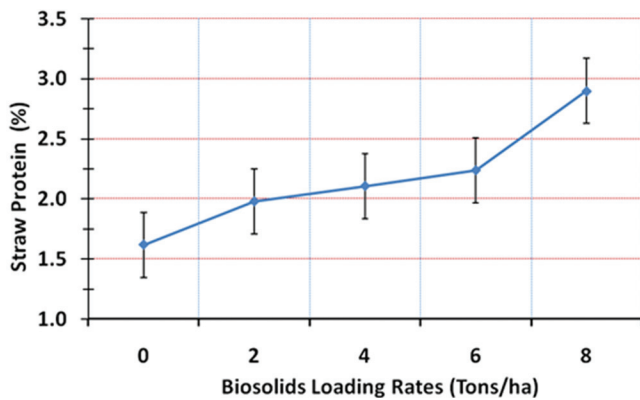


Figure 4. Effect of loading rate on percent straw protein content.

cent straw protein content from 1.6% with zero biosolids to 2.9% at 8 tons/ha biosolids loading rate.

However, for grain protein content (%), the analysis of variance indicates that there was no statistical significant difference between the arithmetic means of the biosolids loading rates treatments with a p -value of 0.275.

Statistical analysis of the four yield parameters presented demonstrates that increasing biosolids loading rate significantly increase the total biological yield to a certain loading rate but not grain yield. At the highest biosolids loading rate straw yield was at its maximum and the thousand grain weight was at its lowest indicating that vegetative growth due to higher levels of nitrogen availability from higher biosolids loading rates is dominant resulting in a lower grain quality (size). This is also supported by the results obtained for the high percent protein content in straw and the non-significant difference amongst the treatments for the percent protein content of grain.

Therefore, it can be concluded based on yield pa-

rameters that the optimum biosolids loading rate should not be greater than 6 tons/ha. Also, at this level of biosolids loading rate grain weight (size) is reduced but the ultimate grain yield did not change (did not show statistical significant difference amongst the treatment means).

Impact of Biosolids Application on Crop Contamination by Enteric Organisms

Samples of barley straws and grains were collected from each experimental plot after harvesting and were tested for microbial pathogens and fecal indicators: *Salmonella*, fecal coliforms, nematode eggs and *Escherichia coli*. Analysis of variance was conducted on each enteric organism using a probability of Type I Error, α of 0.05. The null hypothesis, H_0 , being tested for each pathogen stated that there is no difference in the concentration of the pathogen between all the experimental plots. That can be interpreted to mean that there are no enteric organisms' effects on the straws/grains due to the application of biosolids of different loading rates. The research hypothesis, H_a , stated: that there is difference in the mean concentration or number of enteric organisms due to the application of biosolids at the specified loading rate. An F statistic was calculated and a conclusion was reached to accept or reject the null hypothesis, H_0 , for each specific pathogen and a p -value was calculated.

Table 3 shows the results obtained for each enteric organism in barley straws due to the application of biosolids. The results presented in Table 3 show that there is no significance difference in any enteric organism in the barley straws for the different biosolids treatments.

Table 3. Analysis of Variance Results for Enteric Organisms in Barley's Straws.

Treatment (Ton/ha)	Straw Arithmetic Means for Microbial Parameters			
	<i>Salmonella</i> (MPN/20 g)	Fecal Coliforms (MPN/g)	Nematode Eggs (/20 g)	<i>E. coli</i> (MPN/g)
0	*ND	5.03	ND	5.03
2	ND	11.00	ND	4.33
4	ND	5.52	ND	0.77
6	ND	2.80	ND	0.57
8	ND	5.53	ND	5.53
H_0 : Reject or Accept?	Accept	Accept	Accept	Accept
p -Value	–	0.056	–	0.174

*N.D.: Not Detected

Table 4. Analysis of Variance Results for Enteric Organisms in Barley's Grains.

Treatment (Ton/ha)	Straw Arithmetic Means for Microbial Parameters			
	<i>Salmonella</i> (MPN/20 g)	Fecal Coliforms (MPN/g)	Nematode Eggs (/20 g)	<i>E. coli</i> (MPN/g)
0	*ND	0.03	ND	0.03
2	ND	0.08	ND	0.03
4	ND	0.23	ND	0.23
6	ND	0.26	ND	0.26
8	ND	0.08	ND	0.08
H_0 : Reject or Accept?	Accept	Accept	Accept	Accept
p -Value	–	1.00	–	1.00

*N.D.: Not Detected

Table 5. Analysis of Variance Results for Heavy Metals Concentrations in Barley's Straws.

Treatment (Ton/ha)	Arithmetic Mean of Heavy Metals Concentrations in Straws (mg/Kg)										
	As	Cd	Cr	Cu	Pb	Hg	Mo	Ni	Se	Zn	Co
0	4.7	*ND	2.3	7.2	1.0	29.6	11.8	2.3	7.1	19.9	3.6
2	4.4	ND	2.0	5.6	1.0	27.3	10.9	2.0	6.6	20.3	3.3
4	4.8	ND	2.3	11.1	1.0	29.7	11.9	2.3	7.1	13.5	3.6
6	4.7	ND	2.0	6.6	1.0	29.5	11.8	2.0	7.1	9.5	3.5
8	4.8	ND	2.0	8.1	1.0	29.9	12.0	2.0	7.1	8.7	3.6
Reject or Accept H_0 ?	Accept	Accept	Accept	Accept	Accept	Accept	Accept	Accept	Accept	Reject	Accept
p -Value	1.00	1.00	1.00	0.28	1.00	0.83	0.99	1.00	1.00	0.0008	1.00

*N.D.: Not Detected

Table 4 shows that the microbial quality of barley grains on the biosolids plots did not differ from the controls.

Impact of Biosolids Application on Heavy Metal Concentrations in Crop

Samples from barley's straw and grains were taken from each experimental plot and were tested for the concentration of the eleven heavy metal elements. Analysis of variance was conducted on each element using a probability of Type I Error, α of 0.05. There was no statistical difference in the concentration of each of the eleven heavy metals between all the experimental plots. The research hypothesis, H_a , stated the opposite: that there is a difference in the mean concentration of each of the heavy metals due to the application of biosolids at the specified loading rate. An F statistic was calculated and a conclusion was reached to accept or reject the null hypothesis, H_0 , for each heavy metal concentration and a p -value was calculated.

Table 5 shows the results obtained for the concentration of each of the eleven heavy metals in barley straw due to the application of biosolids. The results presented in Table 5 show that there was no significant

difference in heavy metal concentrations in the barley straw for the different treatments except zinc, Zn. The concentration of zinc decreased significantly with the increase in biosolids loading rate with a p -value of 0.0008.

Table 6 shows similar analysis of variance results for heavy metals concentrations in barley grains. The results in Table 6 indicate that there was no significant difference amongst heavy metals concentrations in barley grains under different biosolids loading rates except for zinc. The concentration of zinc in the grain increased significantly when the biosolids loading rates increased with a p -value of 0.0206.

Therefore, there was no effect in the eleven heavy metals concentrations in barley straw and grain due to the application of biosolids with different loading rates except for zinc. Concentration of zinc decreases in the barley's straws when increasing biosolids loading rates and increases in the grain with increasing biosolids loading rates.

Impact of Biosolids Application on Soil Profile

Four different soil parameters were measured at two soil depths. The parameters are: Hydrogen Ion Con-

Table 6. Analysis of Variance Results for Heavy Metals Concentrations in Barley Grains.

Treatment (Ton/ha)	Arithmetic Mean of Heavy Metals Concentrations in Straws (mg/Kg)										
	As	Cd	Cr	Cu	Pb	Hg	Mo	Ni	Se	Zn	Co
0	4.5	*ND	2.3	6.5	1.0	25.7	10.8	2.4	6.0	33.7	3.2
2	4.6	ND	2.0	9.3	1.0	25.7	11.1	2.1	6.0	32.2	3.1
4	4.5	ND	2.3	6.8	1.0	25.8	11.3	2.3	6.0	31.6	3.5
6	4.7	ND	2.0	7.4	1.0	26.2	12.1	2.1	6.0	32.3	3.6
8	4.8	ND	2.0	7.9	1.0	25.6	12.3	2.0	6.0	40.4	3.6
Reject or Accept H_0 ?	Accept	Accept	Accept	Accept	Accept	Accept	Accept	Accept	Accept	Reject	Accept
p -Value	1.00	1.00	1.00	0.89	1.00	0.99	0.99	0.99	1.00	0.02	0.99

*N.D.: Not Detected

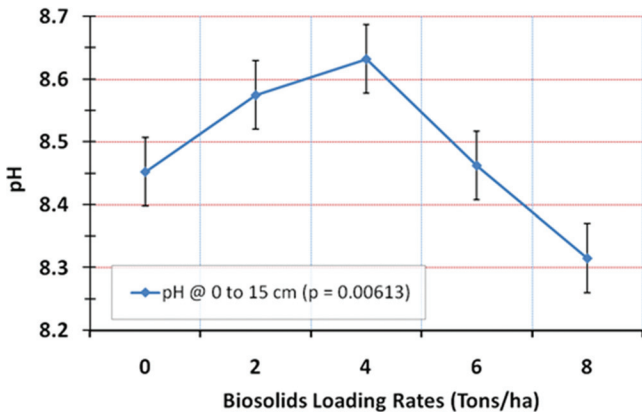


Figure 5. Impact of different biosolids loading rates on soil pH at 0–15 cm depths.

centration (pH), Salinity or Electrical conductivity (EC), concentration of organic carbon (OC), and the concentration of total Kjeldahl nitrogen (TKN). Soil in the different treatment plots were sampled at two depths: 0–15 cm and 15–30 cm.

Analysis of variance was conducted for the different parameters in the experimental plots. There was a significant difference amongst pH means for the different treatments of biosolids loading rates at 0–15 cm soil depth (p -value = 0.00613); and no statistical significant difference was observed at 15–30 cm soil depth (p -value = 0.6755). Figure 5 shows the trend of variations for the different biosolids loading rates at 0–15 cm soil depth.

Soil salinity was found to significantly increase with increasing loading rates for both soil depths as shown in Figure 6. The increase in salinity is more prominent on the 0–15 cm depths with a maximum Electrical Conductivity of 0.4 dS/m at biosolids loading rate of 8 tons/ha.

Organic carbon concentrations were measured for the different experimental plots after harvesting was

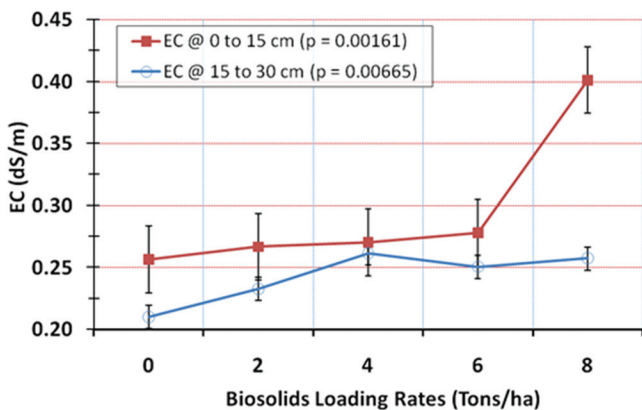


Figure 6. Effects of biosolids loading rates on soil salinity.

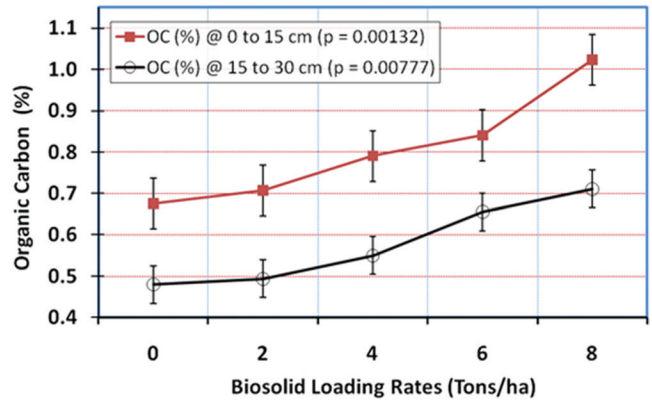


Figure 7. Effect of biosolids loading rates on organic carbon.

completed at the two soil depths: 0–15 cm and 15–30 cm. Statistical analysis indicated a significant increase in organic carbon for both depths at higher biosolids loading rates with a greater affect in the upper soil layer as shown in Figure 7.

Figure 8 shows that there is a statistically significant difference for the concentration of TKN in the two different soil depths. The effects of increasing TKN on the upper soil layer are more prominent with a maximum concentration of about 1194 mg/Kg TKN for the 8 tons/ha biosolids loading rate. However, for the lower soil layer, the maximum effect was observed at the 6 tons/ha biosolids loading rate corresponding to a TKN concentration of 800 mg/Kg.

White *et al.* (1997) and Martinez (2003) found similar results when applying anaerobically digested biosolids to rangeland ecosystems. Higher loading rates were applied once and the effects on soil parameters were monitored for subsequent years. Salinity, OC and TKN were measured and were found to increase each year.

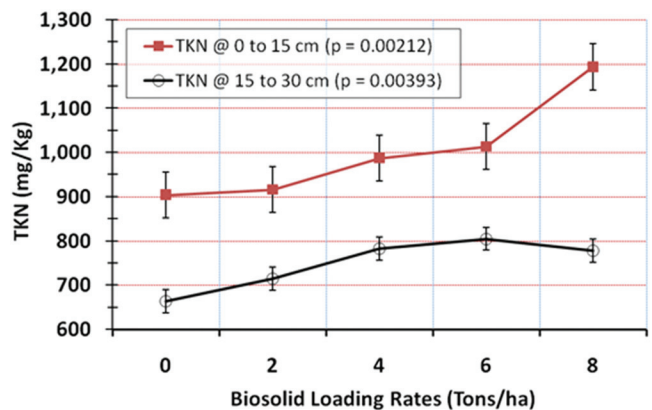


Figure 8. Effects of biosolids loading rates on TKN concentration in soil.

Table 7. Analysis of Variance Results for Heavy Metals Concentrations at 0–15 cm Soil Depths.

Treatment (Ton/ha)	Arithmetic Mean of Heavy Metals Concentration (mg/Kg)										
	As	Cd	Cr	Cu	Pb	Hg	Mo	Ni	Se	Zn	Co
0	4.5	*ND	34.9	17.9	17.0	29.6	11.5	35.7	7.0	56.2	15.1
2	4.5	ND	45.9	23.7	17.0	27.3	10.3	39.1	6.9	71.4	17.5
4	4.9	ND	49.2	24.6	17.9	29.7	12.0	43.2	6.9	75.7	17.8
6	5.0	ND	50.3	24.5	13.2	29.5	11.8	43.4	7.0	76.3	17.9
8	4.6	ND	51.1	24.6	13.2	29.9	11.8	47.1	7.1	78.3	18.0
Reject or Accept H_0 ?	Accept	Accept	Reject	Accept	Accept	Accept	Accept	Reject	Accept	Reject	Accept
<i>p</i> -Value	1.00	1.00	0.00014	0.285	0.216	0.83	0.99	0.0053	1.00	0.00001	0.74

*N.D.: Not Detected

Impact of Biosolids Application on Heavy Metals Concentrations in Soil

Soil samples from each experimental plot were collected at two soil depths: 0–15 cm and 15–30 cm after harvesting. There was no effect on the concentration of heavy metals on the soil due to the application of biosolids at loading rates used in this study.

Table 7 shows heavy metals concentrations at soil depth 0–15 cm due to the application of biosolids. The results show that there is no significant difference in heavy metals concentrations for the different treatments at the 0–15 cm soil depths except for Chromium (Cr), Nickel (Ni) and Zinc (Zn). The concentrations of Chromium, Nickel and Zinc increase significantly with increasing biosolids loading rates with *p*-values of 0.00014, 0.0053 and 0.00001 respectively.

Analysis of variance for the concentration of the eleven heavy metals at 15–30 cm soil depths are shown in Table 8. The results indicate that there is significant difference in heavy metals concentrations for Chromium, Nickel and Zinc with increasing trend as the case for the upper soil layer. This is the same trend observed for the 0–15 cm soil samples. However, a significant decrease in Lead (Pb) concentration with increasing

biosolids loading rates for the 15–30 cm depths was observed.

CONCLUSION

No statistical significant effects on grain yield or on grain protein content was observed due to the application of biosolids in this study. However, a statistically significant decrease in the “thousand grain weight” parameter was observed with increasing biosolids loading rates causing a reduction in barley grain size. Therefore, these results suggest biosolids should be applied to fodder crops that do not produce grains such as Sudan grass and alfalfa. This will increase vegetative growth due to the increase in available nitrogen.

Concentrations of the eleven heavy metals in grains and straw were statistically insignificant. This was probably due to the low concentration of those metals in the biosolids which reflects the case for domestic biosolids generated in Jordan.

It was determined in this study that applying biosolids to rain-fed lands planted with barley significantly increases soil salinity in the top layer. Also, concentration of organic carbon in the soil profile was significantly increased. This is a benefit to desert soils with

Table 8. Analysis of Variance Results for Heavy Metals Concentrations in Soil at 15–30 cm Depth.

Treatment (Ton/ha)	Arithmetic Mean of Heavy Metals Concentrations (mg/Kg)										
	As	Cd	Cr	Cu	Pb	Hg	Mo	Ni	Se	Zn	Co
0	4.6	*ND	36.2	19.5	20.5	25.8	10.9	38.2	6.0	60.3	14.2
2	4.5	ND	45.2	23.8	20.9	25.6	11.0	46.9	6.0	64.5	14.3
4	4.5	ND	48.4	25.0	16.4	25.8	11.5	50.7	6.0	71.6	14.3
6	4.8	ND	50.2	26.0	20.0	26.1	11.8	51.2	6.0	81.2	14.5
8	4.6	ND	50.6	26.1	12.9	25.8	12.0	50.4	6.0	69.5	15.8
Reject or Accept H_0 ?	Accept	Accept	Reject	Accept	Reject	Accept	Accept	Reject	Accept	Reject	Accept
<i>p</i> -Value	1.0	1.0	0.0004	0.1029	0.0297	1.0	1.0	0.0009	1.0	0.0000	0.962

*N.D.: Not Detected

low to none organic matter; and hence application of biosolids to deserts can be considered a form of carbon sequestration which would provide developing countries with carbon credits. Economical cost for transportation and application should however be considered to make this option feasible and attractive to policy makers.

Total Kjeldahl nitrogen concentration in soil was significantly increased when increasing biosolids loading rates in the 0–15 cm soil layer. For the 15–30 cm soil layer, TKN concentration was significantly increased to a maximum level at biosolids loading rate of 6 Ton/ha.

Application of biosolids had significant affects only on the concentration of Chromium, Nickel and Zinc for the two soil layers and on the concentration of Lead in the lower soil layer.

ACKNOWLEDGMENTS

The authors would like to acknowledge the financial support to conduct this applied research by the United States Agency for International Development (USAID) through a cooperative agreement with The University of Arizona.

The authors also would like to thank The Water Authority of Jordan for their assistance and cooperation; and for making the treatment plants and biosolids available to conduct the research study. The assistance and cooperation of the researchers, staff and engineers at Ramtha Regional Experimental Center—Ministry of Agriculture—is greatly appreciated and is one of the factors for the success of this research; Thank You.

REFERENCES

1. Akrivos J, Damais D, Katsara K, Andreadakis A. 2000. Agricultural Illustration of Lime Treated Sewage Sludge. *Journal of Water Science and Technology*; 42(9):203–210.
2. Amajirionwu M., N. Connaughton, B. McCann, R. Moles, J. Bartlett, B. O'Regand. Indicators for managing biosolids in Ireland. *Journal of Environmental Management* 88 (2008) 1361–1372. <http://dx.doi.org/10.1016/j.jenvman.2007.07.003>
3. Athamneh B. Usage of Sewage Sludge for Improving Soil Fertility and Crop Production and it's Impact on the Environment [M.Sc Thesis]. Jordan: Department of agricultural Science at Jordan University of Science and Technology; 2003.
4. Avnimelech Y., Cohen A., and Shkedi D. 1990. "The effect of municipal solid waste compost on the fertility of clay soils". *Soil Technol.*, 3: 275–284. [http://dx.doi.org/10.1016/0933-3630\(90\)90008-Q](http://dx.doi.org/10.1016/0933-3630(90)90008-Q)
5. Beaton K, Graham R, McLaughlin M. 1993. The Influence of Low Rates of Air-dried Biosolids on Yield and Phosphorus and Zinc Nutrition of Wheat (*Triticum Durum*) and Barley (*Hordeum Vulgare*). *Australian Journal of Soil Research*. 41(2) 293–308. <http://dx.doi.org/10.1071/SR02074>
6. Brbarick K.A., and Lppolioto J.A. 2000. "Nitrogen fertilizer equivalency of sewage biosolids applied to dryland winter wheat". *J. Environ. Qual.*, 29: 1345–1351. <http://dx.doi.org/10.2134/jeq2000.00472425002900040043x>
7. Cartmell G., Cartmell E., Gostelow P., Riddell-Black D., Simms N., Oakey J., Morris J., Jeffrey P., Howsam P., and J. Pollard S. 2006. "Biosolids A Fuel or a Waste? An Integrated Appraisal of Five Co-combustion Scenarios with Policy Analysis". *Environmental Science Technology* 45: 649–658. <http://dx.doi.org/10.1021/es052181g>
8. Committee on Toxicants and Pathogens in Biosolids Applied to Land Biosolids Applied To Land: Advancing Standards And Practices. 2002. National Academy Press. 2101 Constitution Ave., N.W. Washington, D.C. 20418.
9. González M., Mingorance M., Sánchez L., Pe-a A. 2008. "Pesticide adsorption on a calcareous soil modified with sewage sludge and quaternary alkyl-ammonium cationic surfactants". *Environmental Science and Pollution Research*, 15:8–14. <http://dx.doi.org/10.1065/espr2007.02.387>
10. Guixin P, Mike B, Glenn B, Peter W. 2004. Effects of Applied Biosolids on Forage Sorghum Production and Soil Major Nutrient Status in an Alluvial Clay Loam Soil in Southeast Queensland. Australian New Zealand Soils Conference, December 2004, University of Sydney, Australia.
11. Hallvard Odegaard. 2003. Wastewater sludge as a resource: Proceedings of the international water association specialist conference, Trondheim, Norway.
12. Jin V. L., M. V. Johnson, R. L. Haney, J. G. Arnold. Potential carbon and nitrogen mineralization in soils from a perennial forage production system amended with class B biosolids. *Agriculture, Ecosystems and Environment* 141 (2011) 461–465. <http://dx.doi.org/10.1016/j.agee.2011.03.016>
13. Kresse E.J., and Naylor L. M. 1983. Municipal sewage sludge: A3 year research effort, Cooperative Extension of Oneida County.
14. Lagae H. J., Langemeier M., Lybecker D., and Barbarick K. 2009. "Economic Value of Biosolids in a Semi-arid Agroecosystem". *Agron. J.*, 101: 933–939. <http://dx.doi.org/10.2134/agronj2008.0209x>
15. Leblanc R.J., Allain C.J., Laughton P.J., Henry J.G. 2003. "Integrated, long term, sustainable, cost effective biosolids management at a large Canadian wastewater treatment facility". In: *Proceedings of the International Water Association (IWA) Specialist Conference*. pp. 225–232.
16. Lomonte C., A. I. Doronila, D. Gregory, A. J.M. Baker, S. D. Koleva. Phytotoxicity of biosolids and screening of selected plant species with potential for mercury phytoextraction. *Journal of Hazardous Materials* 173 (2010) 494–501. <http://dx.doi.org/10.1016/j.jhazmat.2009.08.112>
17. Magesan G. N., Wang H. 2003. "Application of municipal and industrial residuals in New Zealand forests: an overview". *Australian Journal for Soil Research*, 41:557–569. <http://dx.doi.org/10.1071/SR02134>
18. Mantovia P., G. Baldonib, and G. Toderib. Reuse of liquid, dewatered, and composted sewage sludge on agricultural land: effects of long-term application on soil and crop. *Water Research* 39 (2005) 289–296. <http://dx.doi.org/10.1016/j.watres.2004.10.003>
19. Manual of Food Quality Control 4 Rev. 1. Microbiological Analysis. 1992.
20. Martinez F., G. Cuevas, R. Calvo, and I. Walter. J. 2003. Ecosystem Restoration Biowaste Effects on Soil and Native Plants in a Semi-arid Ecosystem. *Journal of Environmental Quality*. 32: pp. 472–479.
21. Mays A. A. Terman G. L., and Duggan J. C. 1973. "Municipal compost: effects on crop yield and soil properties". *Journal of environmental Quality*, 2 (1), pp. 89–92. <http://dx.doi.org/10.2134/jeq1973.00472425000200010011x>
22. Method of Soil Analysis-Part 2 Microbiological and Biochemical Properties, SSSA, 1994. WHO Technical Report No. 778.
23. Ott, R. Lyman and Michael Longnecker. 2001. "An introduction to statistical methods and data analysis". 5th edition. Wadsworth Group: DUXBURY, 51 Forest Lodge Road, Pacific Grove, CA 93950 USA.
24. Oudeh M., Khan M., and Scullion J. 2002. "Plant accumulation of potentially toxic elements in sewage sludge as affected by soil organic matter level and mycorrhizal fungi". *Environ. Pollution*, 116: 293–300. [http://dx.doi.org/10.1016/S0269-7491\(01\)00128-2](http://dx.doi.org/10.1016/S0269-7491(01)00128-2)
25. Pu G., Bell M., Barry G., and Want P. 2004. "Effects of applied biosol-

- ids on forage Zea mays production and soil major nutrient status in an alluvial clay loam soil in southeast Queensland, Australia". 3rd Australian New Zealand Soils Conference, University of Sydney, Australia.
26. Rusan M. and Athamneh B. 2009. "Effect of Cd-Enriched Sewage Sludge on Plant Growth, Nutrients and Heavy Metals Concentrations in the Soil-Plant System". International Plant Nutrition Colloquium, University of California, Davis. Paper 1012.
 27. Schroder J. L., Zhanga H., Zhou D., Bastac N., Rauna W. R., Payton M. E., and Zazulake A. 2008. "The Effect of Long-Term Annual Application of Biosolids on Soil Properties, Phosphorus, and Metals". *Soil Sci. Soc. Am. J.*, 72: 73–82. <http://dx.doi.org/10.2136/sssaj2007.0025>
 28. Skjelhaugen O. J. 1999. "A farmer operated system for recycling wastes". *Journal of Agricultural Engineering Research*, 73: 373–382. <http://dx.doi.org/10.1006/jaer.1999.0429>
 29. Snyman H.G., Terblanche J.S. and van der Westhuizen J.L.J. 2000. Management of land disposal and agricultural reuse of sewage sludge within the framework of the current South African guidelines. *Wat. Sci. Tech.*, 42 (9), 13–20.
 30. Standard Methods for the Examination of Water and Wastewater, 20th Edition, 1998, APHA, AWWA.
 31. State of Science Report: Energy and Resource Recovery from Sludge. 2008. Global Water Research Coalition.
 32. Suleiman, W., C. P. Gerba, A. H. Tamimi, R. J. Freitas, A. Al Sheraidah and B. Hayek. 2010. Management practices and biosolids treatment and disposal in Jordan. *J. Residuals Sci. Technol.* 7 (1):63-67.
 33. Tamimi, A. H., C. P. Gerba, B. Hayek, C. Y. Choi and R. J. Freitas. 2007. Characterization of drying bed treated biosolids in Jordan. *Journal of Residuals Science and Technology* 4(3):111–164.
 34. Tour Guide VIII International Forum on Soil Taxonomy and Agrotechnology Transfer, Jordan, The Arab Center for the Studies of Arid Zones and Dry Lands, 1984.
 35. USEPA. 1993a. Federal Register: February 19, 1993. 40 CFR Parts 257, 403, and 503. The Standards for the Use or Disposal of Sewage Sludge. Final Rules. EPA 822/Z-93/001. U.S. Environmental Protection Agency.
 36. USEPA. 1993b. Federal Register: February 19, 1993. 40 CFR Part 503; as amended at 64 FR 42571, Aug. 4, 1999.
 37. Wang H., Brown S.L., Magesan G.N., Slade A.H., Clinton P.W., and Payn T.W. 2008. "Technological options for the management of biosolids". *Environmental Science and Pollution Research*, 15: 308–317. <http://dx.doi.org/10.1007/s11356-008-0012-5>
 38. Werheim B., Mocquot B., and Mench M. 2000. "Distribution of sludge-borne manganese in field-grown maize". *Commun Soil Sci. Plant Anal.*, 31: 305–319. <http://dx.doi.org/10.1080/00103620009370438>
 39. White C.S, S.R. Loftin, and R. Aguilar. 1997. Application of Biosolids to Degraded Semiarid Rangeland: Nine-Year Responses. *Journal of Environmental Quality* 26: pp. 1663–71.
 40. Yager, Tracy J.B., Smith, David B., and Crock, James G., 2004, Effects of surface applications of biosolids on soil, crops, ground water, and streambed sediment near Deer Trail, Colorado, 1999–2003: U.S. Geological Survey Scientific Investigations Report 2004–5289, 93 p.
 41. Zebarth B. J., Neilsen G. H., Hogue E., and Neilsen D. 1999. "Influence of organic waste amendments on selected soil physical and chemical properties". *J. Soil Sci.* 79: 501–504. <http://dx.doi.org/10.4141/s98-074>

Corrosion Behaviors of Carbon Steel in the Presence of Iron Oxidizing Bacteria Cultured in Reclaimed Water

LI PENG^{1,*}, YAJUN ZHANG¹, PING XU¹ and LIPING LU²

¹Key Laboratory of Urban Stormwater System and Water Environment, Ministry of Education, Beijing University of Civil Engineering and Architecture, Beijing 100044, China

²China Academy of Urban Planning and Design, Beijing, 100044, China

ABSTRACT: The corrosion behaviors of carbon steel in the presence of iron oxidizing bacteria (IOB) in reclaimed water was investigated mainly using the static hanging piece method, electrochemical analysis, SEM, EDAX, FT-IR and XRD. The results showed that IOB accelerated the corrosion of carbon steel by 50–100% by attaching to its surface; the corrosion potential of the system with IOB was higher (23–36% negative) than that without IOB; bacteria grew (biofilm formed) on the surface of carbon steel and pitting corrosion occurred on the coupons in the reclaimed water inoculated with IOB, while no pitting corrosion occurred in the system without IOB. The corrosion products mainly consisted of FeOOH and CaCO₃ whether IOB existed or not but were more complicated in the presence of IOB.

1. INTRODUCTION

DUE to the shortage of water resources, reclaimed water is more and more widely used in industry and agricultural production. Unfortunately, reclaimed water has more adverse effects on pipe walls owing to its complicated water quality conditions compared with drinking water, such as a more serious corrosion problem and microbial growth [1,2].

Iron oxidizing bacteria (IOB) are bacteria that produce power for growth by oxidizing Fe²⁺ to Fe³⁺. The Fe³⁺ ions subsequently deposit as iron oxide-hydroxide and cause various kinds of corrosion [3], such as pitting corrosion [4]. IOB is a paramount part involved in aerobic corrosion and iron oxidizing bacterial activity is the key culprit of metal corrosion. It has been found that IOB induced corrosion damage [5,6].

Up to present, the majority of research associated with microbiologically induced corrosion (MIC) in pipe networks is on sulfate reducing bacteria (SRB) [7]. And the role of other kinds of microbes (e.g., IOB) in MIC has been ignored [8]. Although the mechanisms of MIC by SRB are becoming clearer, but the role of IOB in MIC is still unclear and remains controversial [9].

One study attributed corrosion damage to crevice

corrosion in the presence of IOB [10]. Quite a few researchers have demonstrated the role of IOB in oxygen concentration cell formation in biofilms as iron hydroxides precipitate during IOB metabolism [11]. For carbon steel, IOB are capable of affecting its physical and chemical processes through their joint metabolism with other microbes (e.g., SRB) coexisting in the environment [12]. But a clear corrosion mechanism of metals in the presence of IOB is unknown.

Views are divergent on whether IOB accelerate or inhibit a corrosion process [13]. Quite a few studies have suggested that IOB accelerated metal corrosion [14–15]. However, many scholars have demonstrated that IOB inhibited corrosion processes under certain circumstances [16,17].

What's more, research on metal corrosion in the presence of IOB mainly used waters other than reclaimed water [18–22]. Consequently, the objective of this study was to investigate the corrosion behavior of carbon steel in reclaimed water in the presence of IOB.

The results of this study are expected to help in dealing with the pipeline corrosion issue in reclaimed water diversion and distribution.

2. MATERIALS AND METHODS

2.1. Coupon Preparation

Coupons made of carbon steel and measured 5 cm

*Author to whom correspondence should be addressed.
Email: 278702744@qq.com.

$\times 2.5 \text{ cm} \times 0.2 \text{ cm}$ (20#, GB/T 688-1988) were used in this work, and their chemical composition measured by melting analysis (wt.%) was follows: 0.096%C, 0.011%P, 0.011%S, 0.17%Si, 0.30%Mn, and balance Fe.

The coupons were first cleaned with filter papers, then cleaned with acetone solution to wipe out further anti-corrosive grease, soaked in a 70% ethanol solution, and subsequently stored in a vacuum desiccator for 24 hours before use.

2.2. Reclaimed Water

The reclaimed water used was collected from the Qinghe Water Reclamation Plant, stored at 4°C and used at room temperature (16–23°C).

2.3. IOB Cultivation, Identification and Inoculation

IOB used in this study was cultivated by the most probable number (MPN) test [23] and identified according to the Bergey's Manual of Systematic Bacteriology [24], and then the cultivated IOB were inoculated into the sterilized reclaimed water. Number of IOB was the average of three measurements. Bacterial growth was monitored for growth curve plotting. Bacterial solution of high purity was stored at 4°C before use.

2.4. Polarization Curves

Polarization curve tests were carried out using the potentiodynamic method with a CHI660C electrochemical workstation (Shanghai Chenhua). The electrodes made of 20# steel were first polished with 240#, 360#, 500#, 800#, 1000# and 1200# diamonds successively on a polishing cloth, then cleaned with an ethanol solution and stored in a vacuum desiccator for 24 hours before use. A scan rate of 0.5 mV/s was used for generating polarization curves. Corrosion potentials were measured three times and averages were taken.

2.5. Bacteria and Media

Two portions of 500 mL of reclaimed water were added to two 1000-mL conical flasks, respectively. Then, the two conical flasks were autoclaved for 15 min at $121 \pm 1^\circ\text{C}$. After that, 500 mL bacterial suspension and 500 mL distilled water were added into the two conical flasks, respectively. The number of IOB was 1.2×10^6 CFU/mL. Finally, after the pretreated

coupons and electrodes were hung in and absorbent cottons were inserted, the flasks were incubated at $30 \pm 1^\circ\text{C}$. The experiment was performed in triplicates.

2.6. Weight-loss Measurement

Three carbon steel coupons were taken out at each sampling time for weight-loss measurements.

Average corrosion rate (mm/y) [25] is calculated as follows:

$$\text{The average corrosion rate} = 87600W / T \cdot A \cdot D \quad (1)$$

where W is coupon weight loss in g; T is the time of immersion in hours; A is the total surface area of the coupon in cm^2 ; and D is metal density in g/cm^3 , which is $7.86 \text{ g}/\text{cm}^3$ for 20# carbon steel.

2.7. Surface Analysis and Corrosion Products Analysis

At the 2nd, 8th and 16th days, corrosion products were removed from the coupons and then vacuum dried for 48 hours before use. Biofilm and corrosion morphology were observed with a scanning electron microscope (SEM) coupled with energy dispersive analysis of X-rays (EDAX). Corrosion product composition was analyzed using Fourier-transform infrared spectroscopy (FT-IR) coupled with X-ray diffraction (XRD). XRD data were analyzed using X'Pert High Score Plus software with the PDF2-2004 database.

3. RESULTS AND DISCUSSION

3.1. Growth Curve of IOB

Figure 1 is the growth curve of IOB in the reclaimed water. As shown, the growth of IOB did not experience a delay phase but directly entered the exponential phase (0–2.5 d), indicating that IOB adapted quickly to the reclaimed water environment. Then the bacteria entered a stable growth period (2.5–4 d), maintaining at a high level of activity and a stable metabolic state and reaching a growth peak at the 4th day. After that, the bacteria entered the death phase due to nutrient depletion.

3.2. Corrosion Rate Variation with Time

The corrosion behaviors of carbon steel in the reclaimed water with or without IOB inoculated were

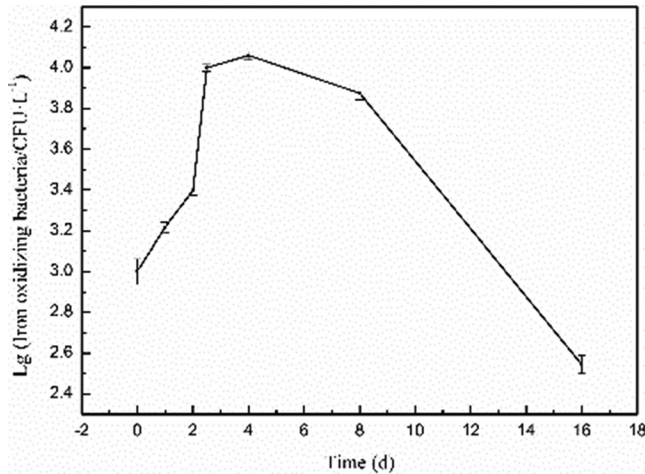


Figure 1. Growth curves of the IOB in the reclaimed water.

evaluated at the 1st, 2nd, 4th, 8th and 16th days. Corrosion rate was determined using the weight-loss method in combination with the electrochemical tests.

3.2.1. Weight-loss Method

As can be seen in Figure 2(a), with or without IOB inoculation, the corrosion rates of carbon steel declined with time, which was consistent with the finding of Wang [4]. In the system with IOB inoculation, the corrosion rate declined from 0.30 mm/y over the first day to 0.14 mm/y over the first 8 days and stabilized afterwards. Liu [2] and Wang [5] reported a similar trend of corrosion rate.

A similar variation trend of corrosion rate was found for the carbon steel in the reclaimed water without IOB inoculation. Specifically, the corrosion rate dropped from 0.16 mm/y over the first day to 0.12 mm/y over the first 2 days, further to 0.10 mm/y over the first 8 days and then stabilized. However, the corrosion rate was 50–100% higher in the reclaimed water with IOB inoculated than in that without IOB. It may be due to the reason that IOB, as a type of aerobic microorganism, obtain energy by oxidizing Fe^{2+} to Fe^{3+} (the electron donor and acceptor are Fe^{2+} and O_2 respectively), and the oxidation reaction reinforces the dissolution of carbon steel. This indicated that the presence of IOB accelerated the corrosion of carbon steel but did not change the variation trend of the corrosion rate.

In addition, Liu [2] documented that carbon steel showed a 1.0–15.8% higher corrosion rate in reclaimed water than in tap water, which may be due to the more complicated and highly-corrosive nature of reclaimed water [1,2].

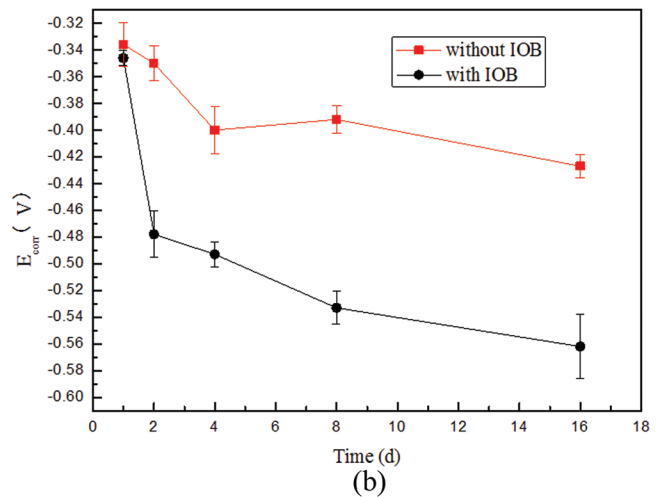
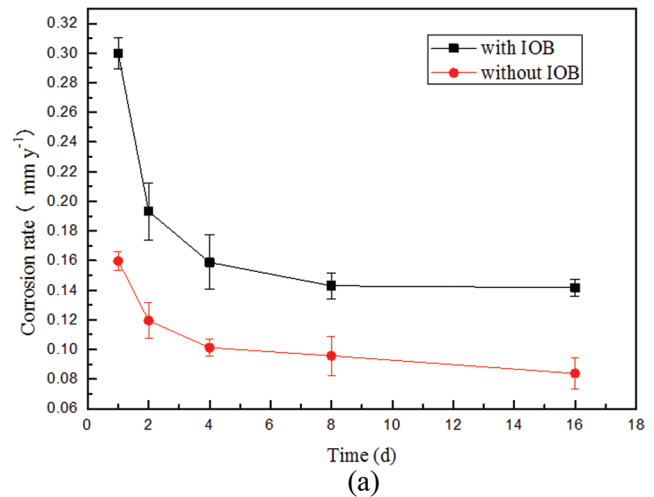


Figure 2. Corrosion rate (a) and corrosion potential (E_{corr}) (b) changes with time in the reclaimed water with or without IOB inoculation.

3.2.2. Corrosion potential versus time

Figure 2(b) shows the E_{corr} changes of the carbon steel electrodes under different experimental conditions. In the first 2–4 days, the E_{corr} increased rapidly towards the negative direction as a result of the exponential growth of the bacteria. Four days later, the bacteria entered the death phase due to nutrient depletion. As a result, the corrosivity of the water decreased. Qi [26] attributed the rapid decline of E_{corr} at the beginning to the formation of a passive layer or biofilms.

Similar trends were also observed for corrosion of cast iron in reclaimed municipal wastewater, Q235 steel corrosion behavior in seawater with IOB and carbon steel corrosion behavior in sedimentary water with IOB [2,15,19]. In particular, Lu *et al.* [25] found that the E_{corr} of carbon steel in seawater inoculated with

IOB dropped from -680 mV over the first few hours to -750 mV over the first 12 days, and then increased to -735 mV over a time period of 1 day or longer, which may be due to the reason that the corrosion products blocked oxygen diffusion and the electro-migration of anions to the carbon matrix, mitigated corrosion damage[2]. Therefore, E_{corr} declined with time.

As shown in Figure 2(b), E_{corr} in the two systems differed widely especially 2 days after the experiment began. The E_{corr} in the system with IOB inoculation was higher (23–36% negative) than that without IOB, which was consistent with the weight loss results above, fully demonstrating that IOB accelerated carbon steel corrosion in the reclaimed water.

3.3. Surface Analysis

3.3.1. SEM Analysis

Morphologies of the corrosion products taken from both systems at the 2nd, 8th and 16th days were observed at a magnification of $500\times$ (Figure 3).

When immersed in the reclaimed water without IOB inoculation, the coupons showed a dense corrosion product layer without evident cracks; and carbon steel didn't undergo localized corrosion anywhere on the surfaces throughout the experiment. The corrosion products formed a thin and uniform layer, covering the surface of carbon steel loosely and unevenly. Extremely little changes in surface morphologies occurred with time.

Conversely, biofilms were observed on the surfaces of the coupons in the system with IOB inoculation throughout the experiment (Figure 3). As shown in Figure 3(a), at the 2nd day, instead of uniform corrosion, pitting corrosion occurred on the surfaces of the coupons in the system with IOB, which may be due to the reason that microbial cells attached on the surfaces of the coupons, inducing crevice corrosion or localized corrosive. Biofilm can effectively bind metals thus accelerate corrosion [27]. In addition, biofilms in thick layers with a slice of tiny cracks and pores all over formed on the metal surfaces. As shown in the figure, the white small flocs indicated that biofilms began to form. At the 8th day, the area of corrosion pits and the coverage of corrosion products expanded. This might be associated with the maturing of biofilm. The coverage of corrosion products further expanded afterwards and almost to the entire surface of carbon steel at the 16th day.

Thus, it was concluded that corrosion damage was

more severe in the presence of IOB than without, which was supported by the corrosion rate results above.

A large number of pores in the corrosion products were observed under high magnification on the coupons immersed in the reclaimed water without IOB [Figure 3(d)] while pompon-shaped biofilms were found on the coupons in the system with IOB [Figure 3(d1)].

3.3.2. EDAX Analysis

Elemental composition ratios of the corrosion scales sampled at different times are showed in Table 1.

The results of EDAX analysis demonstrated that the main elements of the corrosion products were iron and oxygen with carbon and silicon present at a much lower content, revealing that IOB might promote the precipitation of iron oxide and hydroxide.

The corrosion products in the system with IOB had a higher content of carbon and oxygen but a lower content of iron than those in the system without IOB. Similar results were also reported by Zheng [18] and Wu [20] who studied the corrosion behavior of carbon steel in reclaimed water with IOB as well. This can be attributed to the organic substances of extracellular polymeric substances (EPS). IOB promoted the oxidation of ferrous ions to ferric ions which were released from the metal surface. As a consequence, the iron content in the corrosion products decreased[20]. The carbon content of the corrosion products in the system with IOB increased from 1.72% over the first 2 days to 7.89% over the first 8 days, which was because of the EPS produced by IOB during metabolism.

In addition, Lu *et al.* [21] studied the corrosion behavior of metal in drinking water and seawater in the presence of IOB and demonstrated that the corrosion products were mainly composed of iron, oxygen and carbon, indicating that regardless of in seawater, tap water or reclaimed water, carbon steel corrosion products are mainly composed of iron, oxygen and carbon.

Table 1. The Elemental Composition Ratios of the Corrosion Scales Sampled at Different Times by EDAX Measurement (Wt %).

Elements	With IOB			Without IOB		
	2nd d	8td d	16th d	2nd d	8td d	16th d
C	1.72	7.89	5.32	1.03	5.69	4.06
O	30.06	21.93	26.92	16.81	14.13	19.31
Fe	66.7	68.7	64.42	80.03	78.55	74.07
Other	1.52	1.48	3.16	2.13	1.63	2.56

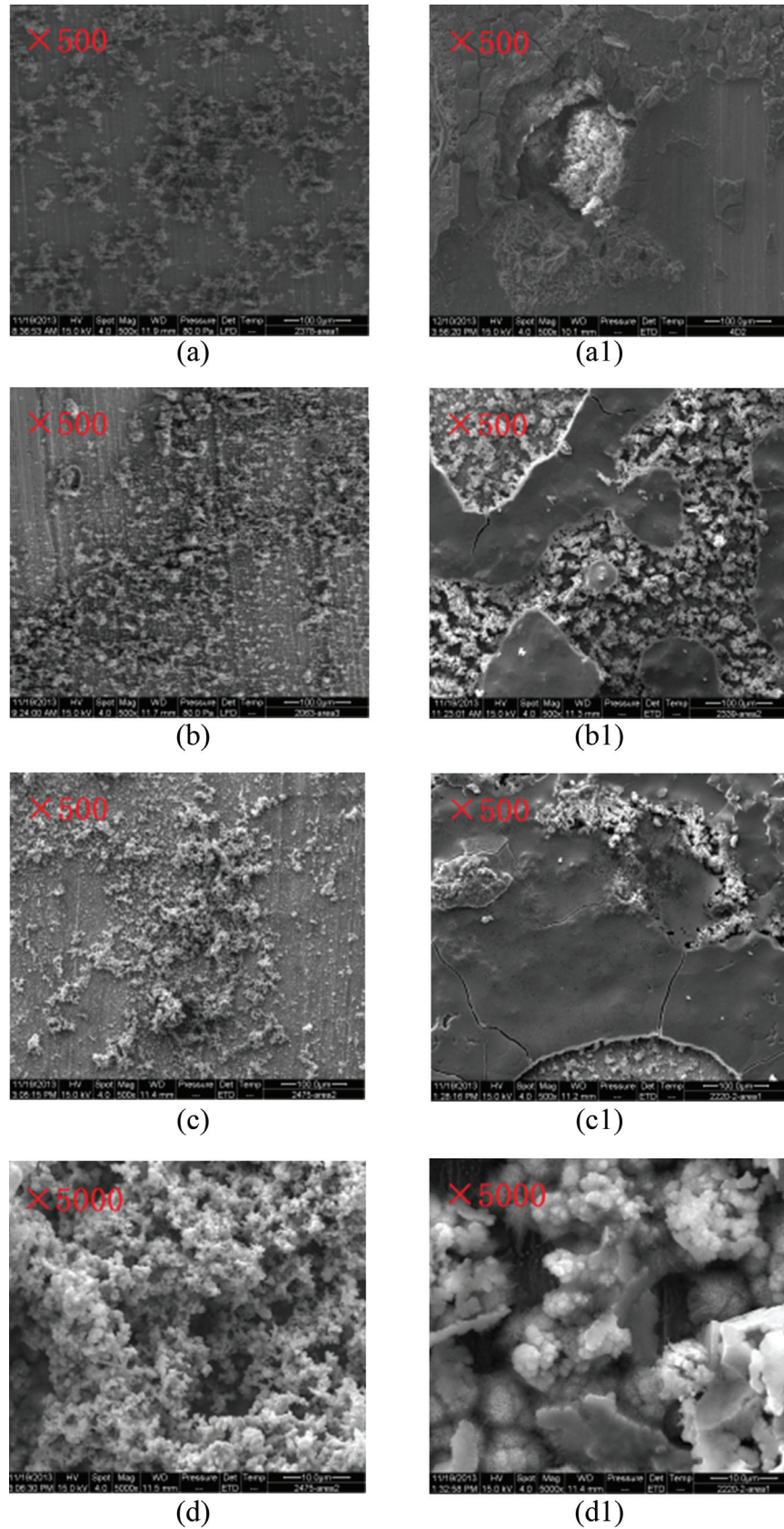


Figure 3. Morphology changes with time of the corrosion products of the carbon steels in the reclaimed water systems with or without IOB inoculation: (a) 2nd d, control; (b) 8th d, control; (c) 16th d, control; (d) 16th d, control; (a1) 2nd d, IOB; (b1) 8th d, IOB; (c1) 16th d, IOB; and (d1) 16th d, IOB.

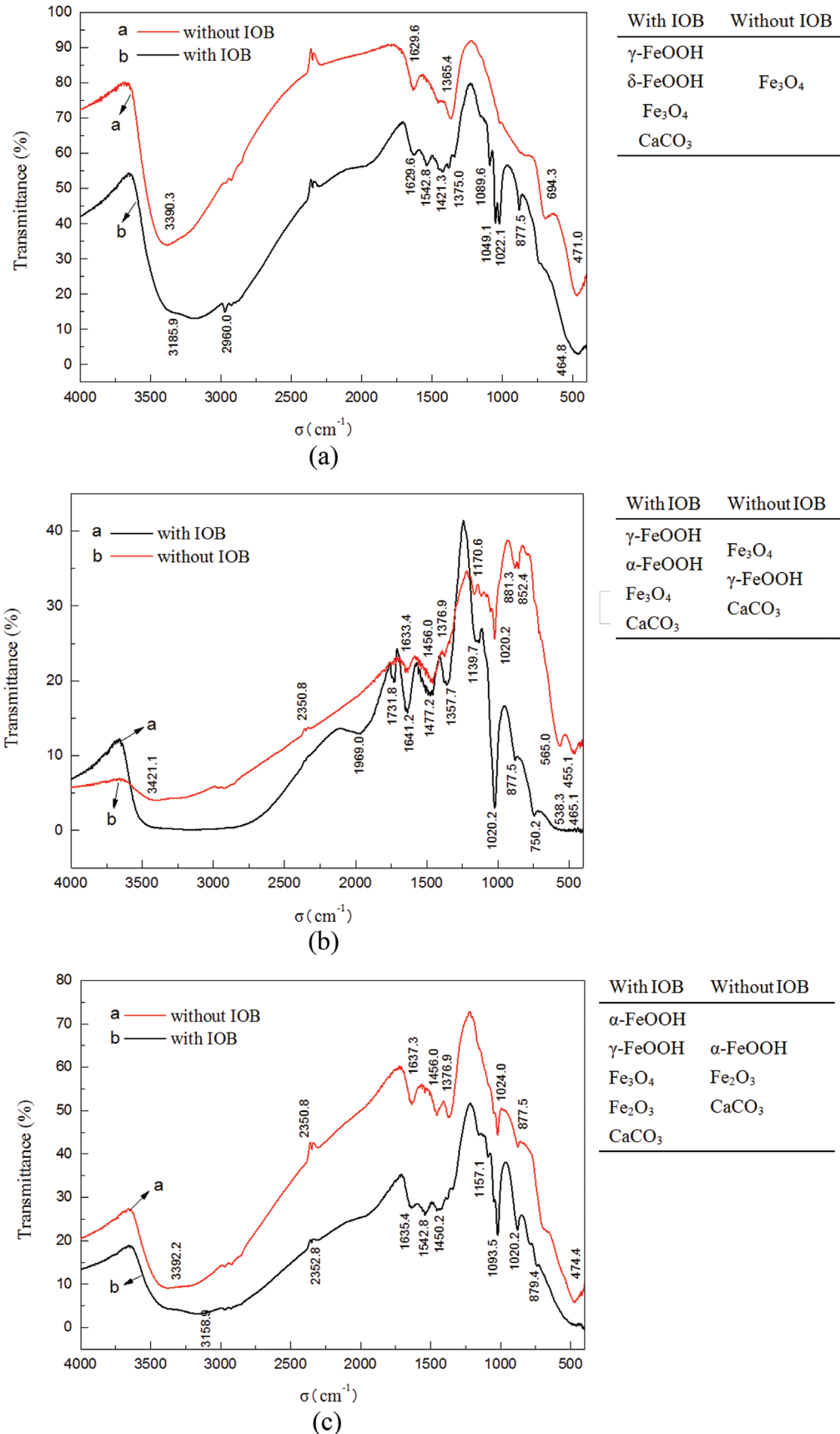


Figure 4. FT-IR spectra of the corrosion products of the carbon steels after immersed for 2d (a), 8 d (b), and 16 d (c).

3.4. Analysis of corrosion products

3.4.1. FT-IR Analysis

The obtained infrared spectra were compared with standard spectral libraries [28] to determine the composition of the corrosion products. The results are summarized in Figure 4.

At the 2nd day, for example, as can be seen in Figure 4(a), there were two distinct peaks at 1022 and 877.5 cm^{-1} , respectively and an additional discernible spectral feature at 464.8 cm^{-1} , indicating the presence of γ -FeOOH which has spectral features at 1020, 880 and 470 cm^{-1} according to Cornell *et al.* [28]. Similarly, the corrosion products were also covered by δ -FeOOH and CaCO_3 as evident from the dominant characteristic infrared spectral peaks at 1375, 1089.6 and 877.5 cm^{-1} , compared to the expected ones at 1378, 1110, 880 and 876 cm^{-1} .

In the frequency ranges of 400–500 cm^{-1} and 500–700 cm^{-1} , both spectra exhibited a broad shoulder, consistent with the characteristic absorption region of Fe_3O_4 , indicating the presence of Fe_3O_4 in the corrosion products of the two systems.

3.4.2. XRD Analysis

Figure 5 shows the variation of the crystalline com-

position of the corrosion scales from the reclaimed water with IOB. The corrosion layer was comprised mainly of γ -FeOOH, CaCO_3 and Fe_3O_4 at the 2nd day, mainly of α -FeOOH, γ -FeOOH and CaCO_3 at the 8th day, and mainly of α -FeOOH, Fe_3O_4 and CaCO_3 with Fe_2O_3 at a minor amount at the 16th day.

In summary, the corrosion products from the two water systems were of a substantially similar composition of mainly FeOOH and CaCO_3 which were reported to be the main components of corrosion products in reclaimed municipal wastewater [29] and tap water [30]. Ashassi-Sorkhabi *et al.* [31] found various forms of FeOOH in corrosion products of carbon steel in sewage inoculated with IOB. In addition, the corrosion product in the system with IOB inoculated had a more complicated composition compared to that in the system without IOB, which might be due to IOB metabolism.

4. CONCLUSIONS

In this study, we explored the corrosion behaviors of carbon steel in reclaimed water in the presence of IOB. The main conclusions of this investigation include:

1. The corrosion rate of carbon steel in the reclaimed water system with IOB was about 50–100% higher than that in the system without IOB. And the

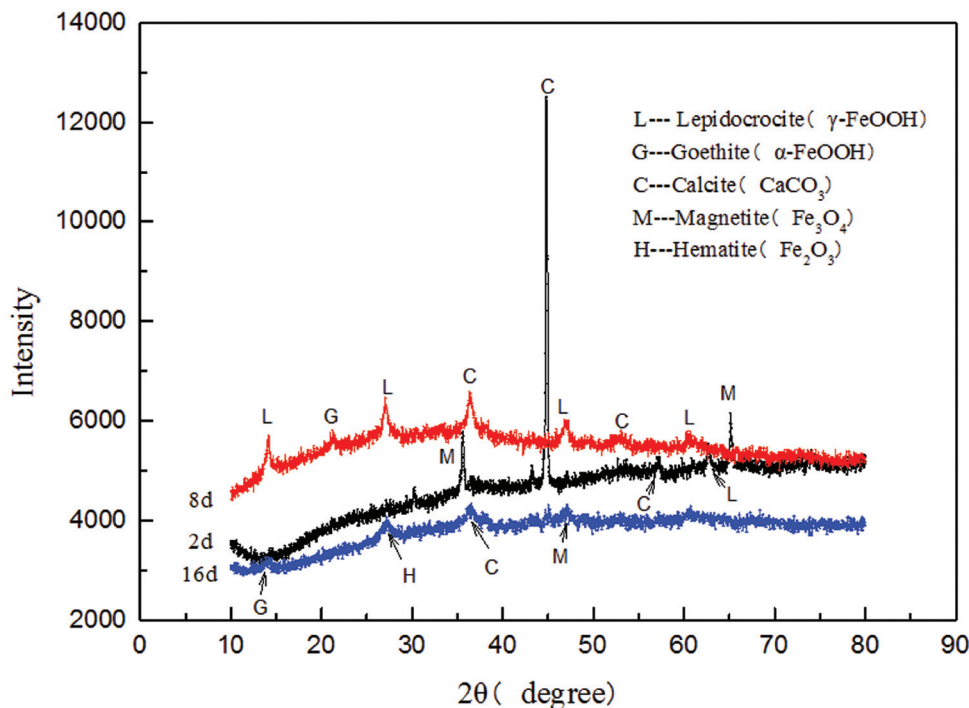


Figure 5. XRD analysis of the corrosion products of the carbon steels in reclaimed water with IOB.

polarization results indicated that the corrosion potential of the carbon steel electrode in the system with IOB was 23–36% negatively higher than that without IOB. The presence of IOB accelerated the corrosion of carbon steel but did not change the variation trend of corrosion rate.

- SEM results showed biofilms and pitting corrosion in the system with the presence of IOB but no biofilms and pitting corrosion in the system without IOB.
- EDAX, FT-IR and XRD results revealed that the main corrosion products were FeOOH and CaCO₃. But the corrosion product in the system with IOB was of a more complicated composition compared to that in the system without IOB.

Finally, the activity of microorganisms (e.g., IOB) is capable of changing the chemical and physical reactions in corrosion processes.

5. ACKNOWLEDGMENT

This paper belongs to a thesis called corrosion mechanisms and water quality regulation principles basing on the interfacial interactions between pipe wall which sponsored by the National Natural Science Fund (51278026).

6. REFERENCES

- Wang, H., Hu, C., Hu, X., Yang, M. & Qu, J. 2012. Effects of disinfectant and biofilm on the corrosion of cast iron pipes in a reclaimed water distribution system. *Water Res*, *46*, 1070–8. <http://dx.doi.org/10.1016/j.watres.2011.12.001>
- Liu, Z., Shi, B., Zheng, H. & Wang, D. 2011. Corrosion of Cast Iron in Reclaimed Municipal Wastewater. *China Water & Wastewater*, *27*, 64–68 (In Chinese).
- Emerson, D., Fleming, E. J. & McBeth, J. M. 2010. Iron-oxidizing bacteria: an environmental and genomic perspective. *Annu Rev Microbiol*, *64*, 561–83. <http://dx.doi.org/10.1146/annurev.micro.112408.134208>
- Wang, H., Ju, L.-K., Castaneda, H., Cheng, G. & Zhang Newby, B.-M. 2014. Corrosion of carbon steel C1010 in the presence of iron oxidizing bacteria *Acidithiobacillus ferrooxidans*. *Corrosion Science*, *89*, 250–257. <http://dx.doi.org/10.1016/j.corsci.2014.09.005>
- Starosvetsky, J., Starosvetsky, D., Pokroy, B., Hilel, T. & Armon, R. 2008. Electrochemical behaviour of stainless steels in media containing iron-oxidizing bacteria (IOB) by corrosion process modeling. *Corrosion Science*, *50*, 540–547. <http://dx.doi.org/10.1016/j.corsci.2007.07.008>
- Kip, N. & Van Veen, J. A. 2015. The dual role of microbes in corrosion. *ISME J*, *9*, 542–51. <http://dx.doi.org/10.1038/ismej.2014.169>
- Venzlaff, H., Enning, D., Srinivasan, J., Mayrhofer, K. J. J., Hassel, A. W., Widdel, F. & Stratmann, M. 2013. Accelerated cathodic reaction in microbial corrosion of iron due to direct electron uptake by sulfate-reducing bacteria. *Corrosion Science*, *66*, 88–96. <http://dx.doi.org/10.1016/j.corsci.2012.09.006>
- Javaherdashti, R. 2008. Microbiologically influenced corrosion: an engineering insight, Springer Science & Business Media.
- Herrera, L. K. & Videla, H. A. 2009. Role of iron-reducing bacteria in corrosion and protection of carbon steel. *International Biodeterioration & Biodegradation*, *63*, 891–895. <http://dx.doi.org/10.1016/j.ibiod.2009.06.003>
- Little, B. J. & Lee, J. S. 2009. *Microbiologically influenced corrosion*, Wiley Online Library.
- Videla, H. 1996. Corrosion inhibition by bacteria. *Manual of biocorrosion*, 121–135.
- Liu, H., Fu, C., Gu, T., Zhang, G., Lv, Y., Wang, H. & Liu, H. 2015. Corrosion behavior of carbon steel in the presence of sulfate reducing bacteria and iron oxidizing bacteria cultured in oilfield produced water. *Corrosion Science*, *100*, 484–495. <http://dx.doi.org/10.1016/j.corsci.2015.08.023>
- Lee, S., Matsui, T. & Yoshikawa, H. 2014. Study of microbial corrosion behaviour of carbon steel both in alkaline liquid medium and liquid medium with anions. *Corrosion Engineering, Science and Technology*, *49*, 562–566. <http://dx.doi.org/10.1179/1743278214Y.0000000194>
- Valencia-Cantero, E. & Pena-Cabrales, J. J. 2014. Effects of iron-reducing bacteria on carbon steel corrosion induced by thermophilic sulfate-reducing consortia. *J Microbiol Biotechnol*, *24*, 280–6. <http://dx.doi.org/10.4014/jmb.1310.10002>
- Qixin, S., Liyahong 2007. Preliminary Studies of the Corrosion of Q235 Steel by Iron Bacteria <http://www.paper.edu.cn>. (In Chinese)
- Cote, C., Rosas, O. & Basseguay, R. 2015. Geobacter sulfurreducens: An iron reducing bacterium that can protect carbon steel against corrosion. *Corrosion Science*, *94*, 104–113. <http://dx.doi.org/10.1016/j.corsci.2015.01.044>
- Liu, H., Zheng, B., Xu, D., Fu, C. & Luo, Y. 2014. Effect of Sulfate-Reducing Bacteria and Iron-Oxidizing Bacteria on the Rate of Corrosion of an Aluminum Alloy in a Central Air-Conditioning Cooling Water System. *Industrial & Engineering Chemistry Research*, *53*, 7840–7846. <http://dx.doi.org/10.1021/ie4033654>
- Zheng, B. 2012. Research on Metal Corrosion by Microorganisms in Circulating Cooling Water. Tianjin University. (In Chinese)
- Chen, D. S., Zhou, Y. Z., Liu, M., Guo, K. W. & Wei, W. J. 2011. Studies on Corrosion Behavior of Q235 Steel by Iron Bacteria, Sulfate-Reducing Bacteria and Total General Bacteria in Sedimentary Water of Storage Tank. *Advanced Materials Research*, *337*, 281–284. <http://dx.doi.org/10.4028/www.scientific.net/AMR.337.281>
- Qing, W., Yun, L., Ya-Nan, L., Yi-Mei, T. & Sen, P. 2014. Influence of iron-oxidizing bacteria in reclaimed water used for recycle cooling water on corrosion behavior of carbon steel. *Journal of the Tianjin Polytechnic University/Tianjin Gongye Daxue Xuebao*, *33*. (In Chinese)
- Lu, Y. 2011. Study on corrosion of steel induced by iron bacteria and SRB in certain aquatic environment. Tianjin University. (In Chinese)
- Schutz, M. K., Schlegel, M. L., Libert, M. & Bildstein, O. 2015. Impact of iron-reducing bacteria on the corrosion rate of carbon steel under simulated geological disposal conditions. *Environ Sci Technol*, *49*, 7483–90. <http://dx.doi.org/10.1021/acs.est.5b00693>
- Examination of bacteria and algae in industrial circulating cooling water—Part 6: Examination of iron bacteria” (GB/T14643.6 2009)
- Seneath PHA, Mair NS, Sharpe ME, Holt JG (1986) *Bergey's manual of systematic bacteriology, 9th edn*. Williams and Wilkins, Baltimore
- Liu G, Yang Z, Zhang L, et al. Imidazoline Corrosion Inhibitor in Metal Acid-Phase Reactors in Anaerobic Digestion[J]. *Journal of Residuals Science & Technology*, 2015, 12(1). <http://dx.doi.org/10.12783/issn.2376-578X/12/1/6>
- Qi, B., Wang, B., Wu, C. & Yuan, Y. 2013. Electrochemical Behavior of Cast Iron in the Presence of Bacteria in Water Distribution Systems. *International Journal of Electrochemical Science*, *8*, 1813–1821.
- Lei Z, Yu T, Ai-Zhong D, et al. Spectral Analysis of Cd, Zn, and Pb Adsorption by Extracellular Polymeric Substances from Activated Sludge[J]. *Journal of Residuals Science & Technology*, 2012, 9(1).
- Cornell, R. M. & Schwertmann, U. 2006. *The iron oxides: structure, properties, reactions, occurrences and uses*, John Wiley & Sons.
- Jin, J., Wu, G. & Guan, Y. 2015. Effect of bacterial communities on the formation of cast iron corrosion tubercles in reclaimed water. *Water Res*, *71*, 207–18. <http://dx.doi.org/10.1016/j.watres.2014.12.056>
- Teng, F., Guan, Y. T. & Zhu, W. P. 2008. Effect of biofilm on cast

iron pipe corrosion in drinking water distribution system: Corrosion scales characterization and microbial community structure investigation. *Corrosion Science*, 50, 2816–2823. <http://dx.doi.org/10.1016/j.corsci.2008.07.008>

31. Ashassi-Sorkhabi, H., Moradi-Haghighi, M., Zarrini, G. & Javaher-dashti, R. 2012. Corrosion behavior of carbon steel in the presence

of two novel iron-oxidizing bacteria isolated from sewage treatment plants. *Biodegradation*, 23, 69–79. <http://dx.doi.org/10.1007/s10532-011-9487-8>

32. Zhang, B.H., Wang, L.J. and Guo, B. 2009. “Load of Non-Point source pollutants from upstream rivers into Three Gorges Reservoir”, *Research of Environmental Sciences*, 22(2): 127–129.

GUIDE TO AUTHORS

1. Manuscripts shall be sent electronically to the Editor-in-Chief, Dr. P. Brent Duncan at pduncan@unt.edu using Microsoft Word in an IBM/PC format. If electronic submission is not possible, three paper copies of double-spaced manuscripts may be sent to Dr. P. Brent Duncan, (Editor of the *Journal of Residuals Science & Technology*, University of North Texas, Biology Building, Rm 210, 1510 Chestnut St., Denton, TX 76203-5017) (Tel: 940-565-4350). Manuscripts should normally be limited to the space equivalent of 6,000 words. The editor may waive this requirement in special occasions. As a guideline, each page of a double-spaced manuscript contains about 300 words. Include on the title page the names, affiliations, and addresses of all the authors, and identify one author as the corresponding author. Because communication between the editor and the authors will be electronic, the email address of the corresponding author is required. Papers under review, accepted for publication, or published elsewhere in journals are normally not accepted for publication in the *Journal of Residuals Science & Technology*. Papers published as proceedings of conferences are welcomed.
2. Article titles should be brief, followed by the author's name(s), affiliation, address, country, and postal code (zip) of author(s). Indicate to whom correspondence and proofs should be sent, including telephone and fax numbers and e-mail address.
3. Include a 100-word or less abstract and at least six keywords.
4. If electronic art files are not supplied, submit three copies of camera-ready drawings and glossy photographs. Drawings should be uniformly sized, if possible, planned for 50% reduction. Art that is sent electronically should be saved in either a .tif or .JPEG files for superior reproduction. All illustrations of any kind must be numbered and mentioned in the text. Captions for illustrations should all be typed on a separate sheet(s) and should be understandable without reference to the text.
5. DEStech uses a numbered reference system consisting of two elements: a numbered list of all references and (in the text itself) numbers in brackets that correspond to the list. At the end of your article, please supply a numbered list of all references (books, journals, web sites etc.). References on the list should be in the form given below. In the text write the number in brackets corresponding to the reference on the list. Place the number in brackets inside the final period of the sentence cited by the reference. Here is an example [2].
Journal: 1. Halpin, J. C., "article title", *J. Cellular Plastics*, Vol. 3, No. 2, 1997, pp. 432–435.
Book: 2. Kececioğlu, D. B. and F.-B. Sun. 2002. *Burn-In Testing: Its Quantification and Optimization*, Lancaster, PA: DEStech Publications, Inc.
6. Tables. Number consecutively and insert closest to where first mentioned in text or type on a numbered, separate page. Please use Arabic numerals and supply a heading. Column headings should be explanatory and carry units. (See example at right.)
7. Units & Abbreviations. Metric units are preferred. English units or other equivalents should appear in parentheses if necessary.
8. Symbols. A list of symbols used and their meanings should be included.
9. Page proofs. Authors will receive page proofs by E-mail. Proof pages will be in a .PDF file, which can be read by Acrobat Reader. Corrections on proof pages should be limited to the correction of errors. Authors should print out pages that require corrections and mark the corrections on the printed pages. Pages with corrections should be returned by FAX (717-509-6100) or mail to the publisher (DEStech Publications, Inc., 439 North Duke Street, Lancaster, PA 17602, USA). If authors cannot handle proofs in a .PDF file format, please notify the Editor, Dr. P. Brent Duncan at pduncan@unt.edu.
10. Index terms. With proof pages authors will receive a form for listing key words that will appear in the index. Please fill out this form with index terms and return it.
11. Copyright Information. All original journal articles are copyrighted in the name of DEStech Publications, Inc. All original articles accepted for publication must be accompanied by a signed copyright transfer agreement available from the journal editor. Previously copyrighted material used in an article can be published with the *written* permission of the copyright holder (see #14 below).
12. Headings. Your article should be structured with unnumbered headings. Normally two headings are used as follows:
Main Subhead: DESIGN OF A MICROWAVE INSTALLATION Secondary Subhead: Principle of the Design Method
If further subordination is required, please limit to no more than one (*Third Subhead*).
13. Equations. Number equations with Arabic numbers enclosed in parentheses at the right-hand margin. Type superscripts and subscripts clearly above or below the baseline, or mark them with a caret. Be sure that all symbols, letters, and numbers are distinguishable (e.g., "oh" or zero, one or lowercase "el," "vee" or Greek nu).
14. Permissions. The author of a paper is responsible for obtaining releases for the use of copyrighted figures, tables, or excerpts longer than 200 words used in his/her paper. Copyright releases are permissions to reprint previously copyrighted material. Releases must be obtained from the copyright holder, which is usually a publisher. Forms for copyright release will be sent by the editor to authors on request.

Table 5. Comparison of state-of-the-art matrix resins with VPSP/BMI copolymers.

Resin System	Core Temp. (DSC peak)	T _E	Char Yield, %
Epoxy (MY720)	235	250	30
Bismaleimide (H795)	282	>400	48
VPSP/Bismaleimide copolymer			
C379: H795 = 1.9	245	>400	50
C379: H795 = 1.4	285	>400	53

General: The *Journal of Residuals Science & Technology* and DEStech Publications, Inc. are not responsible for the views expressed by individual contributors in articles published in the journal.